

**Characterising the neural compass
across the human lifespan - a
multimethod investigation**

Thesis

for the degree of

doctor rerum naturalium (Dr. rer. nat.)

approved by the Faculty of Natural Sciences of Otto von Guericke

University Magdeburg

By M.Sc. Matthieu BERNARD

Born on 24/07/1995 in Saint-Herblain (France)

Examiners: Prof. Dr. Thomas Wolbers

Prof. Dr. Nicolas Schuck

Submitted on 24 January 2024

Defended on 26 August 2024

ABSTRACT

Head direction (HD) cells are important for navigating throughout our environment. They have been found in several brain regions of both rodents and, recently, humans. Their firing rate increases when the animal faces a specific direction and decreases when they move their head away from their preferred orientation. Thus, these cells have been considered to act as an internal compass. However, these HD cells must remain stable in relation to their environment to function properly. This stabilisation can be achieved via landmarks, which are supposed to give concrete directional information. In Chapter 1, we investigated the impact of landmark stability on the HD coding in the human brain. We found that the primary visual cortex (V1) and retrosplenial cortex (RSC) coded the landmark stability similar to previous studies. We also decoded a HD signal associated with stable landmarks in the RSC, unstable landmarks in the thalamus, and both landmarks types in the presubiculum. Moreover, another gap in the HD system literature was the influence of ageing on the system. Indeed, several studies reported a decline in spatial navigation skills due to ageing, but there is a lack of studies on how the HD system is affected. Therefore, Chapter 2 investigated the effect of ageing on the HD system using immersive virtual reality. In addition, to test for the accumulation of noise during a stationary orientation, a delay period was introduced in half of the trials before the response phase. We found that older participants produced higher angular errors than young participants. Additionally, both age groups were negatively impacted by the delay period suggesting an accumulation of noise while stationary. To help explain the differences between age groups, in Chapter 3, we created a model using ring attractor networks, a typical architecture when modelling the HD system. Previous HD models could not correctly assess ageing and the influence of noise sources related to physiological changes. Hence, we assessed ageing by implementing three distinct sources of noise: synaptic changes, loss of cerebral volume and vestibular input. We found that synaptic noises and increased neuron death led to a tendency to get stuck in local minima, which could lead to the increased range of errors observed in older participants. Altogether, the work from this thesis helped to understand in more depth the effect of ageing on the HD system and is a first step in characterising how the system degrades in ageing.

TABLE OF CONTENTS

List of Abbreviations	9
1 General Introduction	11
1.1 The spatial navigation system	11
1.2 The head direction system	14
1.2.1 Seminal work and description	14
1.2.2 Neural substrates in rodent research	17
1.2.3 Neural substrates in human research	20
1.2.4 Behavioural mechanisms of orientation coding in human	23
1.2.5 Computational modelling	25
1.3 The population ageing	29
1.4 Aim of this thesis	32
1.4.1 Chapter 1	32
1.4.2 Chapter 2	32
1.4.3 Chapter 3	33
2 CHAPTER 1: How does the stability of environmental cues affect HD computations?	35
2.1 Introduction	35
2.2 Materials and Methods	37
2.2.1 Participants	37
2.2.2 Design and procedure	38
2.2.3 Environment	38
2.2.4 Learning phase	40
2.2.5 Criterion phase	42
2.2.6 Testing phase	42
2.2.7 MRI data acquisition	44
2.2.8 Behavioural analysis	45
2.2.9 fMRI data preprocessing	46
2.2.10 Brain masks	47
2.2.11 fMRI analysis	48
2.3 Results	53
2.4 Discussion	68
2.5 Contributions	72
3 CHAPTER 2: How does human ageing affect our ability to keep track of orientation?	73
3.1 Introduction	73

3.2	Materials and Methods	77
3.2.1	Participants	77
3.2.2	Experimental design and procedure	77
3.2.3	Environment	78
3.2.4	Learning task	79
3.2.5	Testing task	80
3.2.6	Placement of the tower task	82
3.2.7	Data reduction and statistical analysis	82
3.3	Results	84
3.4	Discussion	94
3.5	Contributions	98
4	CHAPTER 3: A computational modelling approach to characterise age-related changes in the HD circuit.	99
4.1	Introduction	99
4.2	Materials and Methods	101
4.2.1	The base HD attractor model	101
4.2.2	Source of noises	105
4.2.3	Modelling of the HD behavioural task	106
4.2.4	Processing and Analysis of the Simulations	109
4.3	Results	112
4.4	Discussion	132
4.5	Contributions	136
5	General discussion	137
5.1	Summary	137
5.2	Limitations	139
5.3	Implications and Future Perspective	142
	Bibliography	160
	List of Figures	163
	List of Tables	165
	Declaration of Honour	167

List of Abbreviations

AD Alzheimer's disease	ITI inter-trial interval
ADN anterodorsal thalamic nuclei	LMN lateral mammillary nuclei
AHV angular head velocity	MCI mild cognitive impairment
BOLD blood-oxygen-level-dependent	MNI Montreal neurological institute
CCW counterclockwise	MTL medial temporal lobe
CSF cerebrospinal fluid	MVPA multivariate pattern analysis
CW clockwise	PCA principal component analysis
DTN dorsal tegmental nuclei	PFD preferred firing direction
EC entorhinal cortex	PoS postsubiculum
fMRI functional magnetic resonance imaging	ROI region of interest
FWHM full-width-half-maximum	RSC retrosplenial cortex
GLM general linear model	SVM support vector machine
HD head direction	V1 primary Visual cortex
HMD head-mounted display	vm virtual meters
	VR virtual reality

General Introduction

1.1 The spatial navigation system

Navigation is an essential aspect of life. From an evolutionary point of view, the ability to map complex environments and remember important information, such as food locations, are crucial factors in enhancing evolutionary fitness (Darwin, 1859). In their everyday life, humans are constantly navigating, either when going to their work, to their home or when travelling and discovering a new place.

Due to its importance, navigation has been the focal point of many studies with various focuses and objectives for decades. One of those focuses is understanding the different processes and cognitive functions involved in navigation. Indeed, human navigation faces various situations and requires multiple strategies to achieve successful navigation without getting lost (Wiener et al., 2009; Wolbers and Wiener, 2014; Ekstrom and Isham, 2017). The current state of the literature defines two main reference frames: allocentric and egocentric (Figure 1) (Committeri et al., 2004; Burgess, 2006; Wolbers and Wiener, 2014; Ekstrom et al., 2017). Allocentric strategy focuses on learning landmarks and their spatial relations, such as distances or directions, independently from the observer's point of view (Klatzky, 1998). This strategy creates maps of the environment that are helpful for large-scale navigation or planning (Tolman, 1948). Egocentric is focused on the observer's point of view regarding their own body (Klatzky, 1998). It is usually used for small-scale or direct navigation and helps avoid collision with the direct peripheral space (Wang and Spelke, 2000).

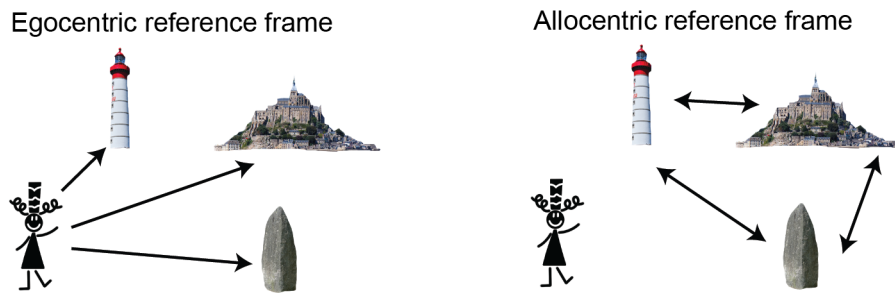


Figure 1: The two reference frames of spatial navigation.

Schematic showing the relation between individuals and environments for the egocentric (left) and allocentric (right) reference frames.

In addition to those reference frames, previous studies defined two specific types of cues. On the one hand, idiothetic cues are related to motion and correspond to self-generated features such as vestibular input, proprioception or motor efference (Gallistel, 1990). On the other hand, allothetic cues include external sensory processes like vision or audition and derive information from the environment (e.g. landmarks) (Gallistel, 1990). As their characteristics are complementary, those two types of cues are often combined and not strictly linked to a specific reference frame (Jain et al., 2017). Finally, it is essential to differentiate human spatial navigation from animal spatial navigation regarding its inputs. Compared to rodents, one of the most commonly used animal models, humans use more vision than other sensory systems, such as audition or olfaction (Ekstrom, 2015).

Another critical research focus is finding the key components of the brain that constitute the navigation system (Grieves and Jeffery, 2017; Ekstrom et al., 2017). One central region that plays a vital role is the medial temporal lobe (MTL), comprising some fundamental regions such as the hippocampus or entorhinal cortex (Figure 2). Brain regions like the thalamus or the retrosplenial cortex (RSC) also belong to the spatial navigation circuit (Figure 2). While some studies have tried to find a specific link between those regions and either egocentric or allocentric frames

(Committeri et al., 2004; Ekstrom et al., 2014), previous works suggest that there is no such strict limitation and that context is more important (Wolbers and Wiener, 2014). Furthermore, such regions are populated with spatial neurons, allowing successful navigation. Many spatial neurons have been discovered and described, such as place cells and grid cells (O'Keefe and Dostrovsky, 1971; Hafting et al., 2005), leading to the award of a Nobel prize in 2014. This thesis will focus on another type of spatial neuron called head direction cells, and the second part of this introduction will give a further explanation.

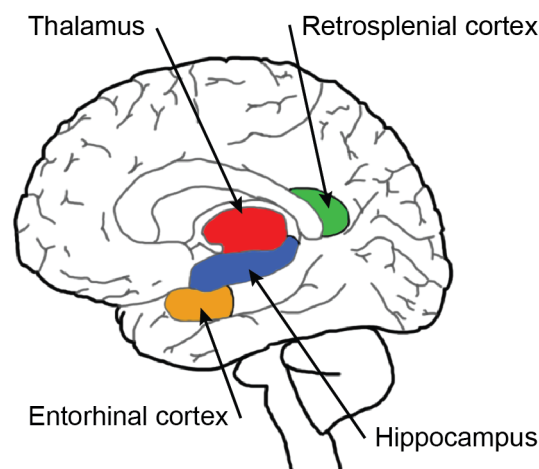


Figure 2: The spatial navigation system in the human brain.

Schematic of the sagittal cut of a human brain representing important spatial navigation regions, including the entorhinal cortex (orange), hippocampus (blue), retrosplenial cortex (green) and thalamus (red).

Even more, literature shows that spatial navigation ability varies between individuals regarding age, gender, experience and cultural differences (Maguire et al., 1999; Ishikawa and Montello, 2006; Hegarty et al., 2006; Wolbers and Hegarty, 2010; Lester et al., 2017; Coutrot et al., 2018). For example, several studies using Sea Hero Quest, a mobile game developed to study spatial navigation across the world, showed that depending on the layout of cities a person grew up in, his overall skills in spatial navigation varied (Coutrot et al., 2022). For example, people living in European cities, with more complex structures of streets and roads, tend to have better spatial

navigation skills than people living in American cities, who usually have straight roads and 90° turns.

1.2 The head direction system

1.2.1 Seminal work and description

Head direction (HD) cells were first discovered and coined by Ranck in an abstract for the Society of Neuroscience conference in 1984. Following this initial discovery, Taube et al. (1990a,b) described the general properties of HD cells in two seminal studies. These studies defined the rodent HD cells as neurons coding for the facing direction of the animal when it is looking at a specific direction (e.g. North). More specifically, there is an increase in the firing rate (number of spikes/second) of a HD cell when the head of the animal aligns with its preferred firing direction (PFD). For example, in Figure 3, if the animal is facing 0°, any HD cells tuned to 0° will fire, and the firing profile will be similar to the red curve on the right side of the figure. If the animal rotates by 90°, the neurons tuned to 0° will have their firing rate decreased, whereas neurons tuned to 90° will fire at their maximum. Since the brain contains an entire network of HD cells with different PFDs spanning the 360-degree range, researchers describe it as the “neural compass of the brain”.

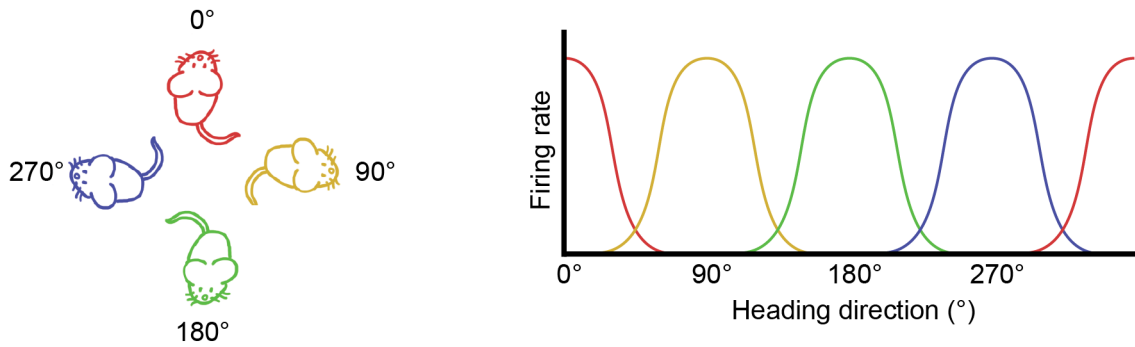


Figure 3: The head direction cell firing.

Four examples of HD cells with separate PFDs and their associated tuning curve when the animal faces each PFD. For example, the orange cell fires maximally when the animal is facing East (90°).

Figure adapted from Sharp et al. (2001b).

Aside from their firing rate, Taube et al. (1990a) described the shape and additional properties of the signal, and multiple studies replicated the findings (Taube, 1995; Blair and Sharp, 1996; Taube and Muller, 1998). First, the shape of the firing rate is similar to a Gaussian curve (i.e. bell-shaped curve) and is called a tuning curve. Its shape originates from the PFD of HD cells as its firing rate increases as the animal faces its PFD and decreases when it moves away. The directional firing range of HD cells is the range of orientation when the neurons fire. It is about 90° on average but can vary from 60° to 110°. Second, the firing rate is usually stable without adaptation when the animal faces the same direction. It means the maximum firing rate does not decrease over time if the animal maintains a fixed orientation. However, the authors observed that the maximum firing rate of a HD cell varies across PFDs and found examples ranging from 6 spikes/second to 100 spikes/second. Third, the PFD of HD cells is independent of the animal's location in its environment. This finding implies that distinct views of the environment do not influence the HD signal. Finally, the PFD of cells remains stable across days when researchers record the animal in the same environment.

Taube et al. (1990b) investigated additional HD cell properties in a changing environment. In a regular context, landmarks are usually fixed and take the form of a cue card in rodent experiments. If the experimenter rotates the cue card by a certain amount (e.g. 90 degrees), the PFD of HD cells follows in the same direction with a similar amount but not equal. When the card is removed from the environment, a shift in the PFD happens by an uncertain amount. Those properties are the first indication that HD cells have a solid relation to landmarks, and Figure 4 summarises all those properties. However, studies found that the HD signal can be updated using solely body-based cues by recording rodents moving around in darkness (Goodridge et al., 1998; Yoder et al., 2011). The authors found that the HD signal was still present even when vision was unavailable, and they observed only a little shift in the PFD. Further studies discovered new properties that give more details about the network and their connections (Jacob et al., 2017; Kornienko et al., 2018; Viejo and Peyrache, 2020; Grieves et al., 2022; Fallahnezhad et al., 2023). However, as they are beyond the scope of the thesis, they will not be described here.

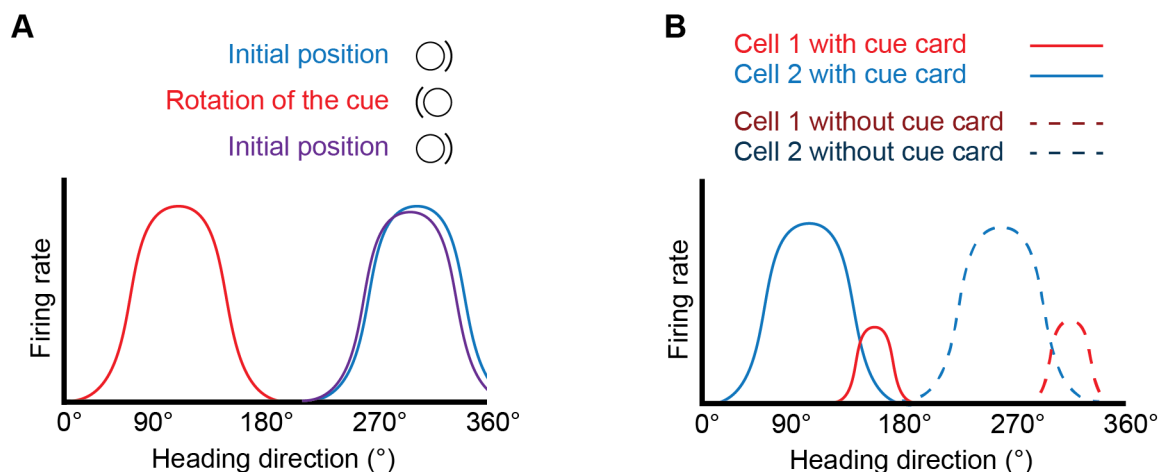


Figure 4: Head direction cells properties in a changing environment.

A, HD cell response after a 180° rotation of the cue card. The PFD of the cell shifted by 180° (red curve) and returned to its initial position following another 180° rotation (purple curve). B, example of two HD cells when the cue card is removed from the environment. The tuning curve was maintained, but the PFD of HD cells shifted to another location (dashed curves). Figure adapted from Taube (2007).

1.2.2 Neural substrates in rodent research

HD cells were first recorded in the postsubiculum (PoS) of the rodent brain (Ranck, 1984). Later electrophysiology studies observed HD cells in several other regions, such as the RSC (Chen et al., 1994; Cho and Sharp, 2001), the anterodorsal thalamic nuclei (ADN) (Taube, 1995; Stackman and Taube, 1998), the entorhinal cortex (EC) (Sargolini et al., 2006) as well as in the dorsal tegmental nuclei (DTN) (Sharp et al., 2001a) and the lateral mammillary nuclei (LMN) (Stackman and Taube, 1998). In addition, lesion studies investigated the contributions of regions in generating and maintaining the HD signal. Lesions to the PoS (Goodridge and Taube, 1997) or EC (Clark and Taube, 2011) do not disrupt the HD signal. In contrast, lesions of the vestibular system (Stackman and Taube, 1997; Stackman et al., 2002), bilateral LMN (Blair et al., 1998; Bassett et al., 2007; Sharp and Koester, 2008) or ADN (Goodridge and Taube, 1997) disrupt the HD signal. Those results suggest that the HD signal is generated from the vestibular system and transmitted via the LMN to the ADN before going to the other cortical regions. However, lesions that do not extinguish the signal lead to some signal alteration. For example, lesion to the RSC leads to unstable PFD in the animal, especially in the case of allothetic cues (i.e. landmark processing), while idiothetic cues would remain intact (Clark et al., 2010).

These different brain regions can be linked, creating two separate pathways corresponding to the different inputs the HD system is receiving. The first pathway, linked to allothetic cues and sensitive to vision, allows the integration of the landmarks. Multiple reports showed landmarks' critical role in the signal's stability (Taube et al., 1990b; Taube, 1995; Knierim et al., 1995; Zugaro et al., 2001, 2003). Therefore, the visual cortex would project to the RSC, the central hub for landmark integration (Auger et al., 2012). The RSC then send this information to the ADN and

PoS to combine with the other inputs (Yoder et al., 2015). The second pathway relies on idiothetic cues such as self-motion with inputs from the vestibular system. Self-motion is another essential input as it allows perception of the head rotation when vision is not available to update the HD (Goodridge et al., 1998; Yoder et al., 2011) and angular head velocity (AHV) cells support it (Stackman and Taube, 1998; Bassett and Taube, 2001). Those cells are located primarily in the DTN (Bassett and Taube, 2001; Sharp et al., 2001b), which has reciprocal connections to the vestibular system and LMN (Liu et al., 1984; Sharp et al., 2001a; Bassett et al., 2007). Those neurons would integrate changes in the head velocity and would be used to update the HD system (Graham et al., 2023). Thus, the pathway is generated from the vestibular system and then moves up to the DTN and LMN before reaching the ADN (Taube, 2007). Finally, both pathways combine their signal in the ADN before being projected to the PoS and EC. Then, the signal is incorporated with the other spatial neurons to contribute to the navigation ability of the animal (Sargolini et al., 2006; Grieves and Jeffery, 2017; Poulter et al., 2018). Figure 5 shows a summary schematic representing the two pathways and the associated regions.

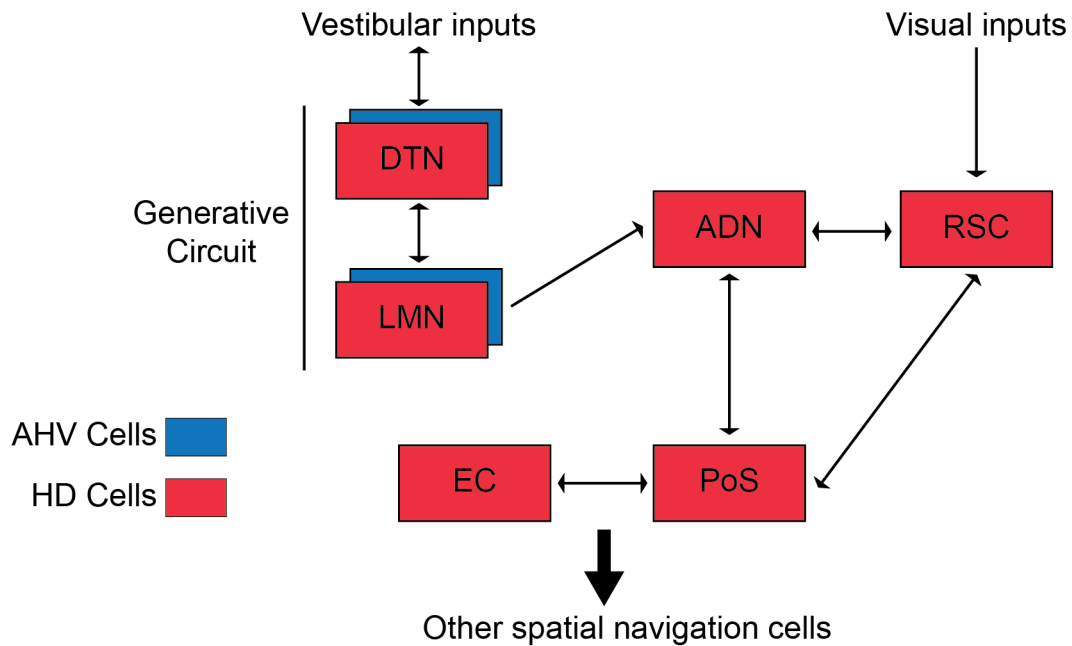


Figure 5: Simplified circuit of the regions involved in the HD system.

Red squares represent regions containing HD cells, and blue squares represent regions containing AHV cells. ADN, anterodorsal thalamus; DTN, dorsal tegmental nucleus; LMN, lateral mammillary nuclei; EC, entorhinal cortex; PoS, postsubiculum; RSC, retrosplenial cortex. Figure adapted from Clark and Taube (2012).

In addition to rodent research, several papers studied other animal models to describe their HD systems. Indeed, recent work from Petrucco et al. (2023) found evidence of the HD system in the zebrafish, and the authors characterise the system similarly to the rodent. The HD system in the fruit fly has also been described for the insects, especially in the modelling context and will be explained later in this introduction (Seelig and Jayaraman, 2015; Green et al., 2017; Kim et al., 2017). Finally, studies also found HD cells in mammals such as bats (Finkelstein et al., 2015, 2019) and primates (Robertson et al., 1999). However, relatively few studies have studied HD cells per se in humans.

1.2.3 Neural substrates in human research

While many studies have been conducted in animal research, only a handful have tried to investigate HD in humans. Among them, most tried to look at HD in behavioural experiments, and only four published papers looked directly at HD using functional magnetic resonance imaging (fMRI).

The first study by Baumann et al. (2010) designed a virtual maze with symbols at the different ends of corridors. After being familiarised with the environment, participants performed a spatial judgement task where they saw a pair of pictures taken from the environment and decided if each picture was on the left or right from the maze's centre. Importantly, each pair of pictures represented either the same direction (e.g. North-North) or a different one (e.g. West-North), but the task performed was independent of HD. Thus, in their analysis, the authors compared novel heading (i.e. different heading) against repeated HD and found a HD signal in the Medial Parietal Cortex (Brodmann area 31).

A second study by Marchette et al. (2014) asked participants to remember four buildings placed in a park with four landmarks at each cardinal point. Each building had a set of objects that participants learned. Next, a judgement of relative direction task tested the participant's performance regarding the individual object positions. Specifically, the task asked if an object was located to the left or right of a second reference object. The authors used a multivariate pattern analysis (MVPA) with Pearson correlations to compare the similarity in the neural pattern if the same direction was repeated across trials, either within or across buildings. The authors found a signal in the RSC in accordance with the rodent literature. They also found that the RSC distinguished local HD, associated with the building's inside geometry, and global HD, related to landmarks.

The third study by Chadwick et al. (2015) designed a four-path square environment with goal objects at each corner and four scenes as a landmark at each side. Then, participants performed a goal direction task where they saw one of the scenes plus an object, and they needed to determine the location of this goal object either from an egocentric (e.g. Left or right) or geocentric way (e.g. which scene). The authors performed a searchlight pattern similarity analysis using Pearson correlation on the pattern of voxel activation, similar to Marchette et al. (2014). They found a signal in a cluster centred on the entorhinal cortex and spreading to the subicular region, and they thought it reflected the HD signal.

Finally, the fourth study done by Shine et al. (2016) used four buildings with pictures of a single category (animals, abstract arts, colour blocks and geometric shapes) in each one of them. In addition, the authors used a head-mounted display (HMD) while learning the environment. They suggested that providing full body-based cues during the training could lead to a recapitulation of such information during the scanning phase, where only visual cues are available. In this study, participants performed a one-back task where they were asked to retrieve the facing direction associated with a picture compared to the one previously seen. The authors analysed the data for evidence of repetition suppression with a general linear model (GLM) and found a signal in the RSC and the thalamus.

These studies found a set of regions in the human brain associated with HD signals similar to the rodent literature: the EC, RSC, subiculum and thalamus using fMRI methods and analysis (Figure 6). Those results suggest that even with head-fixed, i.e. no vestibular inputs, HD signal can be extracted from the human brain. Interestingly, a recent study by Sit and Goard (2023) recorded HD cells in the RSC of head-fixed

mice. They showed evidence that the heading can be encoded separately from the physical head orientation of the animal.

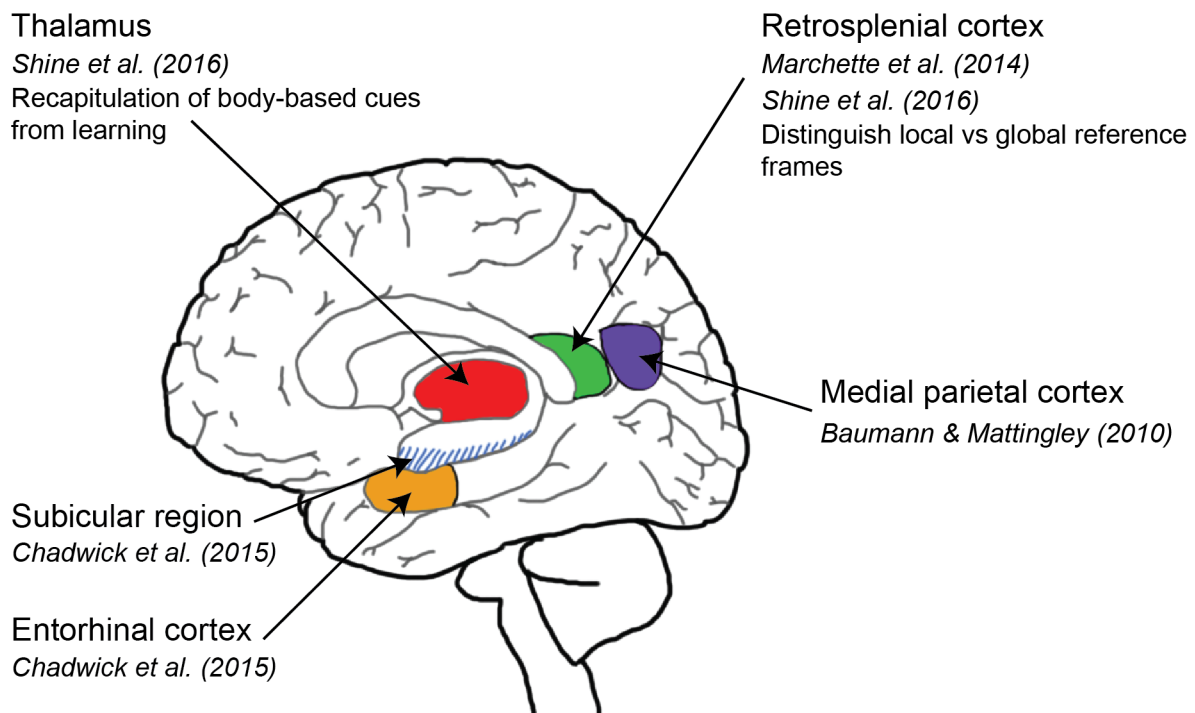


Figure 6: Summary of human brain regions sensitive to HD signal.

Schematic of the sagittal cut of a human brain including the entorhinal cortex (orange), medial parietal cortex (purple), retrosplenial cortex (green), subicular region (dashed blue lines), and thalamus (red).

In addition to those fMRI studies, researchers investigated the impact of RSC lesions on patients' behaviour. Multiple studies reported that after lesions to RSC, patients would usually have impaired spatial navigation skills with some feeling of disorientation (Song et al., 2020; Maguire, 2001; Vann and Aggleton, 2004; Hashimoto et al., 2010; Claessen and van der Ham, 2017). For example, Takahashi et al. (1997) found pure topographical disorientation after RSC lesions where patients could identify landmarks but not establish spatial relations. This disruption in the processing of landmarks is similar to the finding from lesion studies in rodents described above. Lesions to other regions, such as the thalamus or hippocampus, also lead to deficits in spatial navigation, such as path integration, where those

patients would have trouble finding the correct pathway between locations in their environment (Astur et al., 2002; Bartsch et al., 2010; Kim et al., 2013).

1.2.4 Behavioural mechanisms of orientation coding in human

Next to the studies focusing on the neural mechanisms underlying HD computations, only a few studies investigated the HD system using pure behavioural analysis. Sadalla and Montello (1989) investigated if participants could maintain their sense of orientation after performing a rotation. They found that participants were less disoriented when turning on angles close to cardinal directions (0, 90 or 180) and that they tend to remember angles as 90°. In addition, several experiments looked at connected aspects.

The first aspect is visual perspective-taking, defined as the study of changes in the spatial relation between objects after a switch in the imagined point of view (or perspective) (Flavell et al., 1981; Parsons, 1987; Amorim, 2003; Zacks et al., 2003). Common examples that can often happen in our everyday lives are taking another person's perspective while giving instructions for driving or predicting someone else's movement in a crowded place to avoid a collision. While the subject is extensive, our interest is in how HD is involved and studied. Early studies thought that HD was involved due to the misalignment between the actual position and the imagined switch of perspective (May et al., 1995; Shelton and McNamara, 1997). However, later work proposed to differentiate HD and misalignment (Waller et al., 2002; May, 2004; Mou et al., 2004). They explained that misalignment is due to a difference in the participant heading between the learning and testing phases of the experimental task. In contrast, changes in the heading are within a single phase (usually testing) between the real and imagined orientation (Waller et al., 2002; May, 2004; Mou et al., 2004).

Finally, recent work from Ueda et al. (2021) investigated the impact of torso and head rotation during a visual perspective transformation task. Specifically, participants would have to solve an orientation judgement task from several perspectives while seeing a human avatar from different positions with either its torso or head forward to the object or backward. They found evidence in their experiment that if the torso is facing the object, it facilitates and improves performance, while the position of the head has less impact on results. Unfortunately, most studies on perspective-taking do not investigate in more depth how the HD system is involved, and firm conclusions are difficult to draw.

The second aspect is self-motion perception and how studies investigate the influence of different cues (i.e. auditory, visual or vestibular). Those experiments ask the participants to self-rotate or move along a path whether different cues are present (Israël et al., 1997; Siegler et al., 2000; Etienne and Jeffery, 2004; Crane, 2012; Zanchi et al., 2022). Those studies found evidence that removing those cues usually negatively impacts participants' sense of direction, e.g., when navigating in darkness (Israël et al., 1997; Siegler et al., 2000). Moreover, one typical experiment linked to self-motion is path integration. Path integration is defined as the ability to follow a trajectory while continuously updating one's position and orientation by monitoring self-motion cues (Mittelstaedt and Mittelstaedt, 1980). Many studies have looked at path integration (Wolbers et al., 2007; Chrastil and Warren, 2021; Qi and Mou, 2023), but it is challenging to disentangle the involvement of the HD system completely. Indeed, studies investigating how HD influenced the task are usually confounded with how the participants' answers are being measured.

Nevertheless, a recent study from Harootonian et al. (2022) examined how HD integrates path integration and visual landmark navigation. The authors used a

self-rotation experiment where participants were asked to rotate on themselves before facing back the learned position. There was no visual feedback except for some trials where the visual feedback was offset from the actual position, allowing the authors to look at systematic errors participants would make. They used those results to compare it with different theoretical models. The authors found evidence that participants were probably using a mix of both body-based and visual-based cues to solve the task. However, their model did not use the type often used in the context of HD, and they did not model the HD system per se.

Finally, it is essential to remember that experiences from most studies are just an approximation of real life as they used smaller-scale spaces. However, the expansion of the methods available for human research tries to account for this. There has been an increase in the use and development of virtual reality (VR) systems and, more importantly, HMD. Nowadays, most human research studying navigation uses VR environments to mimic ecological context and increase the sense of embodiment (Kilteni et al., 2012; Diersch and Wolbers, 2019). All the experiments made throughout this thesis use VR and HMD. However, trying to get more real-life experiments would contribute positively to the field. Such studies (Maguire et al., 2006; Marquardt et al., 2022; Heward et al., 2023) are starting to be published. For example, Marquardt et al. (2022) looked at adults' navigation performances using a mobile app to track their movement while navigating in the real world to perform a task.

1.2.5 Computational modelling

This next section will present the theoretical model used to study the HD system: the ring attractor network. A theoretical attractor network can be described as

nodes/neurons organised as a conceptual ring with recurrent connections. In 1982, Hopfield introduced the basic equations and properties and in 1989, Amit proposed so-called attractor networks and theorised their dynamics.

It is important to note that one of the first models describing the head direction system was not a ring attractor network. The model from McNaughton et al. (1991) hypothesised an integration of inputs between movement (i.e. angular velocity) and the current HD to create the output being the next state of HD. However, in a refined model from Skaggs et al. (1995), the authors added the ring attractor network architecture accounting better for the connections and dynamics of the system. More precisely, they defined that there should be strong excitatory connections between neighbouring nodes and inhibitory connections to distant nodes. In a stable state, this would produce a cluster of activated cells somewhere on a circle, forming the current bump of activity of the HD akin to a tuning curve (Figure 7). They also described how vision or vestibular input would interact with such a model and how it allowed the model to rotate by having the input either clockwise or counterclockwise, which would drive the HD state to the location of the input.

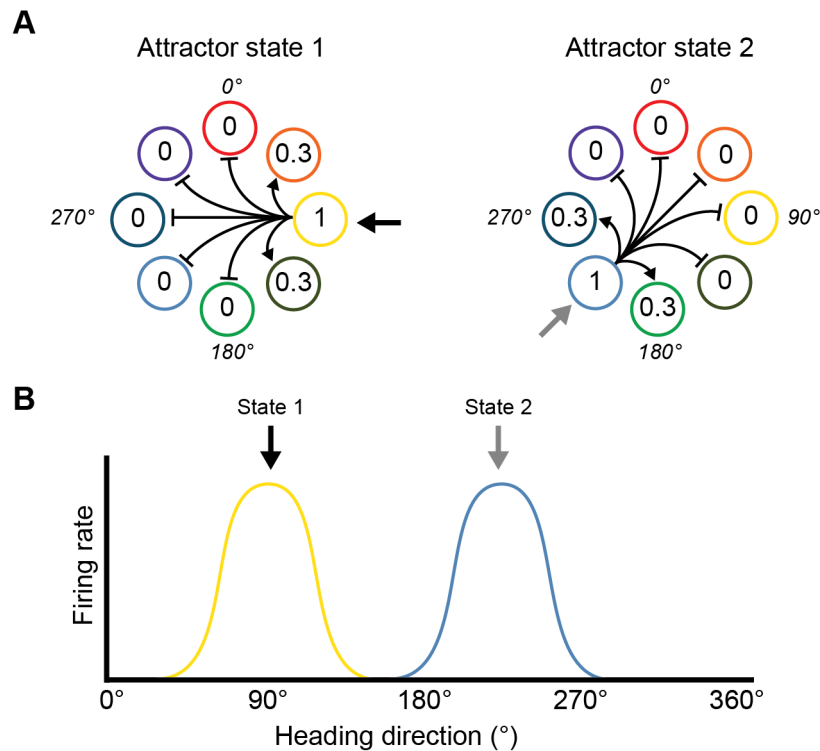


Figure 7: Schematic of ring attractor network dynamics in a HD model.

A, Two states of a ring attractor with 8 neurons (coloured rings) with an example of the pattern of connections (black lines) between a single neuron (yellow on the left and light blue on the right) to the other rings. The connections are excitatory for neighbouring neurons (arrowhead lines), or inhibitory for distant neurons (flathead lines). In the model, every neuron has the same connection pattern. Inside each neuron is a value representing the firing rate of the neurons when a stimulus (represented by the black and grey arrow) is applied to the yellow (left) or light blue (right) neuron. *B*, the tuning curve associated with the state 1 (yellow) and state 2 (blue).

In 1996, a complete model by Zhang was developed and significantly impacted the field. His model is being used since then in several studies (Byrne et al., 2007; Page et al., 2014; Page and Jeffery, 2018; Yan et al., 2021). The model replicated the HD properties described in the rodent literature at the time (i.e. directional tuning, vision based with landmark or vestibular inputs). His model also used the ring attractor network dynamics, similar to Skaggs et al. (1995), with symmetric or asymmetric weights, allowing for the rotation of the activity bump within the ring. While this model is imperfect and has some flaws, especially in terms of physiological plausibility, other models have been developed since then to investigate further properties or try to account for those

(Goodridge and Touretzky, 2000; Song and Wang, 2005; Bicanski and Burgess, 2016; Page and Jeffery, 2018; Yan et al., 2021).

In complement to this theoretical work, researchers tried to investigate the location and generation of this potential attractor network. Substantial evidence supports that the generation of the bump is linked to the vestibular signal and its afferent connection, such as DTN and LMN (Skaggs et al., 1995; Sharp et al., 2001a; Song and Wang, 2005). Even more, the transformation from AHV to HD signal might be done in the sub-cortical part of the system, especially the ADN where the ring could be located (Knierim and Zhang, 2012). However, there is no concrete evidence of whether the signal is a product of some brain properties or is created from a network of neurons similar to a ring attractor architecture.

From the few papers investigating it, a study from (Peyrache et al., 2015) hypothesised that if the HD system was internally organised as a ring attractor model, the relationship between the neurons would persist between wake and sleep states. The authors used Bayesian-based decoding to infer the HD signal and the head orientation of the animal when it was asleep. As hypothesised, they found a robust correlation between the two states (wake and sleep). They also found evidence similar to a property of the ring attractor, which suggests that only a subset of neurons fire simultaneously, creating the bump. However, no neuron topology similar to a ring has been found in the rodent.

However, fruit fly possesses such topology (Seelig and Jayaraman, 2015; Green et al., 2017; Kim et al., 2017). Indeed, a part of the brain called the ellipsoid body has the shape of a ring and acts as a ring attractor network by providing projection to other parts of the brain. Strikingly, studies presented that with rotation inputs, the activity would also move CW or CCW, similarly to the theoretical ring attractor network. Visual inputs also

seemed to connect to the ellipsoid body. No evidence of ring attractor dynamics has been found yet in human studies.

1.3 The population ageing

The last report of the WHO estimates that the world population is getting older and might reach 50% of older adults by 2030 in Europe (Figure 8) (Wilmoth et al., 2023). Henceforth, many studies investigated cognitive changes associated with ageing (for review, see Lester et al. (2017)). It was reported that old adults are impacted by different behaviours, such as being disoriented, lost or not finding personal objects. Such problems arise due to a deficit in spatial navigation skills and point to further complications for this population. Indeed, it can lead to isolation as they cannot navigate outside, which increases the chance of having more severe cognitive decline or neurological disease (Hendriks et al., 2023). Logically, studies focused on spatial navigation as evidence to find which neural circuits are targeted early during cognitive decline.

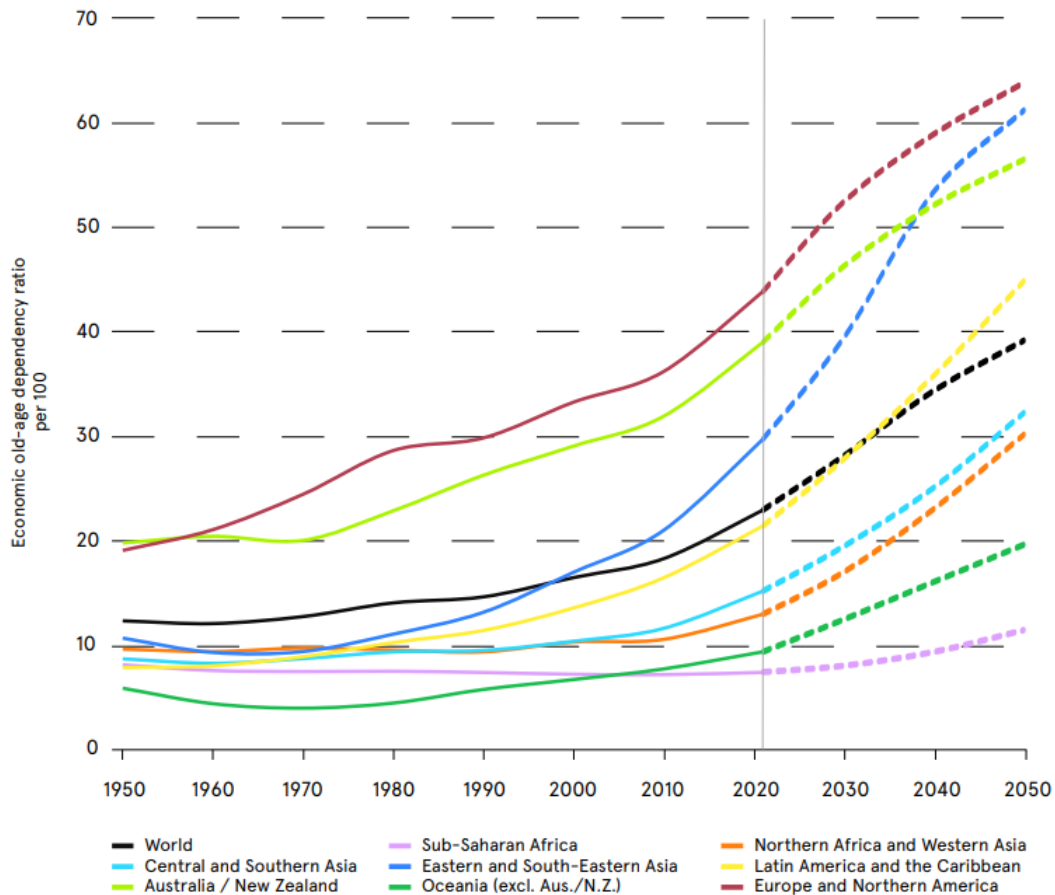


Figure 8: Percentage of people aged 65 years or over across world regions from 1950 and estimated until 2050.

Figure adapted from WHO 2023 report (Wilmoth et al., 2023)

Studies on the ageing brain are numerous and investigate the changes in the input and neural processes of the brain across the lifespan. For the inputs, studies show that vision, one of the dominant sensory inputs for humans, is impaired during ageing (Quillen, 1999; Loh and Ogle, 2004; Swenor et al., 2020). In addition, studies have shown that with ageing, some degree of vestibular loss exists (Neuhauser et al., 2008; Agrawal et al., 2009; Anson and Jeka, 2015). This loss would also lead to a deficit in the navigation system, especially the HD system since lesions in the vestibular of the rodent erase the HD signal (Stackman and Taube, 1997; Stackman et al., 2002).

Furthermore, next to the deficit in inputs, ageing impacts the synaptic connection between neurons (for review, see Morrison and Baxter (2012)) by reducing their numbers and the number of neurotransmitters. This reduction impairs the brain's overall functioning and connected abilities, such as spatial navigation. In addition, multiple studies showed a decrease in cerebral volumes during ageing in several brain regions related to navigation, such as the hippocampus (Burke and Barnes, 2006; Raz and Rodrigue, 2006), the thalamus (Hughes et al., 2012), and the RSC (Moffat et al., 2006). Some studies (Rapp and Gallagher, 1996; Freeman et al., 2008) link loss of cerebral volumes without loss of neurons but loss of neuronal and dendritic connections. However, other studies state that neuron death occurs during healthy ageing and varies between brain regions and individuals (Mueller et al., 1998; Thompson et al., 2003). This subject is up for debate in the field as rodent studies also observe no such loss of neurons in MTL structures (Merrill et al., 2001; Rapp et al., 2002).

Therefore, it is crucial to continue the research on how ageing impacts navigation to help detect cognitive decline early to treat it better. One way to assess it is to define spatial navigation tasks to check if their skills are impaired and to characterise further and understand the mechanics behind it (Moffat, 2009; Bates and Wolbers, 2014; Colombo et al., 2017). Several studies tried to investigate those and found evidence that navigation strategy such as path integration is impaired with ageing (Harris and Wolbers, 2012; Stangl et al., 2018; Segen et al., 2022). In addition, other studies found evidence for impaired allocentric skills, especially related to route learning and landmark knowledge (Wiener et al., 2013; Bécu et al., 2023). Many of those studies have connected those deficits to other types of spatial neurons, such as place cells or grid cells. However, no studies have investigated the effect of ageing on the HD

system in humans. This thesis will try to find more evidence on how ageing impacts the HD system.

1.4 Aim of this thesis

The thesis aims to build and develop how the human brain's HD system works. The thesis will be separated into three chapters reflecting the three experiments undertaken. All of them aimed to increase our understanding of the system in the human brain.

1.4.1 Chapter 1: How does the stability of environmental cues affect HD computations?

As HD needs stable landmarks to maintain its signal, the effect of landmark stability was studied to see its impact. The goal was to see if and how unstable landmarks influence and change the HD signal. The analysis and methods in this chapter used the strength of MVPA to decode the HD signal and characterise the influence of stability. Finally, as human participants had different strategies and behavioural performances when solving a task, those were discussed in relation to the results.

1.4.2 Chapter 2: How does human ageing affect our ability to keep track of orientation?

The second chapter focused on creating a new behaviour experiment examining the HD system. Only a few experiments tried to look at HD specifically from a behavioural point of view. Therefore, the task found a way to get the "purest" measure of HD. In addition, the study was conducted on both young and older adults to see how ageing

affects HD. Since ageing seems likely to impact HD, this chapter tried to understand the mechanisms that are changing with ageing in more depth.

1.4.3 Chapter 3: A computational modelling approach to characterise age-related changes in the HD circuit.

The last chapter focused on developing a model of the HD system to understand the mechanism by which orientation computations are compromised in old age. Building on existing ring attractor models, this new model resolved their pitfalls so ageing could be characterised. Indeed, the goal was to find noise sources, such as synaptic deficit or neuron death, and modify their level to characterise their impact on the HD system. The goal was to be able to describe the potential loss that would happen during ageing and where it would come from in the system. Finally, the model implemented the second chapter's task and tweaked the noise amount. The objective was to see which noise sources best described young or older adults' performance.

CHAPTER 1: How does the stability of environmental cues affect HD computations?

2.1 Introduction

In the general introduction, the different fMRI studies investigating HD have been presented and discussed. However, the experimental designs used in these human studies did not assess the properties of the HD cells. Therefore, the experiment undertaken for this chapter tries to investigate one of the properties of HD: its relation to landmarks.

HD cells are maintained stable relative to the environment (Taube et al., 1990b), and landmarks are crucial in giving such stable directional information (Knierim et al., 1995). There are many landmarks in everyday life, and some are more stable and salient than others. It is essential to identify the permanence of landmarks to avoid getting lost. A study by (Zugaro et al., 2001) investigated the effect of object rotation on the PFD of HD cells when background cues were present or not. The authors show evidence that rodents primarily used the background cues to update the PFD of HD cells compared to foreground cues (i.e. objects). They justified this finding as the background cues would be more salient and stay longer within the animal's retina when moving. In addition, the animal could consider foreground objects unreliable as they would see them from different viewpoints.

Multiple studies investigated the coding of landmark stability in the human brain (Auger et al., 2012; Auger and Maguire, 2013; Auger et al., 2015, 2017; Auger and

Maguire, 2018a,b). The authors found that the RSC, PoS and hippocampus would encode permanent landmarks in an allocentric spatial map of the environment. Moreover, they hypothesised that the HD signal might play a role by firing in response to the reliable permanent landmark. This assumption is supported by the fact that permanent landmark coding and HD signals have been found in the RSC. Moreover, previous studies mentioned a difference in the perception of landmark stability between good and bad navigators (Auger and Maguire, 2013; Auger et al., 2017). Precisely, bad navigators would have a lower activity in the RSC regarding the permanence of items while learning the environment. Finally, this landmark stability has been examined for everyday objects (Auger et al., 2012; Auger and Maguire, 2013) and novel 'alien' landmarks (Auger et al., 2015, 2017; Auger and Maguire, 2018b). Therefore, it would be interesting to investigate the relationship between HD and landmark stability in the human brain. It is unknown whether unstable landmarks would not be integrated within the HD system or would be coded, but the tuning curve associated with them would change.

The analysis of this study will be based on MVPA, a fMRI analysis that can decode which direction the participant is facing with the neural pattern taken from the blood-oxygen-level-dependent (BOLD) signal. This method was developed by Haxby et al. (2001) in order to find a pattern of voxel activity within the brain using classifiers. Different papers investigating the MTL have successfully used this MVPA (e.g. Hassabis et al. (2009); Bonnici et al. (2012)). First, the study of Hassabis et al. (2009) decoded place responses by training classifiers differentiating the position of participants within two different environments. In addition, Bonnici et al. (2012) also looked at pattern completion in the MTL through the morphing of two scenes. The authors successfully decoded the choice of the participants in the hippocampus.

Therefore, a new experiment should be carefully designed to allow MVPA decoding and study HD properties, such as the impact of landmark stability.

The study aimed to investigate how the stability of landmarks, whether stable or unstable, influences the neural signal in the human brain. Regions related to HD, such as the EC, hippocampus, RSC and thalamus, were measured. Using immersive VR, participants learned a simple environment with two stable and two unstable landmarks. This setup provided participants with full body-based cues during training. Then, participant neural signals were recorded during fMRI while passively moving within the learned environment. The prediction would suggest that decoding of heading toward stable landmarks would be stronger than the one toward unstable landmarks and that RSC would be able to differentiate between stable and unstable landmarks.

2.2 Materials and Methods

2.2.1 Participants

Twenty healthy young adults aged between 18 and 30 years (25.68 ± 4.8 , female $n=9$) participated in the study. Participants were fluent in German, did not report any physical or mental disorders, and were not colourblind. The local ethics committee approved the experiment, and all research was performed under relevant guidelines and regulations. Written informed consent was obtained from each participant before starting the experiment. Participants were compensated financially for their participation. We excluded one participant due to insufficient performance compared to the others in the pointing task during testing.

2.2.2 Design and procedure

The study was performed in a balanced, within-subject design (Figure 9). Every participant came for two consecutive days, performing the learning of the environment during the first day in immersive VR using a HMD. More precisely, during the whole learning phase, participants were wearing an HTC Vive HMD with a wireless adapter, and they could actively walk in an area of 5 by 5 metres without constraint. On the second day, participants did the testing while being in an MRI scanner. For details on the tasks, see the descriptions below.

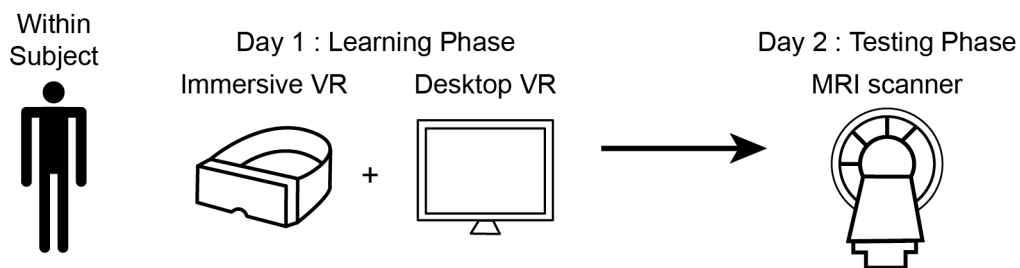


Figure 9: Design of the task.

Within-subject design of the experiments with participants performing the learning on day 1 using immersive and desktop VR. On day 2, participants did the testing phase inside a MRI scanner.

2.2.3 Environment

The virtual environment was created using Unity software (version: 2019.2.0f1). The ground had a moon-like texture with no apparent pattern preventing orientation. The skybox also had a star pattern without a specific pattern. In addition, the skybox was rotated randomly during every trial, preventing participants from using it to locate themselves. Four landmarks designed as planets were positioned in each cardinal direction to allow participants to orient. Each had a different colour (green, red, blue or orange) and different texture so participants could easily differentiate them. The colour and texture were different across participants. Importantly, those four planets

had different stability, meaning their position within the environment would change. Henceforth, the “North” and “South” landmarks were stable and stayed at the same position during the whole experiment. On the contrary, the “East” and “West” landmarks were unstable, and their position changed every trial within a range from 25° to 155° for the East and 205° to 335° for the West. Finally, two other smaller “planets”, called “moons”, were positioned at the diagonal of the environment (115 and 290) and had separated colours from the main landmarks (purple and grey, also switching between participants). Those “moons” were used in a pointing task to test participants’ memory of the spatial relation between the moons and the permanence of landmarks. Figure 10 shows a bird’s eye view of the environment.

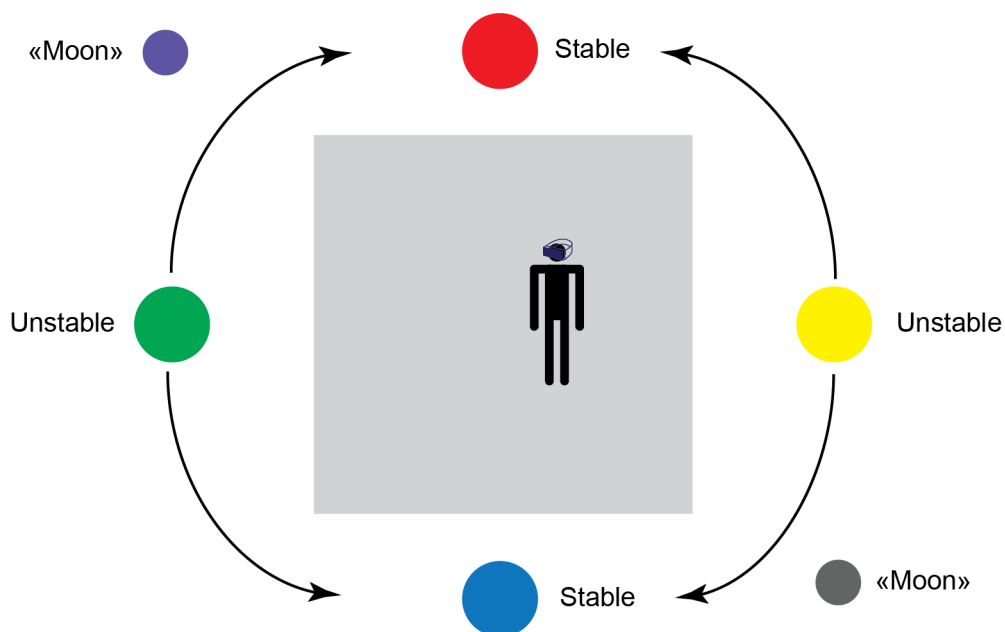


Figure 10: Environment of the task.

Bird-eye view schematic of the environment learned by participants. It comprises 4 landmarks, 2 stable (red and blue) and 2 unstable (green and yellow). Unstable landmarks changed position every trial of the task within a given range as shown by the black arrows. Two small objects called “moon” were positioned at the diagonal of the environment and were only used for a pointing task

2.2.4 Learning phase

We separated the learning phase into learning blocks. Each block included three tasks: the actual learning task and two checking tasks to see if the participant learned the environment. The learning blocks were repeated until the participant passed the checking tasks (Figure 11). In every trial, the unstable planets' position change occurred during a fade-in/fade-out phase, so participants could not watch the switch.

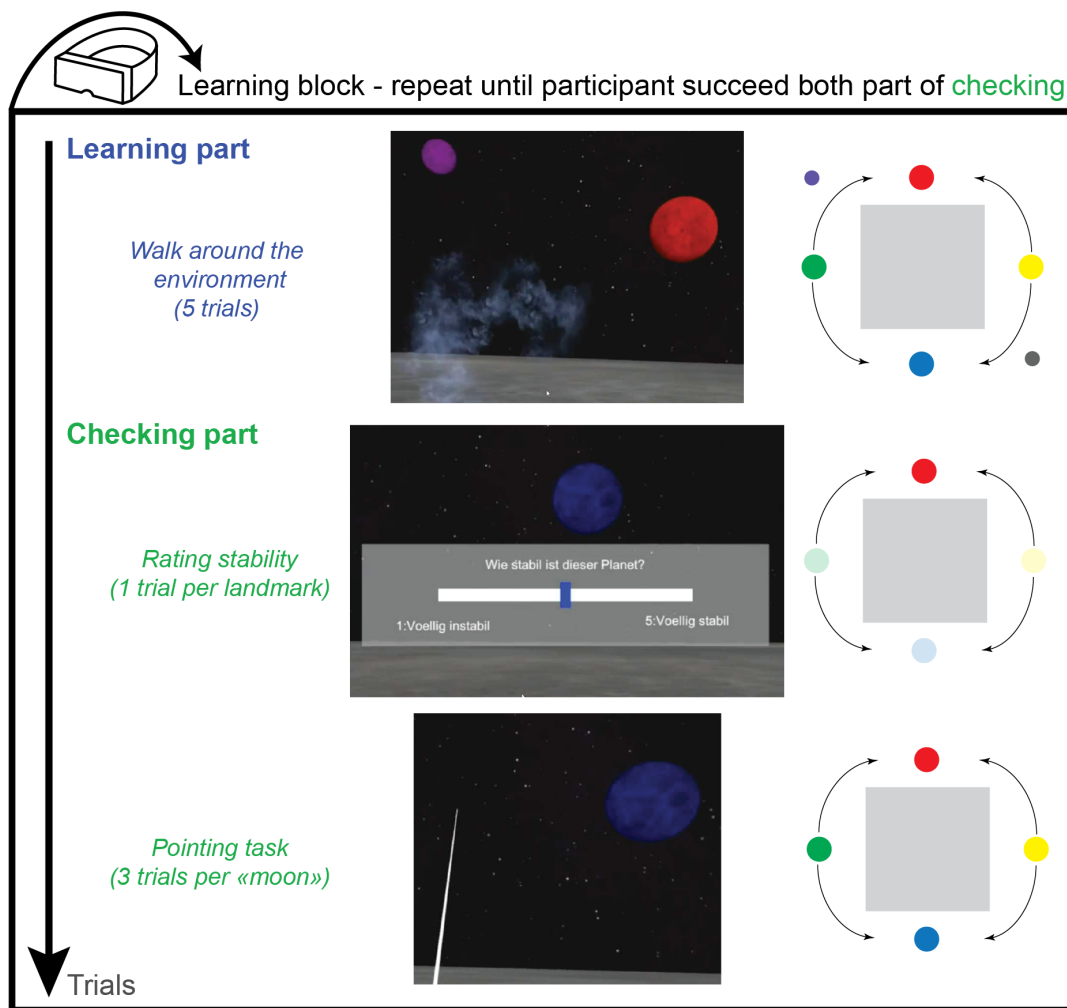


Figure 11: Design of the learning phase.

The black box is an example of a learning block with the 3 different tasks. Top, the learning part where participants walked in immersive VR and saw the entire environment. Middle, the rating of stability task to test participant on their perception of landmark permanence. They saw only one landmark at a time, and the moons were not present. Bottom, the pointing task where participants had to point to the position of moons while seeing the four landmarks. Participants repeated a learning block if they failed one of the checking tasks.

During the learning task, the participant could see the whole environment (four planets and two moons) and performed five trials for each block. During each trial, participants moved around the environment by picking up an object (represented by a gas canister). In addition, during two out of the five trials, participants had to perform a pointing task. The goal of that task was to point to one of the two moons while seeing only one of the landmarks.

After performing those learning trials, participants performed the stability rating. For each trial, participants had to move to a random location within the environment indicated by a blue circle on the ground. Upon reaching the circle, participants rotated to face one of the four landmarks. Then, a scale appeared in front of the participants, asking them to rate the landmark's stability. The scale ranged from one, completely unstable, to five, completely stable. After picking the answer, participants moved to another random location to rate the next landmark until all of them were rated once. For the participant to succeed in this checking task, they had to correctly identify stable landmarks as stable (i.e. rating 5) and unstable landmarks as unstable (i.e. rating 1 or 2). The rating for the unstable was decided to be either 1 or 2 since those landmarks would move only on half of the environment.

As the last step in this phase, participants performed a pointing task. Compared to the one done during the learning task, every landmark was visible simultaneously. The task asked the participants to move to a random location within the environment, indicated by a blue circle on the ground. Then, they needed to point to one of the two moons using their controller. The target moon was indicated by displaying its picture next to the controller. To complete this task, participants needed to point to the correct moon with an accuracy of 15° degrees for every trial. Participants performed six trials in total, with three pointing for each moon. If the participant succeeded in the stability rating

and the pointing task, they moved to the next phase of the experiment. However, if participants did not pass at least one task, they would perform another learning block composed of the same three tasks.

2.2.5 Criterion phase

After completing the learning phase, participants performed a last task on the desktop the same day. The environment was the same as in the learning phase and followed the same stability rules. This task aimed to ensure participants could transfer their knowledge and perception of the immersive VR environment experienced during the HMD to the one on desktop VR. The task was another pointing task where participants saw a single landmark in front of them, and they had to use a joystick to point to the location of the target moon. For each trial, participants had 1 second to see a picture of the target moon and the landmark they were facing. Then, they had up to 2.5 seconds to use the joystick to point to the correct position of the moon. Participants performed 24 trials, 6 trials per landmark, and they needed an accuracy of 40° to pass this phase. Only the trials related to the stable landmark were used to calculate the accuracy since participants could not know the position on the moon from an unstable position. If the participants could not succeed in this task, they would return to the learning phase to complete another block. If the participants succeeded, they completed the experiment's first day and came back the next day for the testing part.

2.2.6 Testing phase

On the second day, participants arrived at the MRI scanner to perform the testing phase. Upon arrival, we asked them to fill out a questionnaire asking for the stability rating,

similar to the learning phase, with the same scale. The goal was to ensure participants remembered the landmarks' stability before entering the scanner.

Before the main scanning phase, participants performed the training of the testing task (Figure 12). For each trial, participants saw one of the landmarks in front of them for 2 seconds. Then, they were passively moved toward it for 5 seconds. Finally, an inter-trial interval (ITI) with a fade in/fade out was presented for a mean of 3 seconds (ranging from 1 to 5 seconds). After the passive movement, a pointing trial similar to the criterion phase could happen. Indeed, participants could see only one of the landmarks in front of them and had to rotate to one of the moons using a joystick.

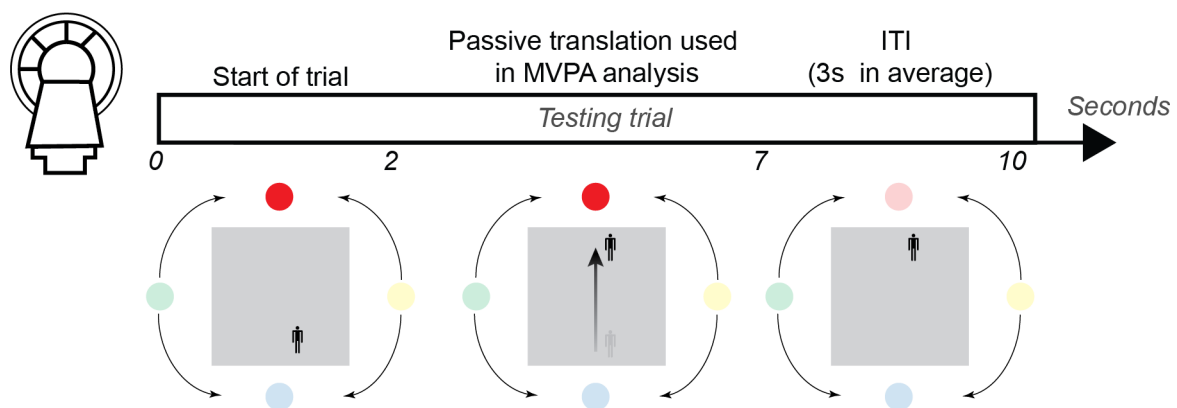


Figure 12: Design of a testing trial.

During the testing in the MRI scanner, participants performed multiple testing trials. Each trial started with a 2-second period where they could see a landmark in front of them. Next, participants were passively moved toward it for 5 seconds. Lastly, an ITI of 3 seconds on average with a fade-out screen would appear. Another trial would start afterwards.

For each scanning run, every landmark had ten regular trials and two pointing trials. Participants performed eight runs, so each direction was sampled 80 times. Finally, the trial sequence was optimised using de Bruijn sequence to enhance the analysis results (Aguirre et al., 2011). In brief, this optimisation improved the detection power for MVPA analysis by counter-balancing the order of directions across runs.

2.2.7 MRI data acquisition

The imaging data were acquired using a 3T SIEMENS Prisma scanner with a 64-channel phased array head coil. Several scans were included: a three-dimensional structural T1-weighted anatomical image with 1 mm isotropic resolution (voxel size = 1 mm; TR/TE/Inversion time = 2500/2.82/1100 ms; flip-angle = 7 degrees; FOV = 256 mm; 192 slices; MPRAGE sequence); a high resolution T2-weighted structural image including the EC and hippocampus was acquired perpendicular to the long axis of the hippocampus using a turbo-spin-echo sequence (voxel size = 2 mm; TR/TE = 6000/71 ms; FOV = 224 mm²; 64 slices); the gradient echo field maps (slice-thickness = 2 mm; TR/TE1/TE2 = 700/4.92/7.38 ms; flip-angle = 60 degrees; FOV = 220 mm²; 72 slices); eight runs with 260 volumes of T2*-weighted functional images were acquired with a partial-volume echo-planar imaging sequence (Figure 13), the image were first aligned with the long axis of the hippocampus but shifted by 7 slices to the superior part of the brain, this allowed the capture of more region of interest (ROI) such as the precuneus (slice thickness = 2 mm; TR/TE = 2000/30 ms; flip angle = 90 degrees; FOV = 216 mm²; 30 slices; GRAPPA acceleration factor 2). Finally, a single run of T2*-weighted functional with whole brain volume echo-planar imaging sequence was comprised, allowing for a more precise coregistration of functional and structural images (slice thickness = 2 mm; TR/TE = 4400/30 ms; flip angle = 90 degrees; FOV = 216 mm²; 70 slices; GRAPPA acceleration factor 2).

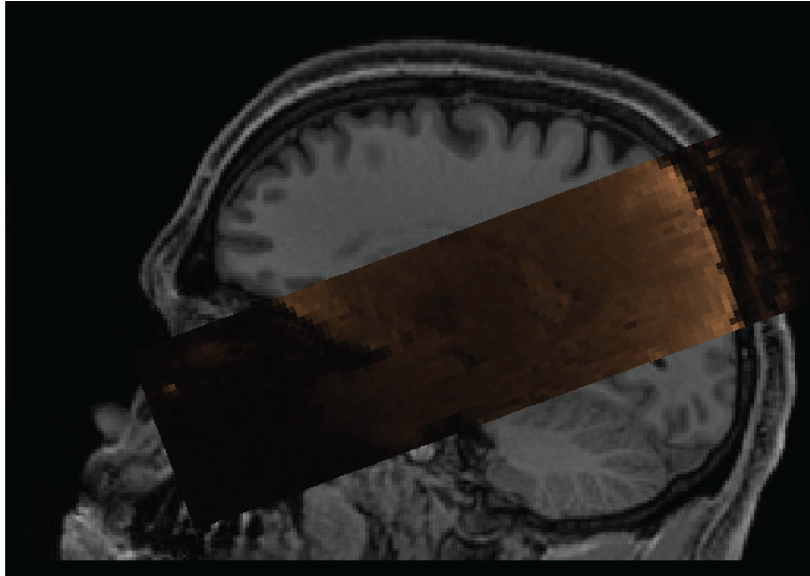


Figure 13: EPI slab of the brain.

EPI slab of the brain (orange) used in the neuroimaging analysis overlay on top of the structural T1 image (grey).

2.2.8 Behavioural analysis

Data reduction relied on Python (version: 3.7.4) and statistical analysis on R (version: 4.1.3). First, we computed the stability rating for each learning block and the number of total blocks done. In addition, we determined the number of learning blocks done after rating the stability correctly. Finally, the time spent in VR when participants used the HMD was extracted from the learning data.

Furthermore, the pointing accuracy during the checking task was used to examine the error distribution over learning blocks. We calculated it by taking the absolute angular error computed between the target's correct position and the participant's answer. Even more, for each pointing trial, we calculated the percentage of time within a trial when the participant was facing one of the landmarks. To do so, we checked if the landmark was in the centre field of view of the participant $\pm 20^\circ$ and then counted for how many seconds the heading of the participant was within that range. In addition, we added a

separate variable to mark if the unstable landmark was located between the position of the moon and the stable landmark associated. The statistical analysis relied on repeated measures ANOVAs and Spearman correlations.

Lastly, we extracted the pointing accuracy from each participant during the criterion phase. Then, the circular mean and standard deviation were calculated for each landmark's last learning block (i.e., the last successful block). The same data reduction was done for the pointing trial completed during the testing phase on the second day. The statistical analysis used repeated measures ANOVAs and paired t-tests.

2.2.9 fMRI data preprocessing

The preprocessing was done using FSL (version 5.0.9), ANTs (version 3.0.0) and Python 3 (version 3.7.4) with the main packages nipy (version 1.2.2) and Nilearn (version 0.10.1). We created the whole preprocessing pipeline with nipy, including multiple steps, which we described below.

First, the anatomical scans were bias-field corrected three times using ANTs to increase the contrast in the image. We used a FSL function to remove part of the neck if its proportion was too high. Then, the images were skullstripped using the BET function from FSL with individual parameters for each participant to achieve the best results. In addition, the structural image was normalised to the Montreal neurological institute (MNI) standard image 1mm using non-linear registration from the ANTs suite.

Second, the magnitude fieldmap was skullstripped using BET with individual parameters and eroded by five voxels to remove any skull leftovers. Then, we used a FSL function to transform the phase and magnitude fieldmap to a single image with the correct units (rad/s).

Third, the eight runs of EPIs (annotated EPIslab for simplicity here) were all concatenated together to find the mean image. Next, each run was motion-corrected by realigning the EPIslab to the mean image. Six motion parameters (the three translations and three rotations around the x, y and z axis) were extracted and stored for the main analysis. Similarly, for the single EPI run covering the whole head (annotated EPlwb), the mean image was extracted and used for motion correction for the EPlwb volumes.

Fourth, the mean image of the EPlwb was registered to the structural image and the prepared fieldmap was included for warping correction. Then, a second registration was done between the mean image of the EPIslab and the EPlwb unwarped. This registration allowed the unwarping of the EPIslab.

Finally, we smoothed the EPIslab data with a 4mm Gaussian kernel. An additional step was done to account for voxels at the edge of the brain being smooth within the data, incorrectly decreasing those values. To correct the brain mask, we smoothed it with the same 4mm kernel and divided it from the EPIslab data to account for voxels with values of 0.

2.2.10 Brain masks

The individual structural images were segmented using Freesurfer (version 6), and the precuneus, EC, and RSC (defined as the posterior ventral cingulate cortex) were extracted using the 'Destrieux' cortical atlas (Destrieux et al., 2010). We also extracted a mask of the ventricles containing the cerebrospinal fluid (CSF) and a white matter mask using the 'Desikan-Killiany' atlas (Desikan et al., 2006). The hippocampus and thalamus masks were extracted using FSL first, which has been shown to segment those regions better (Patenaude et al., 2011). The primary Visual

cortex (V1) mask was taken from the MNI brain template using the ‘Juelich’ Histological Atlas and was subsequently thresholded at 50%. Next, the affine matrices calculated during the preprocessing were used to warp the masks from the MNI space to the structural image space. Finally, all the masks were warped from the structural space to the EPIslab space to be included in the analysis (Table 2.1).

Name of the mask	Software used	Neuroimaging space used	Encyclopedia used
Retrosplenial cortex (RSC)	freesurfer	Individual space	‘Destrieux’ cortical atlas
Entorhinal cortex (EC)	freesurfer	Individual space	‘Destrieux’ cortical atlas
Precuneus	freesurfer	Individual space	‘Destrieux’ cortical atlas
Thalamus	fslfirst	Individual space	FSL first
Hippocampus	fslfirst	Individual space	FSL first
Cerebrospinal fluid (CSF)	fsl space	MNI	‘Juelich’ Histological Atlas
Primary visual cortex (V1)	freesurfer	Individual space	‘Desikan-Killiany’ atlas
White Matter	freesurfer	Individual space space	‘Desikan-Killiany’ atlas

Table 2.1: Brain masks defining the ROIs used in the analysis

2.2.11 fMRI analysis

Analysis of the fMRI was done in both univariate and multivariate ways. For univariate, we achieved a ROI and a whole brain analysis. Specifically, those

analyses tried to compare the BOLD signal between stable vs unstable landmarks. For the ROIs, a GLM was constructed for each run and then combined using a fixed-effects model. The design matrix of the GLM included two main regressors of interest. Specifically, they were created by taking the five seconds translation periods when participants were going either towards stable landmarks (North or South) or unstable landmarks (West or East). We included another regressor taking the period during which participants performed the pointing trial. Then, the time derivative of those regressors was calculated. In addition, multiple noise regressors were included, such as the six motion parameters and “physiological noise” (Behzadi et al., 2007). The latter was computed by taking the signal from the white matter and CSF of the participant on each run and including it on a principal component analysis (PCA). Next, we used a broken stick method (Jackson, 1993) to determine the number of principal components to select for each participant. An example of the design matrix can be found in Figure 14. We ran a contrast comparing if the signal was higher for stable compared to unstable landmarks. The individual t-stat maps were averaged and compared to 0 to check for a significant difference between the two conditions. The same GLM was computed for every run and combined using the fixed effect for the whole brain analysis. Next, a second-level analysis was run with a random effect to account for the participants. Finally, the resulting z-score map was thresholded at $Z > 2.3$, and a cluster extent of $p < 0.05$ was applied to identify continuous clusters and to control for family-wise error (FWE) rate.

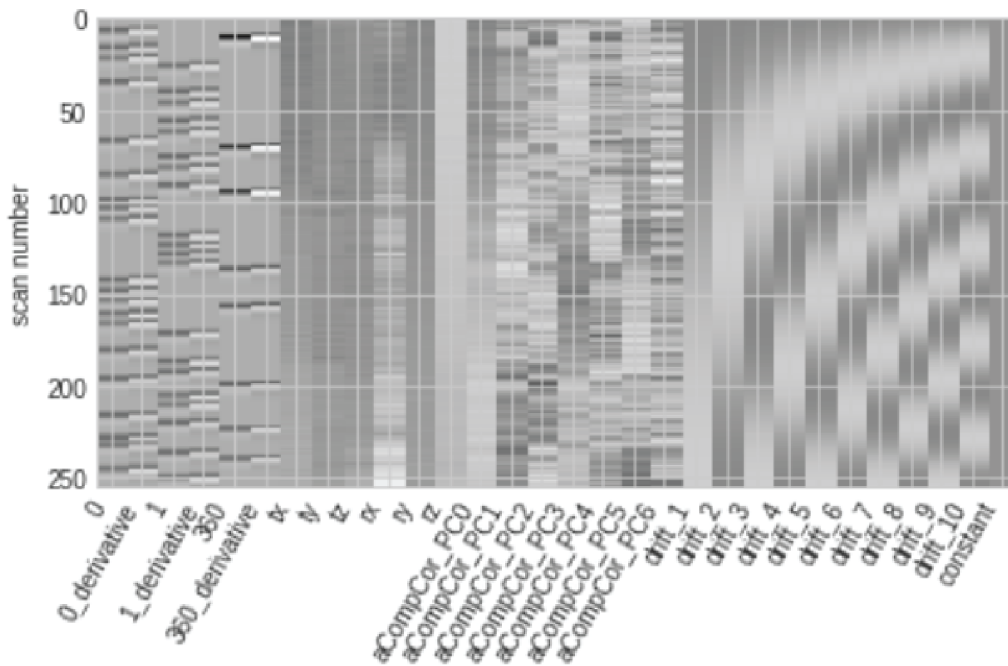


Figure 14: Example of a design matrix created for univariate analysis and run-wise decoding.

Additionally, we implemented a multivariate pattern analysis (MVPA) with two separate types of decoding: run-wise and trial-wise (Figure 15). The run-wise MVPA was performed to decode the brain signal for stable vs unstable landmarks, similar to the univariate analysis within each ROI. We decided to use run-wise decoding as the literature showed it gave better stability of decoding accuracy across cross-validation (Allefeld and Haynes, 2014). The first step was to acquire t-stat brain maps using the same GLM as the univariate but without computing a fixed effect across the GLM. We extracted individual t-stat maps for each run and each condition (stable or unstable), leading to 16 maps separated between the eight runs. Then, a classifier was used to separate the runs between training (7 runs) and test (1 run) sets. In the training set, the data were first standardised, and a feature selection was run to include only a percentage of the most responsive voxels within the ROI. Next, we computed a linear support vector machine (SVM) to differentiate between the two conditions of interest.

In order to optimise the model, a grid search was executed to have different combinations of the C parameter for the SVM (controlling the steepness of the curve separating the condition) and the percentage of selected voxels. The C parameters ranged from 0.001 to 1000 with multiples of 10, and the percentile used were 25, 50 and 100%. The training set was further divided into the proper training set (6 runs) and a validation set (1 run). Every combination of parameters was tested to find the best pair of parameters used to calculate the decoding accuracy in the leftover testing set. Cross-validation was performed, so every run was used as the testing set. This led to calculating eight decoding accuracies that were subsequently averaged for each participant. To test for statistical significance, simple t-tests were computed to compare the average decoding accuracy of participants against chance level (0.5). The choice to not perform permutations was motivated by the limited number of possible unique permutations (128), leading to a really low statistical power.

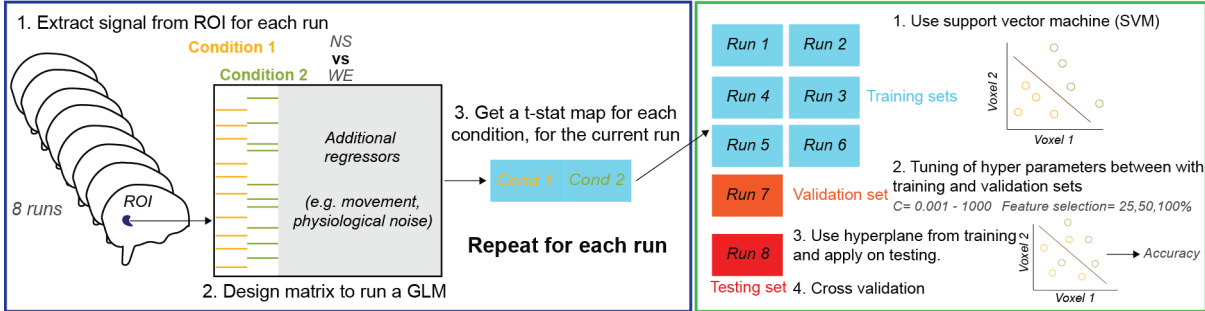


Figure 15: MVPA analysis for run-wise and trial-wise decoding.

On the left, the blue box shows the steps to extract t-stat maps from the brain signal in each ROI. The example given is for run-wise decoding. For trial-wise decoding, the design matrix would be different, but the output would still result in t-stat maps for the conditions for each run. On the right, the green box presents the steps to obtain the decoding accuracy.

The trial-wise MVPA aimed to decode the neural signal between two conditions: North vs South or West vs East. We used trial-wise analysis to decode directions as we could include ten times more samples in the MVPA than run-wise, increasing the detection power. Indeed, the main difference compared to the run-wise was the computation

of the regressors of interest in the GLM. We modelled each trial separately, meaning that the first regressor included only the trial of interest (e.g. the first trial when moving toward North), the second regressor included the other trials of interest (all the other trials when moving toward North or South) and finally the third regressors included the other trials not included in the MVPA (e.g. trials toward West and East) as shown in Figure 16. This led to the creation of 20 t-stat maps per run. Next, we calculated the decoding accuracy between the two conditions in the same way as the run-wise MVPA described above (Figure 15). Statistical significance was assessed by comparing the average decoding accuracy of the participants to a null distribution. The null distribution was created by calculating 1000 random permutations by shuffling the correct labels during the training of the model.

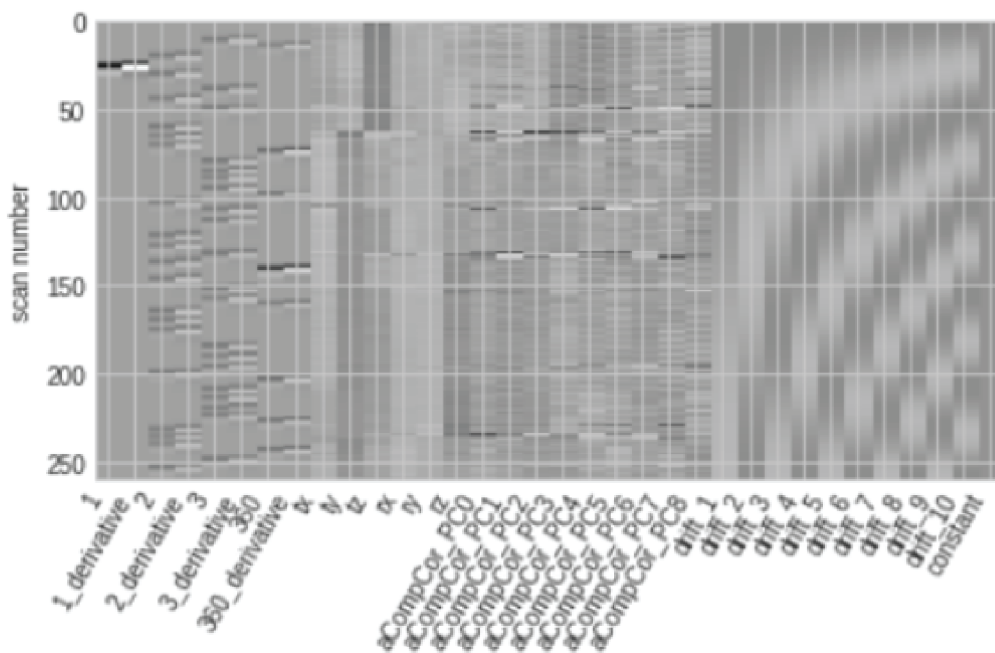


Figure 16: Example of a design matrix created for trial-wise decoding.

Finally, a last analysis was calculated to investigate if there was a similarity in the signal when moving in the same direction. The goal was to check the brain signal's stability when passively moving toward the same landmark. For example, highly correlated

signals would be linked to the brain signal repeating itself as the participant moved in the same direction. On the contrary, uncorrelated data could be due to the brain signal changing directions every time, similar to unstable landmarks. To test those hypotheses, we extracted the t-stat maps for individual trials across the four directions, similar to the trial-wise decoding. Then, a correlation matrix was computed between the trials going in the same direction, resulting in 45 unique correlations for each run and direction. Lastly, those values were entered into a linear mixed-effect model that comprised a nested random effect between participants and runs. The model was run using R (version: 4.1.3) with the packages nlme (version: 3.1) and investigated for each ROI if there was a difference between stable and unstable landmarks.

2.3 Results

Participants learned and memorised the stability of each landmark across the experiment.

Every participant successfully completed the learning phase within the limit of 25 learning blocks (Figure 17A). However, the number of learning blocks done to finish the task (mean=12; std=5.03) and the time spent in immersive VR (mean=85.68; std=45.68) varied across participants. Similarly, the number of learning blocks done before participants learned the stability of the four landmarks (mean=4.73; std=3.30) differed. Indeed, some participants took longer to learn the stability of the landmarks (Figure 17A), while others took longer to succeed in the pointing task by reaching the correct threshold (15°, red line in Figure 17C).

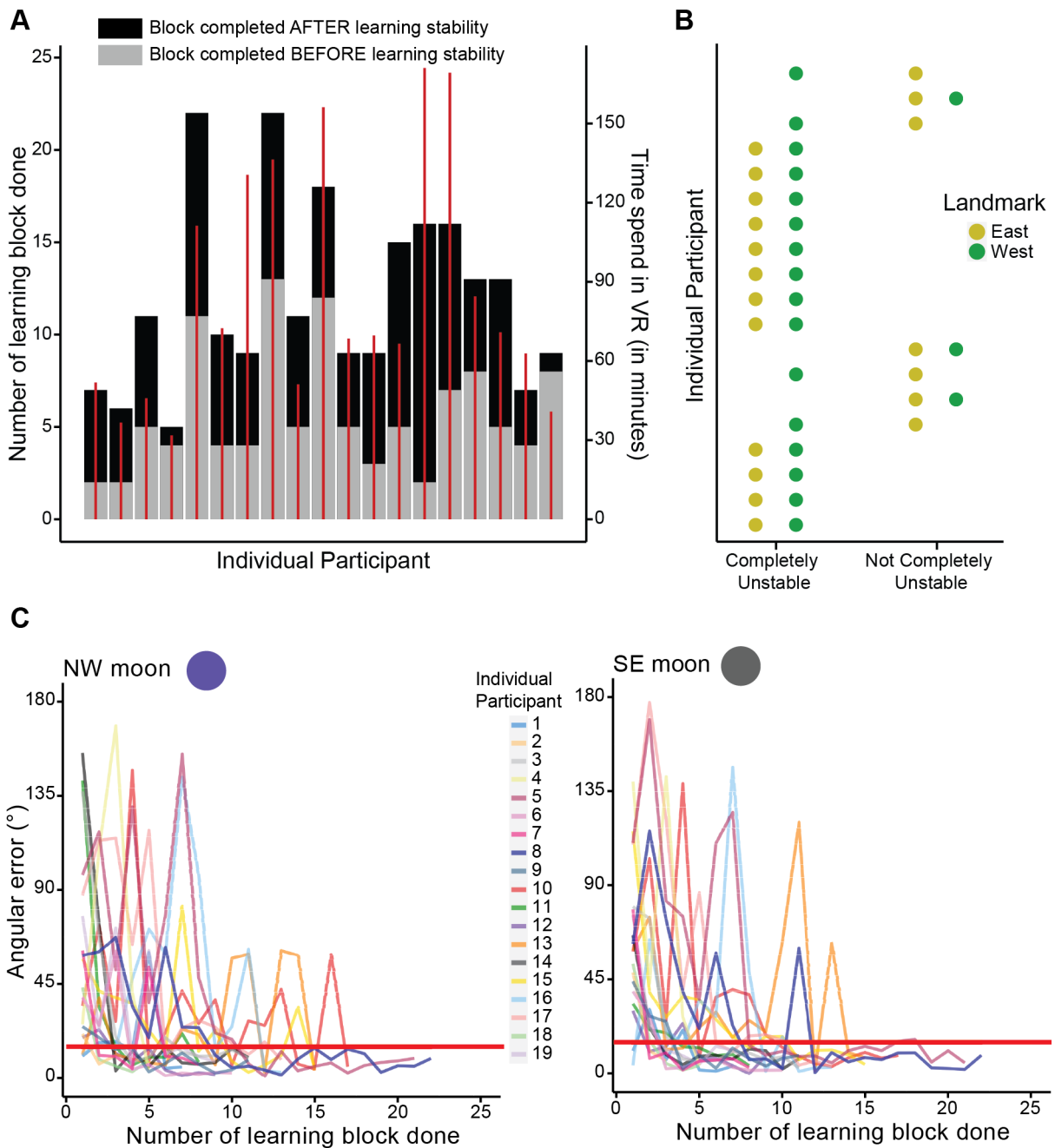


Figure 17: Learning results from participants.

A, number of learning blocks (bars) and time spent in VR (red line) for each participant. Grey bars represent the blocks done before learning the stability of landmarks. Black bars represent the blocks done after learning the stability of landmarks. *B*, final rating of individual participants regarding the two unstable landmarks West (green) and East (yellow). *C*, average angular error of participants during the pointing task in the learning phase when pointing to the North West moon (left) or South East moon (right). The red line represents the learning threshold of 15°.

The majority (63%) of participants rated both unstable landmarks as completely unstable (1 out of 5 on the scale) (Figure 17B). Nevertheless, 4 participants thought

the East landmark was less unstable than the West landmark. Also, 3 participants rated East and West landmarks as “not completely unstable” (2 on the scale). Interestingly, the West landmark was never rated as “not completely unstable” unless participants rated both landmarks as 2 on the scale. Finally, participants repeated the same answers when rating the landmarks again on the 2nd day for the testing in the fMRI.

Participants learned the position of the moons in immersive VR in relation to their associated landmarks.

During the pointing task in immersive VR, participants could see the four landmarks at the same time. To determine if they used more stable than unstable landmarks to point to the moons, the percentage of time that participants faced each of the landmarks was calculated during the last successful learning block (Figure 18). An ANOVA suggested a main effect of landmarks for both the North-West (NW) moon ($F(3,54)=12.04$; $p<0.001$) and the South-East (SE) moon ($F(3,54)=6.03$; $p=0.001$). However, the unstable landmarks could be positioned between the stable landmarks and the position of the moons. Therefore, those trials would have an inflated time for the facing direction of the unstable landmark even if the participant does not necessarily try to face those. To measure the impact of those trials, they were discarded and another ANOVA was calculated. We found no main effect of landmarks for the NW moon ($F(3,51)=1.873$; $p=0.15$) or the SE moon ($F(3,48)=0.62$; $p=0.61$). Nevertheless, at the individual level, some participants had an increase in the facing time related to stable landmarks across the task (Figure 19).

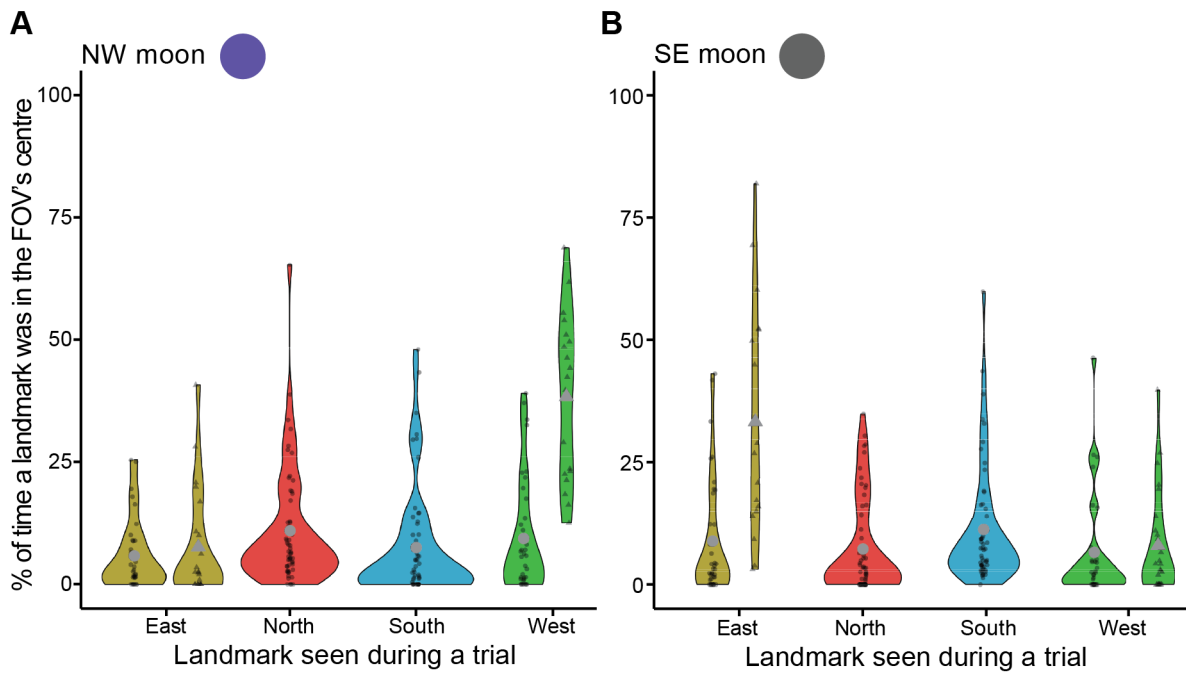


Figure 18: Percentage of time a landmark was seen by a participant during a pointing trial.

Pointing trial results during the learning phase for the North West moon (A) and South East moon (B). Violin plots show the distribution of the percentage of time a stable (North in red, South in Blue) or an unstable landmark (West in green, East in yellow) was in the FOV's centre. Individual data points are shown in black, and participant means in grey. Triangles represent trials where the unstable landmark was between the moon and the associated landmark.

Finally, Spearman correlations were computed between the facing time for each landmark versus the absolute angular error across every trial and participant. Hence, a positive correlation was found for South ($R=0.26$; $p<0.001$) and East ($R=0.18$; $p<0.001$) landmarks when pointing to the NW moon. Similarly, a positive correlation was also found for the North ($R=0.19$; $p<0.001$) and West ($R=0.16$; $p<0.001$) landmarks for the SE moon. This result would suggest that across the pool of subjects, they performed worst when facing non-associated landmarks (stable or unstable) for each moon.

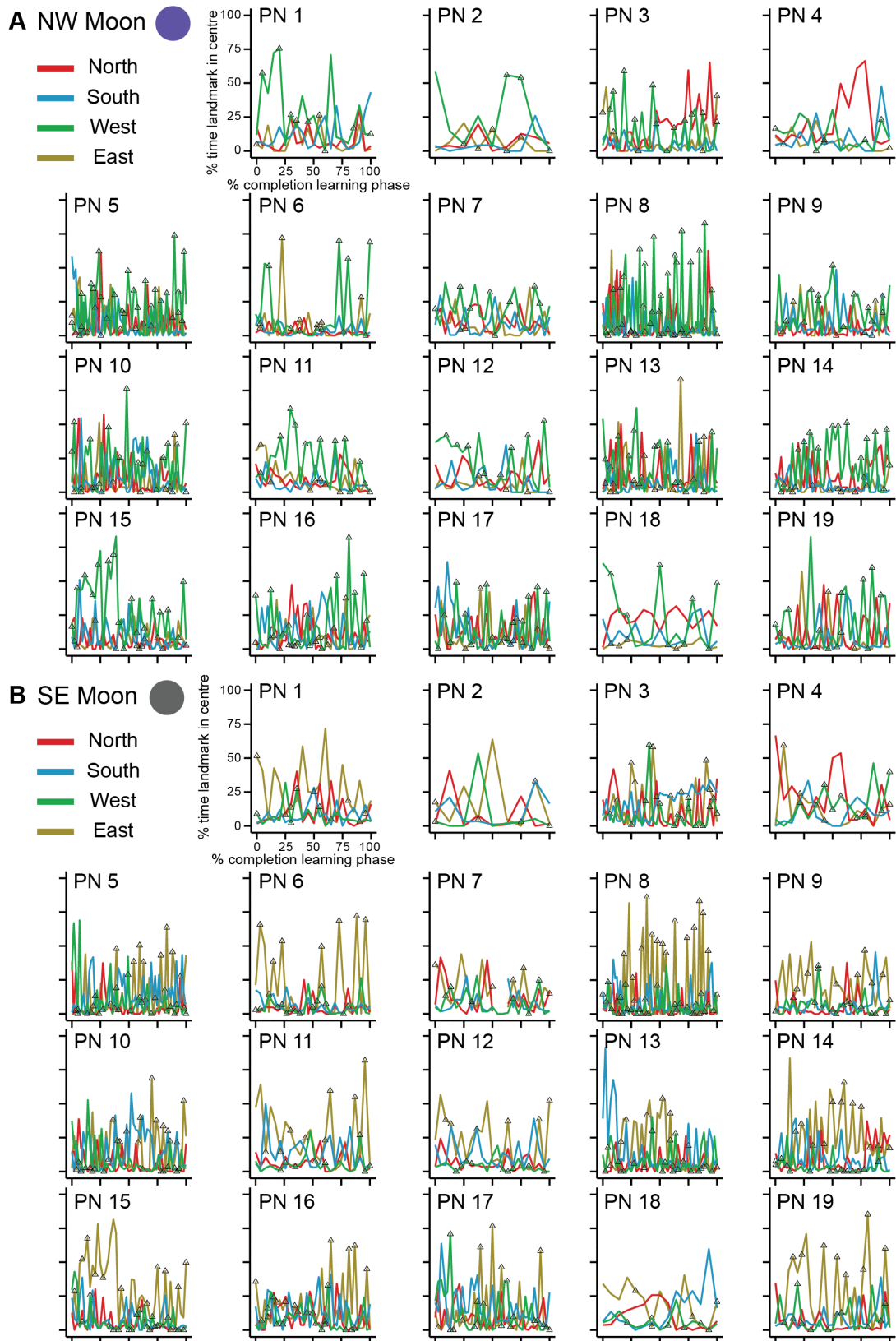


Figure 19: Percentage of time a landmark was seen during a pointing trial across the learning phase for each individual participant.

Detail on the next page

Figure 19: *Pointing trial results during the learning phase for the North West moon (A) and South East moon (B). Colour lines represents the percentage of time a stable (North in red, South in Blue) or an unstable landmark (West in green, East in yellow) was in the FOV's centre across the learning blocks performed by each participant. Triangles represent trials where the unstable landmark was between the moon and the associated landmark.*

Participants used different pointing strategies when seeing a single landmark.

Compared to the pointing done in immersive VR, participants could only see a single landmark at a time in the desktop version (criterion and testing phase). The pointing toward stable landmarks was within $\pm 30^\circ$ around the correct position of the moon as the learning threshold was set to 40° (Figure 20). Interestingly, the task design allowed the participant to point to any direction desired when looking at an unstable landmark. This led to the participants adopting different strategies to answer (Figure 21). We assessed the spread in the response by calculating the circular standard deviation of the pointing direction across trials for each landmark (Figure 20). An ANOVA found a main effect of the circular standard deviation across landmarks for criterion ($F(3,54)=5.70$; $p=0.002$) and testing ($F(3,54)=4.49$; $p=0.005$). For the criterion phase, additional paired t-tests found a significant difference between East and North ($t(19)=-2.64$; $p=0.017$), East and South ($t(19)=-3.09$; $p=0.006$), West and North ($t(19)=-2.44$; $p=0.025$) and West and South ($t(19)=-2.80$; $p=0.012$). For the testing phase, paired t-tests found a significant difference between East and North ($t(19)=-2.48$; $p=0.023$), West and North ($t(19)=-3.40$; $p=0.003$) and West and South ($t(19)=-2.10$; $p=0.05$). However, when using Bonferroni correction to account for multiple comparisons, only East and South during criterion ($t(19)=-3.09$; $p_{\text{adj}}=0.038$) and between North and West during testing ($t(19)=3.40$; $p_{\text{adj}}=0.019$) survived.

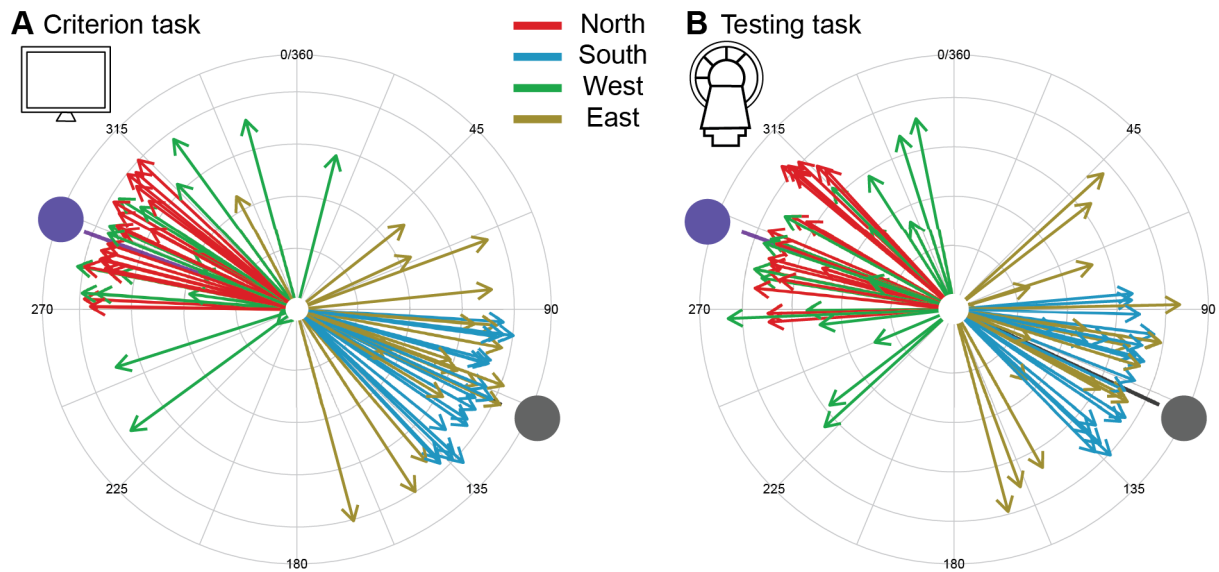
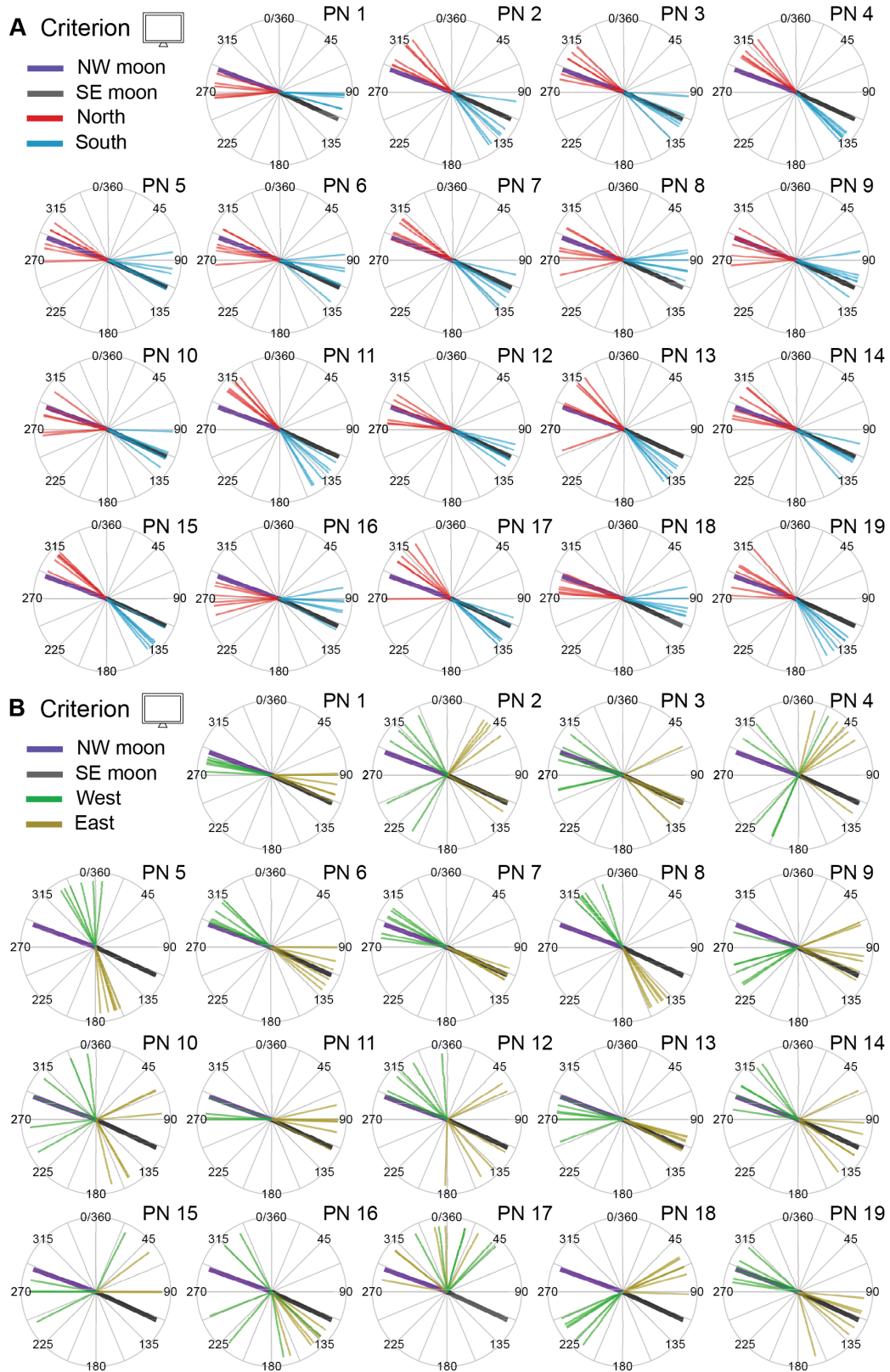


Figure 20: Average pointing answer to the moons for participants during the criterion and testing tasks for each landmark.

Each arrow represents the average pointing answer of a participant when they saw the North (red), South (blue), West (green) or East (yellow) landmark. The length of the arrow represents the inverse circular standard deviation with a shorter length describing a larger standard deviation (i.e. larger spread of answers). Participants had to point to the NW moon (purple) when they saw the North and West landmark, and to the SE moon (grey) when they saw the South and East.

Furthermore, a visual inspection of the individual plots suggested different strategies employed by participants regarding the unstable landmarks (Figure 21). The first would be associated with a large spread of answers, such as participant 2, 9 or 16. The second one would be linked to clustered answers aligned with the correct position of the moon, such as participant 1, 7 or 19. Finally, the third strategy also had clustered answers but pointed to another location within the environment, such as participant 4, 8 or 18.



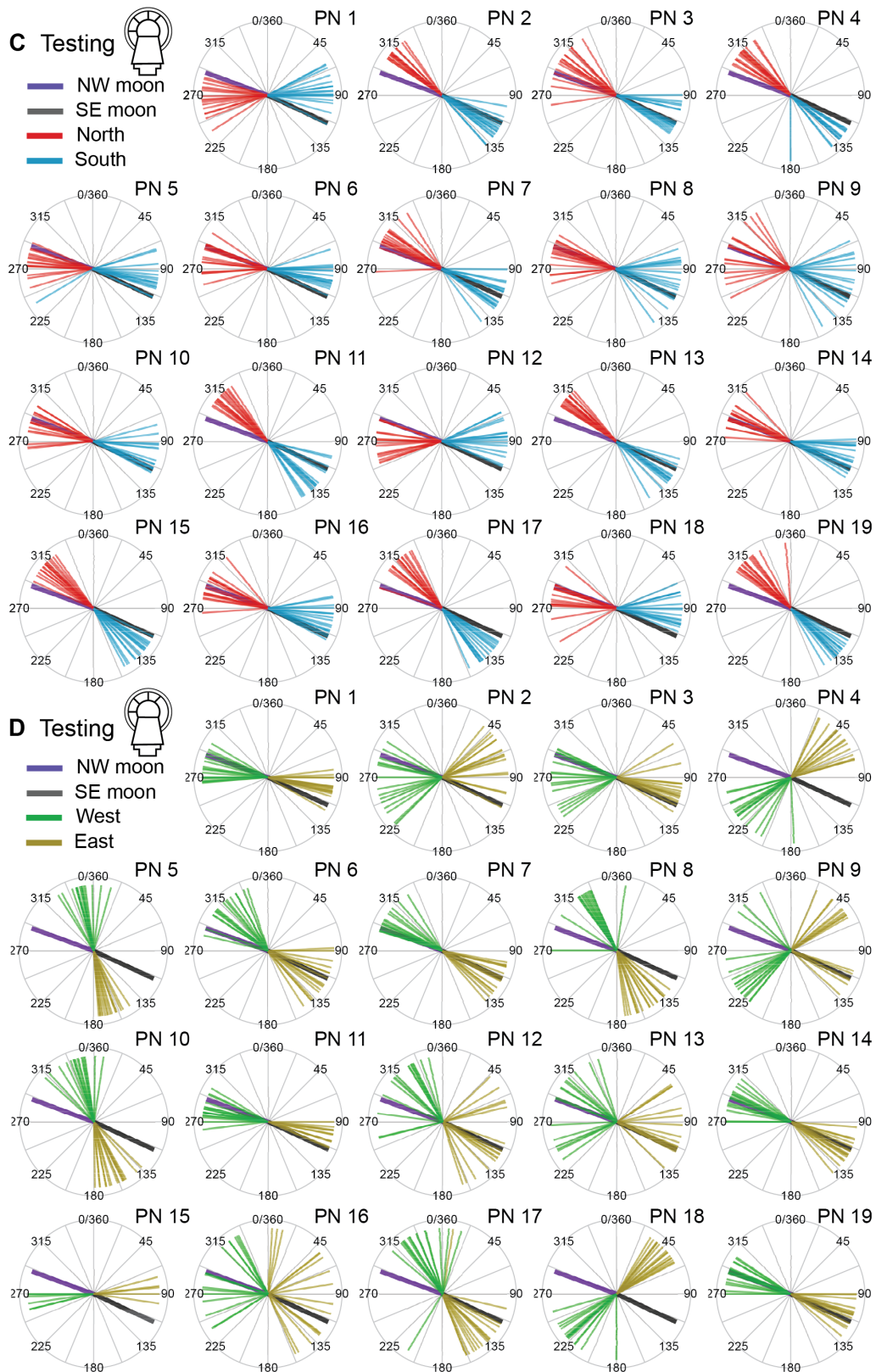


Figure 21: Pointing answer to the moons during the criterion task and testing phase for each individual participant.

Detail on next page.

Figure 21: *Each line represents a pointing answer of a participant when they saw the North (red), South (blue), West (green) or East (yellow) landmark. Participants had to point to the NW moon (purple) when they saw the North and West landmark and to the SE moon (grey) when they saw the South and East. A-B, the data shown are from the criterion block from the last learning block performed. C-D, the data shown correspond to all the pointing trials participants performed across scanning runs.*

Decoding of signal differentiating stable and unstable landmarks.

We assessed whether there was a signal related to the stability of landmarks associated with heading direction (Figure 22). A MVPA was computed to the signal when participants were moved toward stable (North and South) compared to unstable (West and East) landmarks. We found significant decoding above chance level (0.5) in the RSC ($t(18)=3.02$ $p=0.007$), precuneus ($t(18)=2.28$ $p=0.035$) and V1 ($t(18)=2.8$ $p=0.011$). To test if this effect was indeed linked to stability, the landmarks were mixed (e.g. North and West vs South and East; North and East vs South and West), so both stable and unstable landmarks were included in each condition. We found no significant decoding after running another MVPA on those mixed stability conditions. Finally, our ROIs and whole-brain univariate analysis did not find significant differences between signals related to stable and unstable landmarks.

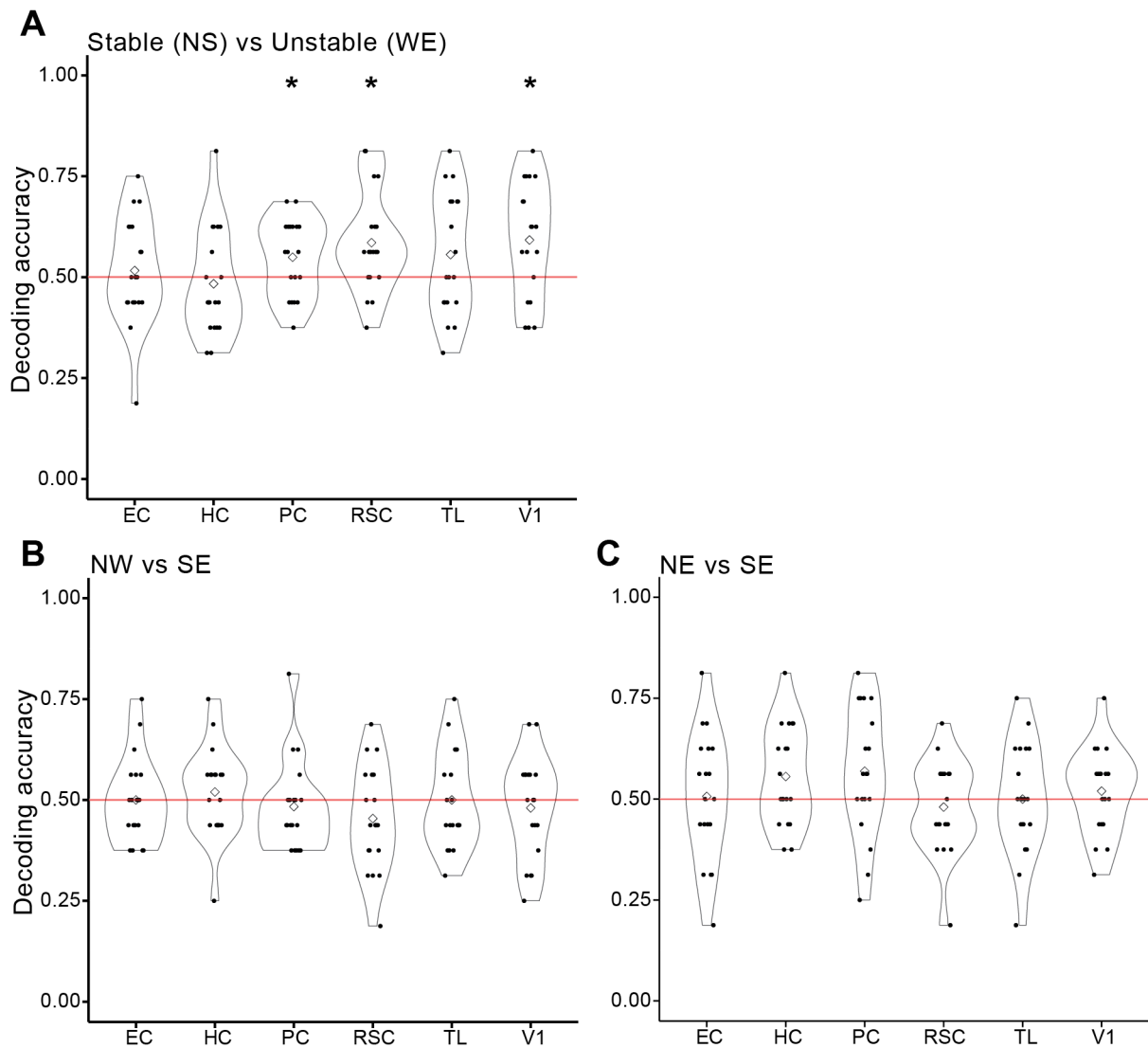


Figure 22: Decoding results for stable vs unstable landmarks and control conditions.

Decoding results when comparing (A) stable vs unstable landmarks or (B,C) a mix of stable and unstable landmarks for each ROI. The dots represent the average decoding accuracy for the individual participants, and the diamond is the average among participants. The red line corresponds to the chance-level at 0.5. EC, entorhinal cortex; HC, hippocampus; PC, precuneus; RSC, retrosplenial cortex; TL, thalamus; V1, primary visual cortex. * denotes significant decoding ($p < 0.05$).

Decoding of HD signal differentiating stable and unstable landmarks.

In addition, we investigated if we could find HD signals in the different ROIs associated with the HD system and if the stability of landmarks impacted the decoding. We examined the decoding accuracy of North vs South (stable landmarks) and West vs East (unstable landmarks). Then, we derived the associated p-value from a null distribution generated via 1000 permutations of the condition labels (Figure 23). For North vs South, we found significant decoding in the RSC ($p < 0.001$) and V1 ($p = 0.022$) but not in thalamus ($p = 0.25$), hippocampus ($p = 0.071$), EC ($p = 0.064$) or precuneus ($p = 0.26$). For West vs East, significant decoding was found in the thalamus ($p = 0.01$), hippocampus ($p = 0.005$) and EC ($p = 0.04$) but not in RSC ($p = 0.44$), precuneus ($p = 0.351$) and V1 ($p = 0.741$).

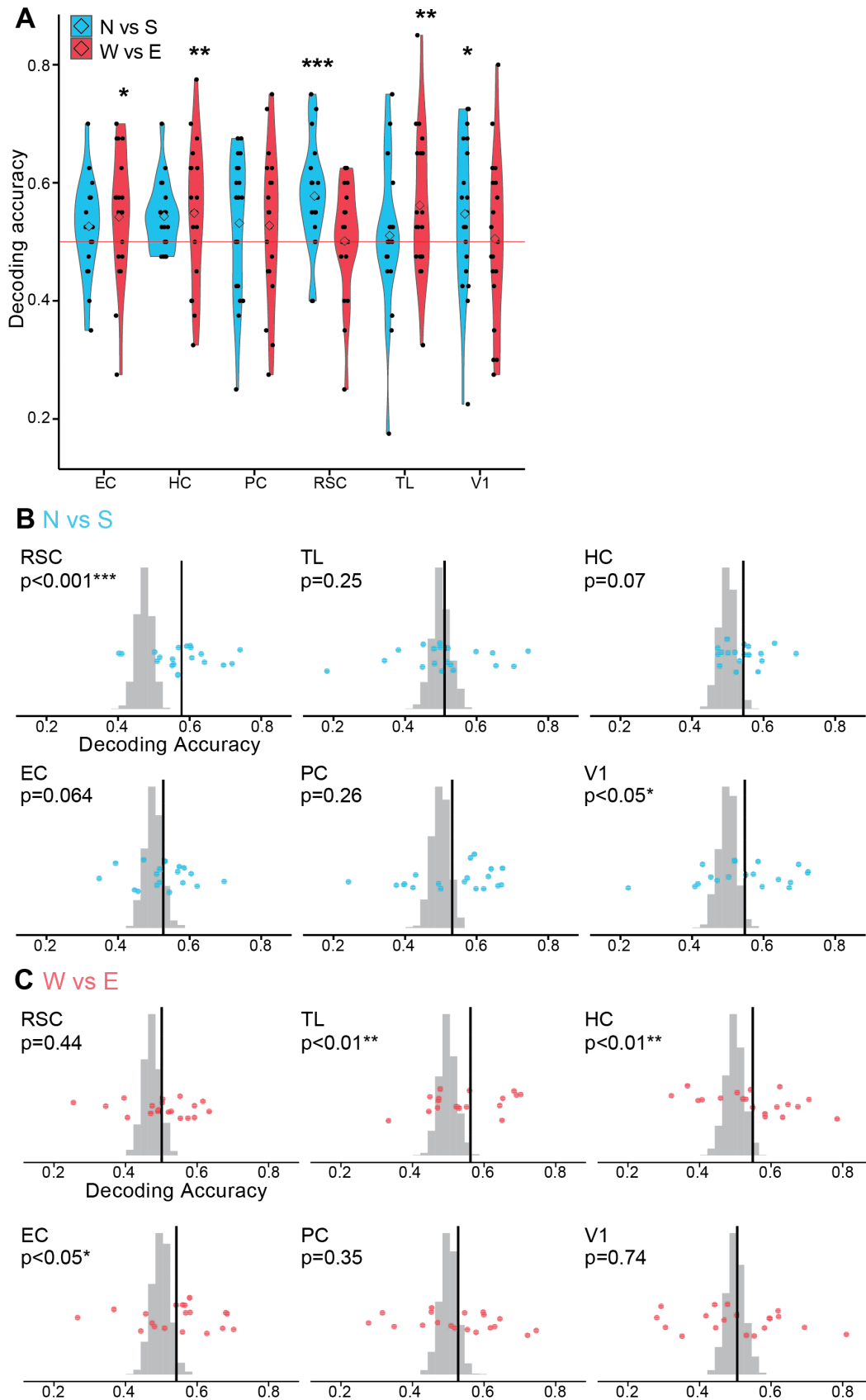


Figure 23: Decoding results for North vs South (Stable) and West vs East (Unstable) for the ROIs.

Detail on next page.

Figure 23: A, decoding results when comparing North vs South (blue) and West vs East (red). The dots represent individual data, and the diamond is the average among participants. The red line corresponds to the chance-level at 0.5. The null distribution from permutations (grey bars) can be seen for (B) North vs South and (C) West vs East. The dots also represent individual data and the vertical black line is the average among participants. EC, entorhinal cortex; HC, hippocampus; PC, precuneus; RSC, retrosplenial cortex; TL, thalamus; V1, primary visual cortex. * $p < 0.05$; ** $p < 0.01$, *** $p < 0.001$.

Furthermore, we segmented the thalamus and the hippocampus to extract the presubiculum, a critical region within the HD circuit, to decode the HD signal (Figure 24). For the presubiculum, we observed significant decoding for North vs South ($p=0.002$) and West vs East ($p=0.035$). For the segmentation of the thalamus, we did not find significant decoding for North vs West in the anterior thalamus ($p=0.07$), lateral thalamus ($p=0.507$), medial thalamus ($p=0.191$) and posterior thalamus ($p=0.834$). For West vs East, we found significant decoding in the posterior thalamus ($p=0.003$) but not in the anterior ($p=0.148$), lateral ($p=0.161$) and medial ($p=0.40$) thalamus.

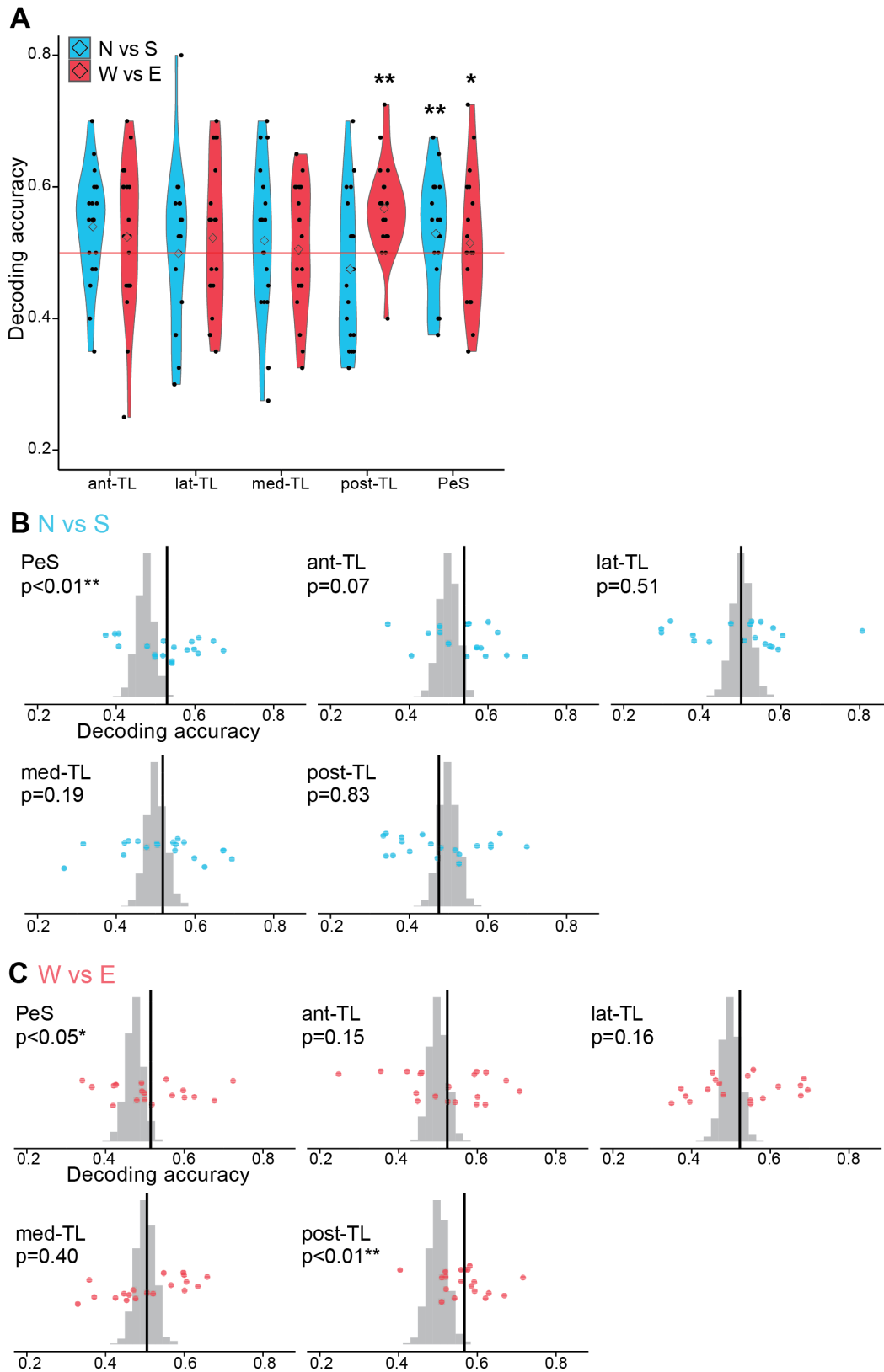


Figure 24: Decoding results for North vs South (Stable) and West vs East (Unstable) for the segmented ROIs

Detail on next page.

Figure 24: A, decoding results when comparing North vs South (blue) and West vs East (red). The dots represent individual data, and the diamond is the average among participants. The red line corresponds to the chance-level at 0.5. The null distribution from permutations (grey bars) can be seen for (B) North vs South and (C) West vs East. The dots also represent individual data and the vertical black line is the average among participants. PeS, presubiculum; ant-TL, anterior thalamus; lat-TL, lateral thalamus; med-TL, medial thalamus; post-TL, posterior thalamus. * $p < 0.05$; ** $p < 0.01$.

Finally, a last analysis investigated if the signal was consistent across trials when participants moved in the same direction. This analysis could tell us if the HD signal, an approximation of the tuning curve, would stay the same for stable landmarks, i.e. high correlation values, or change for unstable landmarks, i.e. uncorrelated values. We calculated correlation matrices between the t-stat maps related to trials moving in the same direction for each run. Then, we entered all the matrices for each participant and directions within a random mixed-effect model. The goal was to assess if the stability of the landmarks for each ROI could explain the correlation results. However, we found no significant difference between stable vs unstable landmarks for EC ($t(27207)=0.59$; $p=0.55$), hippocampus ($t(27207)=0.08$; $p=0.94$), precuneus ($t(27207)=-0.49$; $p=0.62$), RSC ($t(27207)=0.56$; $p=0.57$), thalamus ($t(27207)=-0.52$; $p=0.60$) or V1 ($t(27207)=-1.37$; $p=0.17$).

2.4 Discussion

In the present study, we found evidence for stability coding in RSC, precuneus and V1 when comparing stable vs unstable landmarks. These results are in line with previous findings from the literature (Auger et al., 2012; Auger and Maguire, 2013; Auger et al., 2015, 2017; Auger and Maguire, 2018b) that found permanence coding of landmarks in the RSC. However, our paradigm linked the landmarks with directional information compared to those studies. This allowed the analysis to decode HD signals when

participants were moved toward stable or unstable landmarks. We found that the RSC and V1 could decode the HD signal when moving toward stable landmarks but not for unstable landmarks. These results replicated the ones from both rodent studies (Knierim et al., 1995; Cho and Sharp, 2001; Jacob et al., 2017) and human studies (Marchette et al., 2014; Shine et al., 2016; Koch et al., 2020) that found HD signal in the RSC. The HD signal found in V1 was similar to the finding from Koch et al. (2020), which found significant decoding accuracy of walking direction in the early visual cortex. Nevertheless, those regions could not decode HD signals related to unstable landmarks. One explanation could be that RSC and V1 are thought to rely almost exclusively on visual inputs (Tong, 2003; Alexander et al., 2023). Indeed, participants might be unable to differentiate their heading when moving toward unstable landmarks precisely. It would make decoding more difficult as the extracted brain signal would differ for the unstable landmark. Even more, a recent computational model developed by (Yan et al., 2021) investigated how visual information, such as landmarks, could be included in the HD system. In their study, the authors manipulated the environment by changing the position of landmarks. They found that the HD signal associated with unstable cues could be disconnected from the RSC if they were treated as not salient or did not give information.

In addition, HD signals related to unstable landmarks were found in the thalamus, hippocampus and EC. Those three regions also have been found in previous findings to be related to HD signals in rodents (Ranck, 1984; Taube et al., 1990a; Taube, 1995; Stackman and Taube, 1998; Sargolini et al., 2006) and human studies (Chadwick et al., 2015; Shine et al., 2016). Surprisingly, we found no HD signal when comparing directions related to stable landmarks. One hypothesis is that the thalamus could decode this HD signal using the recapitulation of body-based cues from the learning phase while they were in immersive VR, also suggested by Shine et al. (2016). Then,

this signal would be sent to the next part of the HD hierarchical pathway (i.e. from the thalamus to the hippocampus and to the EC (Taube, 2007)). Moreover, we segmented the hippocampus and found that the presubiculum could decode both directions when moving towards stable or unstable landmarks. This result could be evidence that the signal from the RSC (coding for the stable landmark) and the thalamus (coding for the unstable landmark) would merge in this region. This would align with the current state of the literature describing the structure and connection within the HD system (Taube, 2007; Clark and Taube, 2012).

Another important question of the study is whether or not the instability of the landmark influences the HD signal itself. Our results suggest that HD signals related to unstable landmarks are still integrated within the HD circuit, especially in the end part of the circuit, such as the presubiculum. Since our participants learned that the position of the unstable landmarks moved in different orientations, we can hypothesise that the tuning curve associated with the landmark would also move. This would suggest that the PFD associated with the landmark would switch, but the width of the tuning curve would remain the same. To test this hypothesis, we investigated if correlations between the brain signals when passively moved toward the same landmark are related to its stability. If there is a higher correlation in the signal for stable compared to unstable, it could be seen as an approximation that the signal is more similar for stable landmarks, meaning the PFD would not change. In contrast, the signal and the PFD would vary across trials due to direction changes for the unstable landmarks. However, we found no difference in the correlations between stable and unstable. Hence, another hypothesis is that the PFD would remain the same, but the width of the tuning curve would get broader and cover the whole range of instability of the landmark. While this was not tested in the current study, some studies applied methods that could investigate it (Nau et al., 2020; Koch et al., 2020).

For example, (Nau et al., 2020) used von Mises distributions of different widths (from 10° to 60°) and convoluted them with the HRF signal. Then, they trained and tested their model to find which widths of distributions explain the time course of the neural signal. Future work could use a similar approach to create several width distributions and see if it correlates with the signal for stable and unstable landmarks.

An important observation that emerged in our study was linked to the behavioural variability across participants. Indeed, while the measures regarding stable landmarks were controlled and similar across all participants, answers regarding the unstable landmarks differed between participants. First, their answers varied when they were asked to rate the stability of unstable landmarks. Second, not all participants faced and tried to use the unstable landmark during the pointing in the learning phase. Third, they showcase a high variability in their pointing during the desktop version when they only saw a single landmark at a time. Several patterns of answers have been used between the participants, indicating various strategies. On the one hand, some participants had a high spread of answers, suggesting that they probably encoded that the unstable planet could be anywhere. On the other hand, we observed highly clustered answers which could suggest specific hypotheses. First, participants might have pointed to an average orientation by sampling all the positions of the landmarks they experienced while in immersive VR. Then, this position could either be a random orientation or linked to the cardinal direction, which would produce a correct answer when pointing to the moon. Lastly, some participants, who knew their answers did not matter, could repeat the same motor movement they performed when seeing a stable landmark. However, how this would impact the representation of the unstable landmark and its relation to the HD signal is still to be determined. While this question could be addressed in future studies, a few hypotheses can be already discussed. Indeed, if the spread of answers is related to the internal

representation of the landmark, participants with clustered answers could have a stable tuning curve, resulting from the average of direction sampled. On the contrary, individuals with spread-out answers could have a broader tuning curve and would repeatedly sample from it and get highly variable responses.

Nevertheless, the fact that participants express such differences could also limit the study's findings. Indeed, effect sizes in fMRI studies are usually small and require the experimenter to create and analyse the data carefully (Geuter et al., 2018). Usually, fMRI experiments require a comparable behaviour performance among subjects to look at the desired effect. Hence, while participants rated the stability of the landmarks in a similar way, intra-individual differences in the other tasks could have led to higher noise within the fMRI analysis. Therefore, follow-up studies should find a way to address this issue and find a way to increase the detection power. An example could use a within-subject design encouraging behavioural variability and thoroughly exploring multiple metrics from a smaller sample of participants. On the opposite, participant strategies and performances could be uniform to decrease the variability and have a homogenous sample of participants.

2.5 Contributions

Matthieu Bernard (MB) completed this project in a collaborative effort with Jonathan Shine (JS), Asema Hassan (AH), Malika Schaumburg (MS) and Thomas Wolbers (TW). MB, JS and TW conceptualised the work. MB managed the project administration. MB and AH programmed the VR task. MB and MS acquired the data. MB analysed the data and visualised the results. TW supervised the work.

CHAPTER 2: How does human ageing affect our ability to keep track of orientation?

3.1 Introduction

Few studies investigated and measured the HD system using behavioural experiments (Sadalla and Montello, 1989; Warren et al., 1989; Harootonian et al., 2022). Indeed, HD measure is usually extracted from other types of experiments, such as perspective taking (Flavell et al., 1981; Parsons, 1987; May et al., 1995; Shelton and McNamara, 1997; Amorim, 2003; Zacks et al., 2003; Waller et al., 2002; May, 2004; Mou et al., 2004) or path integration (Mittelstaedt and Mittelstaedt, 1980; Wolbers et al., 2007; Chrastil and Warren, 2021; Qi and Mou, 2023). However, this often leads to a measure of the HD system confounded with other behavioural measures such as mental rotation or movement (either passive or active). Therefore, one of the goals of this chapter is to create a clearer readout of HD.

While many studies looked at the effect of ageing regarding spatial navigation (Lester et al., 2017), almost no study investigated it from the HD system point of view. However, much evidence points to a probable HD system dysfunction during ageing. Studies found some deficit in ageing for navigation tasks related to spatial landmarks such as path integration, and older participants performed worse than young participants when making turns (Harris and Wolbers, 2012; Stangl et al., 2018; Segen et al., 2022). In addition, several studies found deficits in the perception of self-motion in older participants that lead to a misperception of heading (Warren et al., 1989).

From a physiological aspect, previous studies found degradation with age of essential brain structures belonging to the HD circuit, such as the hippocampus (Burke and Barnes, 2006; Raz and Rodrigue, 2006), thalamus (Hughes et al., 2012) or RSC (Moffat et al., 2006). Moreover, degeneration of the vestibular system has been reported (Neuhauser et al., 2008; Agrawal et al., 2009; Anson and Jeka, 2015) and could impact downstream functions like the HD circuit. All those deficiencies would logically lead to issues in the HD system, but previous ageing studies did not investigate how this system could be impacted. Hence, this study will compare the performance between young and old adults and assess how ageing affects the HD system.

A previous HD model hypothesised how increased noise could impair the HD system. Indeed, one property of the HD model from Zhang (1996) can be interesting to investigate in the context of ageing: the reduction of the representational space. Specifically, it is described by the reduction of the possible range of preferred heading directions. In other terms, a system at the equilibrium with a precise coverage of 360° would drift to a selected few peaks with time (Figure 25). This effect emerges when noise is added to the system, making connections between neurons unstable, as it could happen with ageing. Renart et al. (2003) also described this phenomenon in another modelling study. The authors investigated working memory function using a continuous network structure (similar to a ring attractor). They placed “points” in equally spaced locations around a circle, included noise in the system, and simulated the model for six seconds. After the simulation ended, the authors found that the points moved from their origin space to a limited number of clustered positions. However, those models are theoretical, and knowing if this property translates behaviourally is essential.

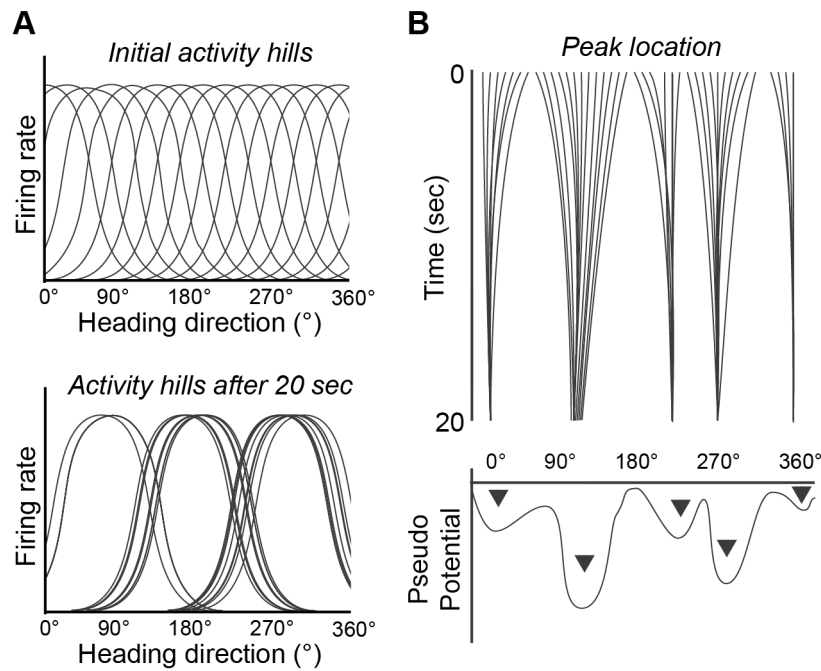


Figure 25: The reduction of the representational space.

A, when noise is added to the HD system, it is hypothesised that the coverage of activity hills would be reduced to a limited number of peaks after a delay period. B, this effect is explained by the pseudo-potential activity having local minima where the peaks would fall into (arrowheads on the bottom panel).

Figure adapted from Zhang (1996)

Shinder and Taube (2014) tried to shed some light on this by rotating head-fixed rodents to different orientations and maintaining them fixed for 30 seconds while recording in the ADN. The authors found a reduction in firing rate when the animal faced away from their PFD compared to facing it. They hypothesised that this could be due to increased noise, making the neuron spiking less predictive of the animal HD. The authors discussed different hypotheses, as this finding could be due to a drift of the PFD, but they argued that it was unlikely. However, this study did not investigate ageing, and the reduction of the representational space may happen only for high noise levels.

Translating this to humans, if the reduction of the representational space is a property of the HD system that would increase with noise, older participants would have a more imprecise coverage of the 360° rings. To test this, we developed a task that included a

20-second delay period before answering, which led to the formulation of two separate hypotheses. On the one hand, we could observe a clustering of answers after the delay period since the heading coverage would be reduced to a limited amount of stable direction, as Zhang (1996) suggested (Figure 26, right panel). On the other hand, if the drift during the delay is random, there would be an increase in error but not necessarily a clustering of answers (Figure 26, left panel).

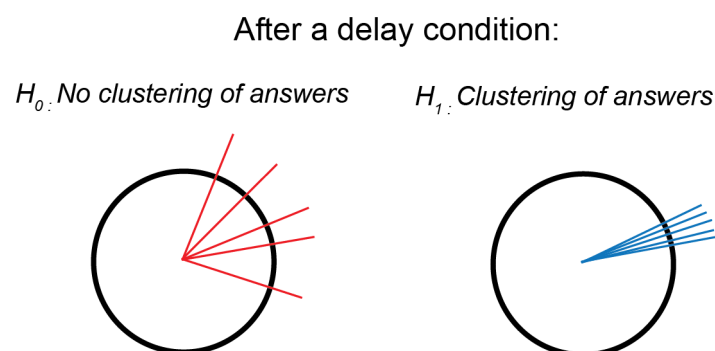


Figure 26: Testing the hypothesis of the reduction of the representational space with the task.

This hypothesis can be tested by including a delay period in the behavioural task and investigating if clustering of answers happens, rejecting the null hypothesis.

To answer those hypotheses, we carefully designed a behavioural experiment where participants used immersive VR to learn the position of a single distant landmark within a circular arena. Then, participants had to retrieve the position of the landmark from different orientations with or without a delay period before they answered. Hence, we predict that older adults would perform worse than young participants across the rotations. Moreover, the impact of delay should be higher for the older participants as their system might be more noisy, and the drift during delay would be faster than for young participants.

3.2 Materials and Methods

3.2.1 Participants

Thirty healthy young adults aged between 18 and 30 years (23.77 ± 3.20 , female $n=17$) and thirty healthy older adults aged between 60 and 80 years (68.31 ± 5.58 , female = 15) participated in the study. Participants were fluent in German, did not report physical or mental disorders and were not colourblind. The experiment was approved by the local ethics committee, and all research was performed in accordance with relevant guidelines and regulations. Written informed consent was obtained from each participant before starting the experiment. Participants were compensated financially for their participation. One older participant was excluded due to an incomplete dataset.

3.2.2 Experimental design and procedure

Every participant came on two consecutive days. On the first day, participants performed three different colour tests (Ishihara test, colour arrangement and colour matching) to verify that they were not colourblind and to assess their colour perception. Then, participants performed the learning task in immersive VR using a HMD followed by the testing task (description in detail below). Each day, participants performed two blocks of the testing task with a break in the middle. After each block, they completed a task where they needed to place the learned landmark. Participants returned on the second day to repeat the learning task and two new blocks of the testing task. During the entire experiment, participants wore a HTC Vive HMD with a wireless adapter and could actively walk in a space of 5 by 5 metres without constraint.

3.2.3 Environment

The virtual environment was created using the Unity software (version: 2019.3.0f6). The ground was made of a grass texture without any visible pattern, and the skybox also did not have a specific pattern. In addition, a circular arena with a diameter of 100 virtual meters (vm) surrounded the participant with a height of 4.5 vm (Figure 27). The distance between the cylinder and the participant was far enough, so the participant could not reach it. The texture applied to the cylinder was a colour gradient with the different colours of the rainbow (Figure 27). Furthermore, a large black rectangle acting as a distant landmark with a width of 34.8 vm was placed on the other side of the cylinder and centred at the position of 0° . The landmark covered 10° of the participant's field of view when they directly faced it from the centre of the environment. Its position was constant across the whole experiment and between participants.

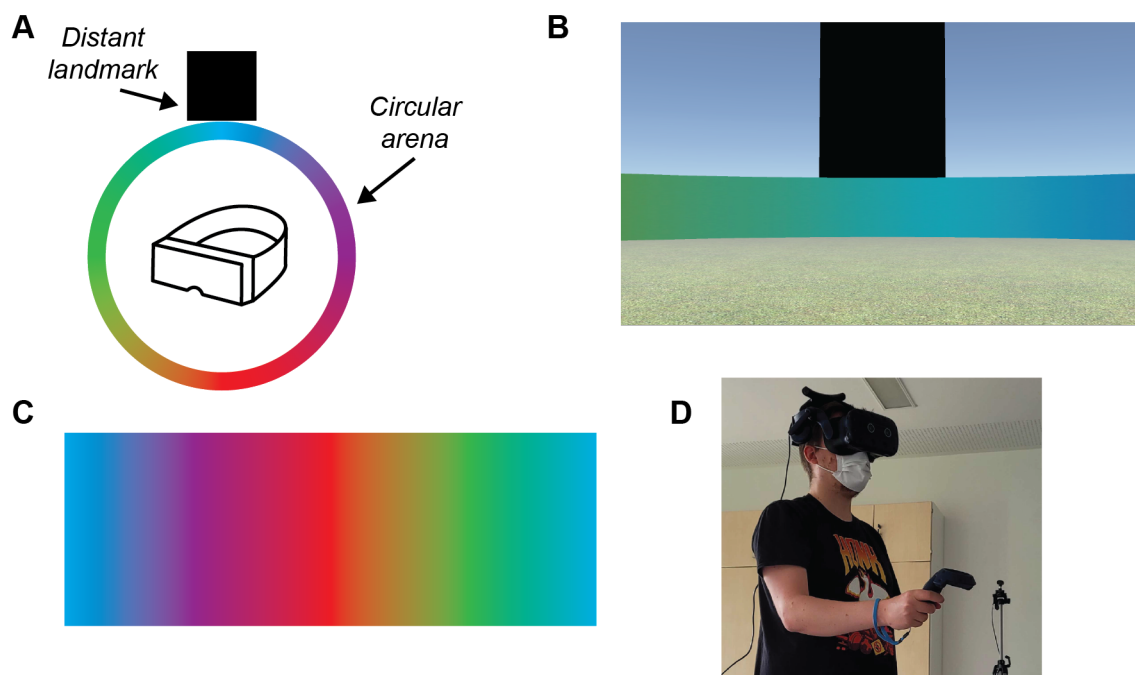


Figure 27: Virtual environment used in immersive VR.

A, bird-eye view of the environment composed of a distant landmark and a circular arena. B, view of the participant when using the HMD in VR. C, colour gradient mapped into the circular arena. D, participant wearing the wireless headset and performing the task.

3.2.4 Learning task

The goal of the task was to learn the position of the landmark, and participants had up to 100 trials to remember the correct position. For each trial, participants walked to a random starting location indicated by a blue circle on the ground. Upon stepping on it, the arena and the landmark disappeared. Then, a 3D arrow appeared in front of them, prompting the participants to rotate either left or right by a fixed amount. The amount was controlled to be either small (50°), medium (105°) or large (160°). After making the rotation, participants heard an auditory cue and saw a text asking them to answer immediately. We added the auditory cue tone to ensure older participants would not overturn and stop at the correct orientation. To answer, participants were instructed to rotate physically to face back the position of the landmark. After giving their answers, participants received feedback in the form of smileys shown in front of them. Feedback was calculated using the absolute angular error computing the difference between the landmark's actual position and the participant's facing direction when he answered. They had either a red (if the error was over 45°), orange (error between 45° and 20°), yellow (error between 20° and 8°) or green smiley (error below 8°). To complete the learning, participants had to pass a threshold calculated by taking the average of the last five angular errors. If the average was below 8° , participants passed the learning phase and could proceed to the testing task. If not, they continued the learning until they succeeded or reached the limit of 100 trials. Every participant in this analysis passed the learning before the 100-trial threshold. A schematic of the task can be seen in Figure 28.

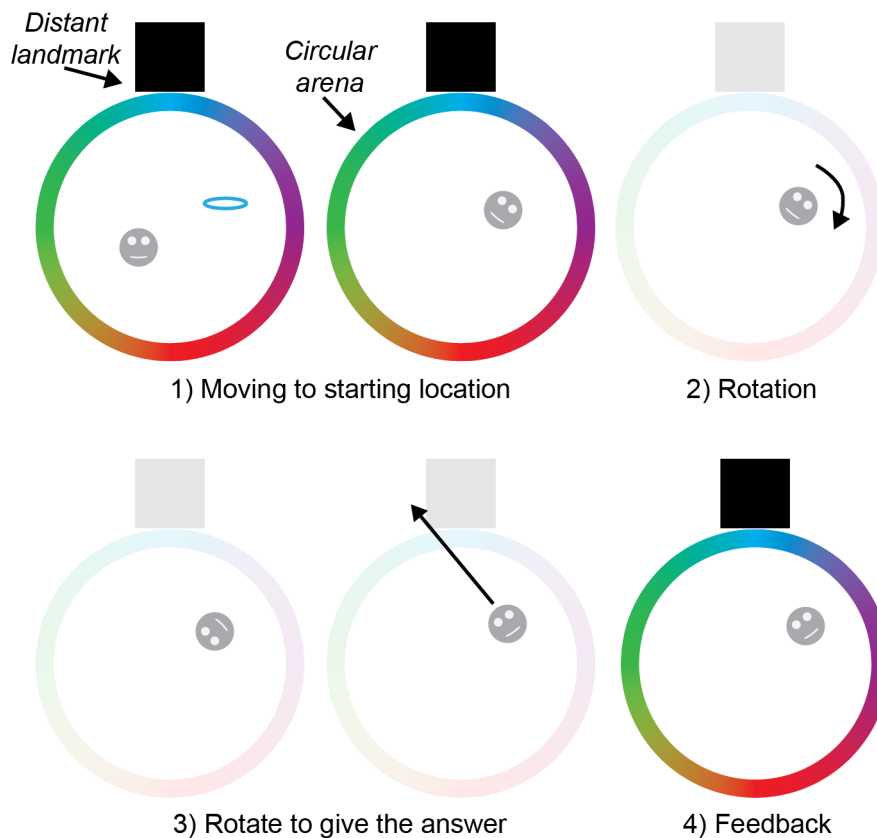


Figure 28: Design of the learning task with a trial example.

Participants could see both the arena and the landmark when the environment was present. 1, participants walked to the starting location indicated by a blue circle on the ground. 2, they rotated by following an arrow presented in front of them. 3, they physically rotated back to face the landmark. 4, they received feedback, and another trial would start.

3.2.5 Testing task

The testing task was done in the same environment, with the only difference being that the landmark was not visible, only the arena. Participants started a trial by walking to a random location indicated again by a blue circle on the ground. Upon reaching it, a 3D arrow asked the participant to rotate until they reached the correct facing direction for the start of the trial. Next, they decided when to press the trigger button of the controller to start the first turn. The arena disappeared when they pressed the trigger, and another 3D arrow made participants rotate left or right by a controlled amount, similar to the learning task. After rotating, a delay of 20 seconds happened for half of

the trials. During this delay, participants were asked to perform a backward counting task with steps of 2, with a starting number generated randomly between 90 and 110. The goal was to distract the participants during the delay period and prevent them from rehearsing their answers. The experimenter ensured that the participants were counting correctly during the whole task. After the delay or no delay, participants had to answer by physically rotating to face the landmark, similar to the learning task. When participants answered, no feedback was given, the arena appeared again, and another trial started. A schematic of the task can be seen in Figure 29.

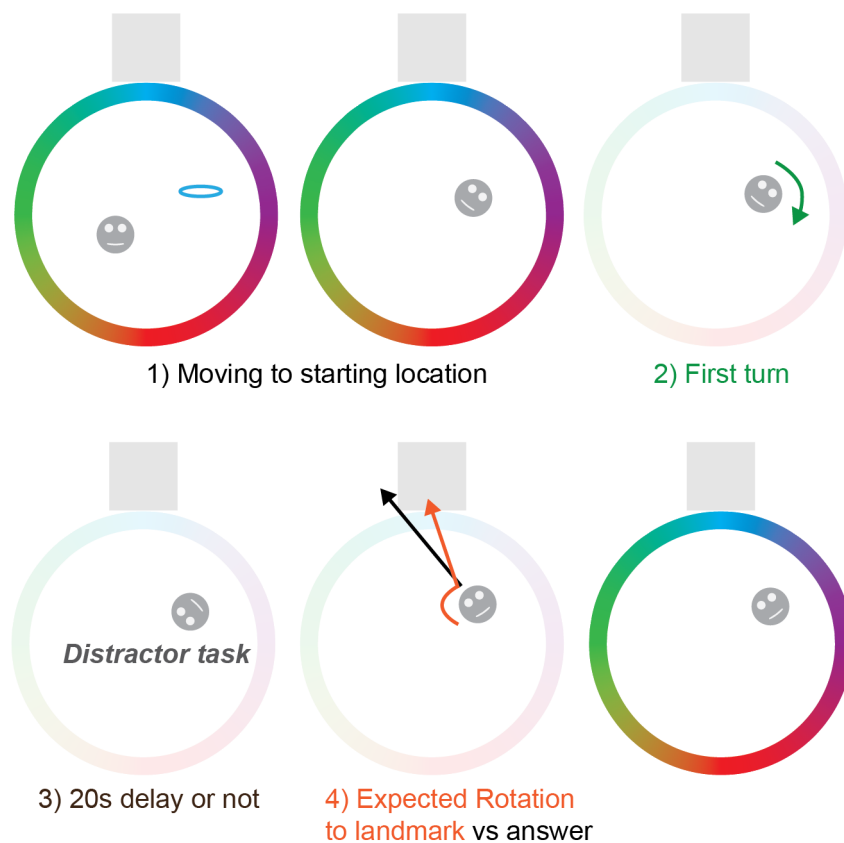


Figure 29: Design of the testing task with a trial example.

Participants could only see the arena during this task. 1, participants walked to the starting location indicated by a blue circle on the ground. 2, they rotated by following an arrow presented in front of them. 3, the delay condition occurred, and participants either performed the distractor task for 20 seconds or answered immediately. 4, they physically rotated back to face the landmark. In the analysis, we investigated their answer (black) against the expected rotation to the landmark (orange).

The trial sequence was created prior to the start of the experiment and was composed of 48 unique trials, each repeated three times. For the unique trials, they were made using the different rotations (small, medium and large), the delay conditions (0 or 20 seconds) and the expected amount of rotation needed to face the landmark (0°, 45°, 90°, 135°, 180°, -135°, -90°, -45°). All 144 trials were separated into four blocks of 36 trials, with 72 trials done per day. Finally, at the start of each block, participants could see the correct position of the landmark for as long as they desired.

3.2.6 Placement of the tower task

At the end of each block, participants were asked to place the landmark within the environment. The goal was to get a direct measure of the memory of the landmark for each participant. Then, we could ensure that they memorised correctly its position across the experiment. During the task, they only saw the arena and placed the landmark by facing the correct position and pressing the trigger button. Then, the landmark appeared at the position currently faced by the participant. Next, participants could refine their answers by using the controller to move its position either left or right. Lastly, they locked their answer and continued the testing task.

3.2.7 Data reduction and statistical analysis

Data reduction relied on Python (version: 3.7.4) and statistical analysis on R (version: 4.1.3). The statistical analysis involved repeated-measures ANOVAs and t-tests. For learning, we extracted the number of trials completed between the two age groups for both days from the datasets. The placement of the landmark was also taken for each participant.

For the testing task, the absolute angular error was calculated similarly to the learning task, i.e., the difference between the landmark's actual position and the participant's facing direction when answering. However, we corrected those values by taking the position of the landmark placed by the participant and using it as the reference when calculating the angular error. In addition, we took the heading of the participant during the delay period and calculated its circular standard deviation. The goal was to assess if participants moved their heads during the delay period. Moreover, the angular error for the trials where participants faced the landmark before answering was further analysed. Since the correct answers for those trials would be to answer without rotating, the analysis focused on the impact of delay and first turn. We look at whether participants moved by assessing the rotation performed by the participant. For each trial, we checked if the movement was below 5° and calculated the percentage of time when the participant moved. We decided to take 5° as the threshold since participants make slight head movements, as seen during the delay period. Lastly, to investigate if there was a clustering of answers, the raw heading of the participant after answering was extracted, and the circular standard deviation was calculated across the different repetitions of the unique trials.

Finally, the scores for each control colour test were calculated for each participant. For the Ishihara test, the percentage of successful trials was computed. For the test assessing colour arrangement (i.e. perception of gradient over similar colour), the number of trials to get a perfect answer was average for each arrangement. Then, those values were averaged to create a percentage of accuracy. For the colour-matching tests, the mean value over the trials of each difficulty (easy, medium and hard) was calculated. Next, those values were either average to create an overall colour-matching score or separated to get a score for each difficulty.

3.3 Results

Both age groups learned the position of the landmark.

First, we computed t-tests to compare the performance in the colour tests between the two age groups. The goal was to ensure that our results were not confounded with differences in colour perception. For the Ishihara tests, we found no significant difference ($t(54.99)=0.23$, $p=0.81$) between older (mean= 98.38 ± 3.60) and young (mean= 98.17 ± 3.14). For the arrangement test, a significant difference was found ($t(32.13)=-3.31$, $p=0.002$) between older (mean= 96.30 ± 4.17) and young (mean= 98.96 ± 1.14). This difference was most likely due to an older participant who performed at around 80%. Lastly, a significant difference was found in the colour-matching test when we included every difficulty ($t(40.77)=3.25$, $p=0.002$). However, the colour gradient mapped onto the circular arena had bright colours and was more related to the easy difficulty of the task. We ran another t-test including only the easy difficulty, and we observed no difference ($t(54.04)=-0.87$, $p=0.39$) between older (mean= 32.48 ± 9.91) and young participants (mean= 29.96 ± 12.01).

All participants could learn the landmark's position on both days for both age groups (Figure 30). When running an ANOVA, we found a main effect of age ($F(1,57)=12.39$, $p<0.001$) and day ($F(1,57)=9.79$, $p=0.003$), but no interaction ($F(1,57)=1.04$, $p=0.31$). Additional t-tests showed significant differences between young and older participants on day 1 ($t(54.19)=-3.22$, $p=0.002$) and day 2 ($t(51.61)=-2.22$, $p=0.03$). In addition, older participants learned significantly faster on the second day than the first ($t(28)=-2.65$, $p=0.01$). This was not the case for young participants ($t(29)=-1.68$, $p=0.10$).

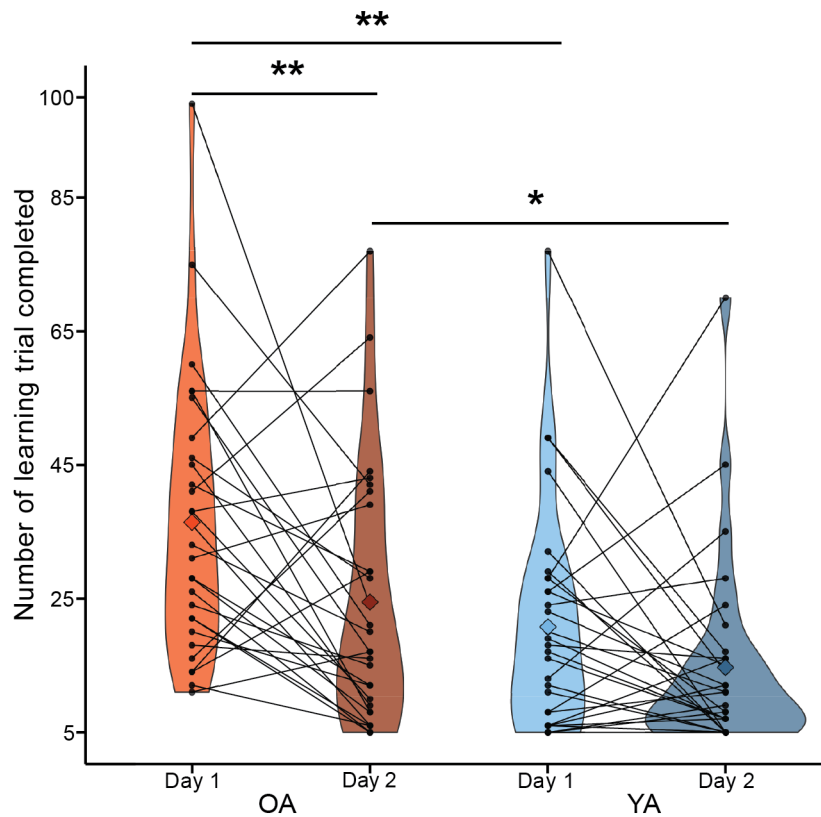


Figure 30: Learning performance across days.

*Number of learning trials completed before passing the threshold for young (YA) and older (OA) adults on Day 1 and Day 2. Violin plots show the distribution of data. The dots represent individual data, and the diamond is the average across individuals. * $p < 0.05$; ** $p < 0.01$.*

Moreover, we investigated whether participants placed the landmark close to the real position for each block (Figure 31). An ANOVA show a main effect for days ($F(1,57)=5.69$, $p=0.02$) but not for age groups ($F(1,57)=0.20$, $p=0.88$) nor an interaction effect ($F(1,57)=1.30$, $p=0.26$). In addition, subsequent t-tests showed that older participants were more accurate when placing the landmark on the second day ($t(28)=-2.18$, $p=0.04$). Young participants did not show such differences ($t(29)=-1.05$, $p=0.30$).

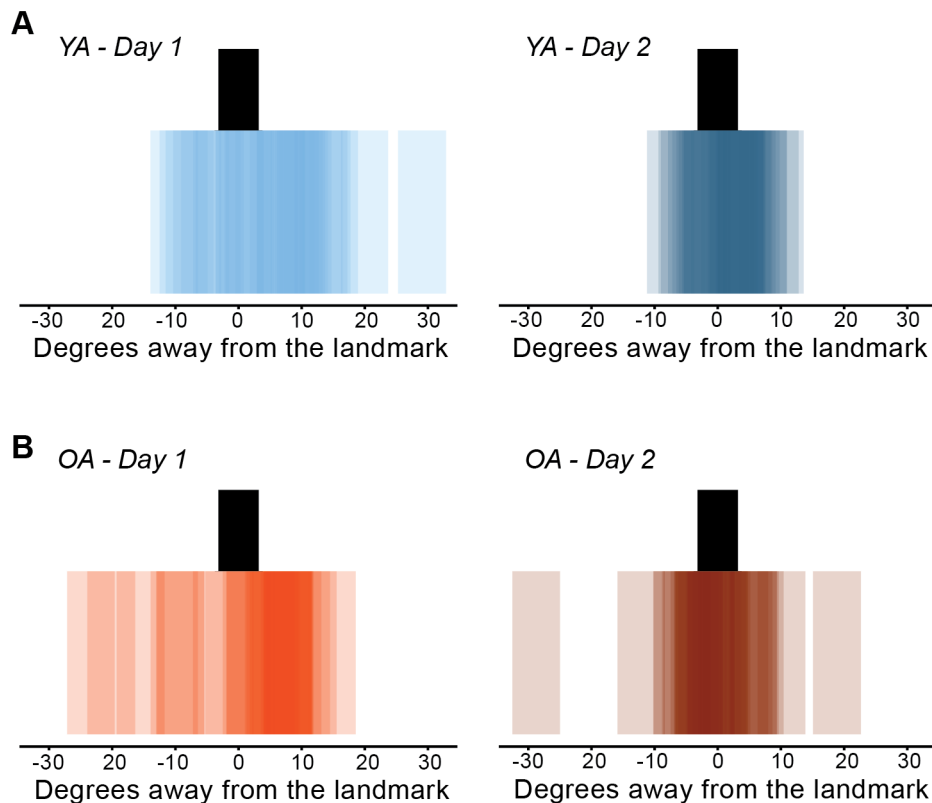


Figure 31: Landmark placement between days

A, placement of the landmark by young adults on Day 1 (left) and Day 2 (right). B, placement of the landmark by older adults on Day 1 (left) and Day 2 (right). The black bar represents the correct position of the landmark, and the coloured bars represent the individual data.

Older participants performed worst on average and both age groups were negatively impacted by the delay condition.

The experiment was performed for two consecutive days. We checked if we could combine the data across the two days by taking the average corrected angular error and comparing it between the two days (Figure 32A). An ANOVA showed a main effect of age ($F(1,57)=9.83$, $p=0.003$) but no main effect of days ($F(1,57)=2.11$, $p=0.15$) nor interaction ($F(1,57)=0.0002$, $p=0.99$). This result would suggest that the performance was not different across the testing days and allow subsequent analyses to look at the dataset as a whole. In addition, another control was performed to check if participants were moving their heads during the delay phase (Figure 32B). We found that the range

of motion of young participants (mean= $2.03^\circ \pm 5.26^\circ$) was not different compared to older participants (mean= $1.67^\circ \pm 2.97^\circ$) ($t(53.27)=1.42$; $p=0.16$).

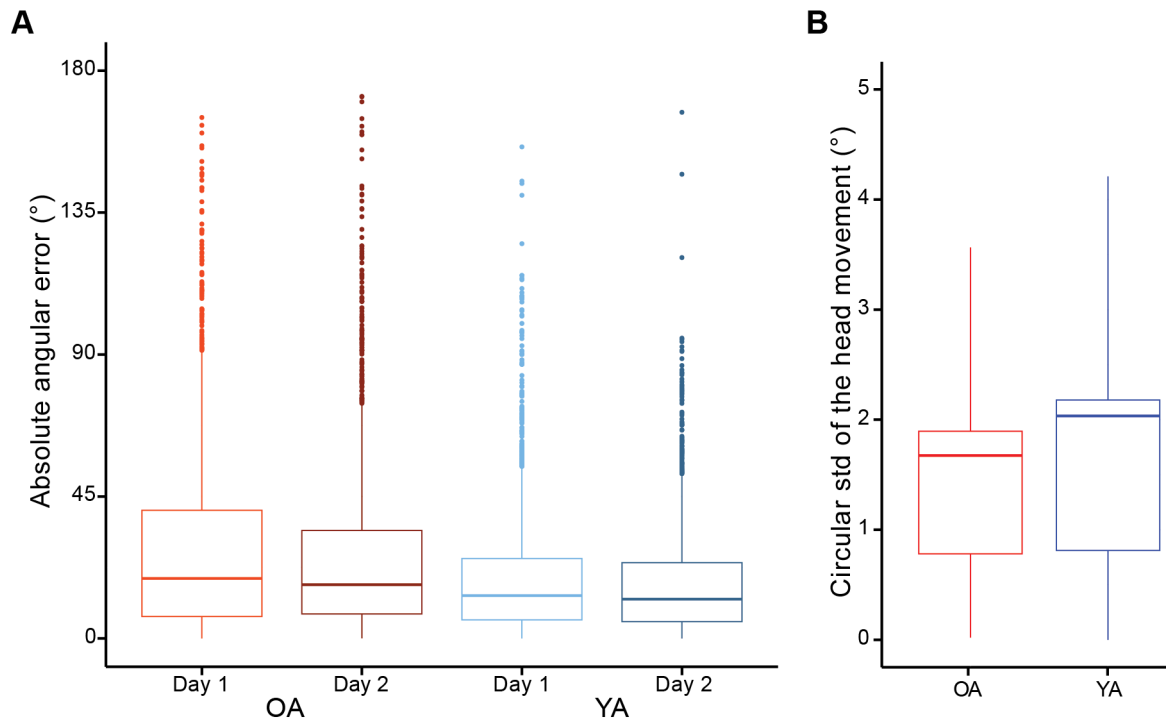


Figure 32: Control measures for equal performance between testing days and head movement during the delay phase.

A, Corrected angular errors separated between age groups and testing days. B, the circular standard deviation of the head movement performed by the participants during the delay period. OA, older adults; YA, young adults.

To assess the effect of age and delay, we separated the data by the “expected rotation to the landmark” (Figure 33A), corresponding to the amount of rotation necessary for the participant to face the landmark. For example, if the expected rotation to the landmark is 180° , the participants must perform a 180° turn to achieve a perfect answer. Hence, a first ANOVA found a main effect of age ($F(1,57)=9.83$, $p=0.003$), delay ($F(1,57)=36.93$, $p<0.001$) and expected rotation ($F(7,399)=4.79$, $p<0.001$). In addition, an interaction effect between delay and expected rotation was also found ($F(7,399)=3.21$, $p=0.003$). However, we found no interaction between age and delay ($F(1,57)=1.12$, $p=0.29$), age

and expected rotation ($F(7,399)=1.64$, $p=0.12$), nor a triple interaction ($F(7,399)=1.87$, $p=0.072$).

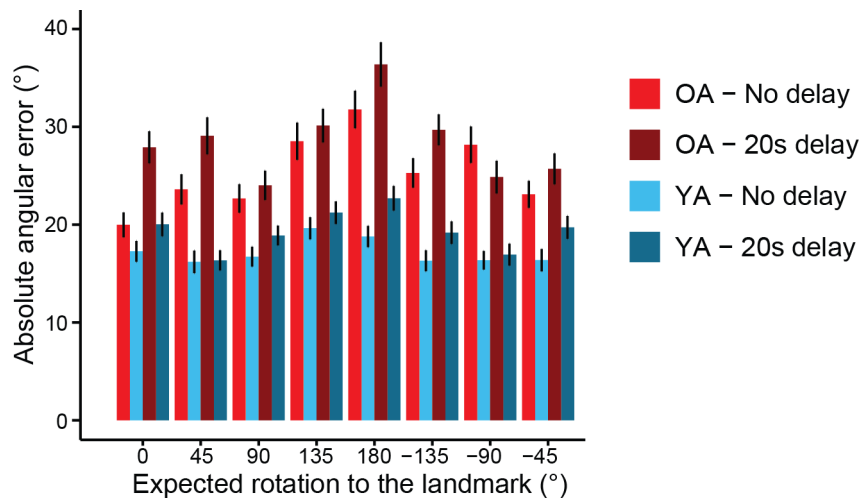


Figure 33: Average angular error across delay conditions and age groups.

Average absolute angular errors (coloured bars) for young (YA) and older (OA) adults for the two delay conditions. The vertical black lines represent the standard error for each bar.

We further analysed the data pattern by considering the different amounts of rotation in the expected rotation to the landmark. Specifically, we divided the absolute angular error by its associated expectation rotation value to obtain a ratio (Figure 34A). This prevented the analysis of the 0° expected rotations, and we conducted a separate analysis. An ANOVA showed a main effect of delay ($F(1,57)=24.34$, $p<0.001$) and expected rotation ($F(7,399)=297.51$, $p<0.003$) but not age ($F(1,57)=3.05$, $p=0.086$). An interaction effect was also found between age and expected rotation ($F(7,399)=2.30$, $p=0.002$) and delay and expected rotation ($F(7,399)=22.38$, $p<0.001$) but not age and delay ($F(1,57)=3.64$, $p=0.06$). Lastly, a triple interaction was found between age, delay and expected rotation ($F(7,399)=3.50$, $p=0.001$). Interestingly, when separating the data by the first turn performed (Figure 34B/C), the influence of the first turn seemed to be larger for smaller expected rotations such as 45° .

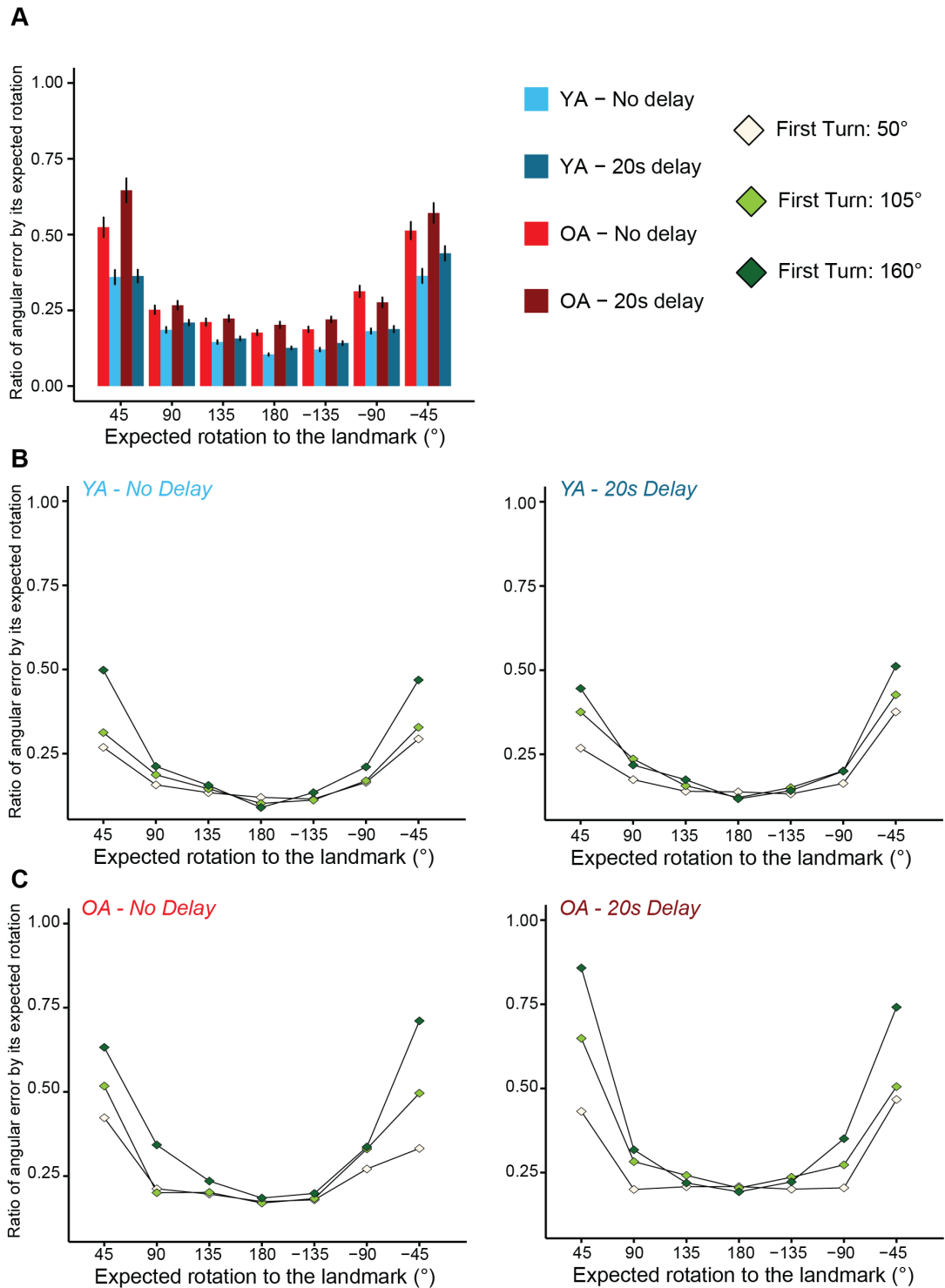


Figure 34: Ratio of angular error by expected rotation across delay conditions and age groups.

A, average ratio of the absolute angular errors divided by the associated expected rotation to the landmark for young and older adults for the two delay conditions. The vertical black lines represent the standard error for each bar. The average ratio is separated by the first turn executed for young (*B*) and older (*C*) adults after the delay conditions.

Both age groups were impacted by the 20-second delay when already facing the correct orientation before answering.

We decided to investigate the particular case when participants were already facing the landmark before answering (i.e. expected rotation of 0°). Indeed, in this condition, the main impact of the error should come from either the first turn or the delay period. When looking at the distribution of participant answers across delay conditions (Figure 35A/B), we observed an increase in the spread of answers both for young ($t(29)=2.83$; $p=0.008$) and older ($t(28)=3.09$; $p=0.004$) participants after the 20-second delay period. In addition, we looked at the amount of rotation performed by participants across delay conditions (Figure 35C). The goal was to check if participants moved as a perfect answer required participants to maintain their orientation. The results from an ANOVA indicated a main effect of delay ($F(1,57)=14.82$; $p<0.001$) but not age ($F(1,57)=0.0008$; $p=0.98$) nor an interaction ($F(1,57)=0.91$; $p=0.34$). Paired t-tests show a higher amount of rotation after the delay period for young ($t(29)=-3.12$; $p=0.004$) and older ($t(28)=-2.29$; $p=0.03$).

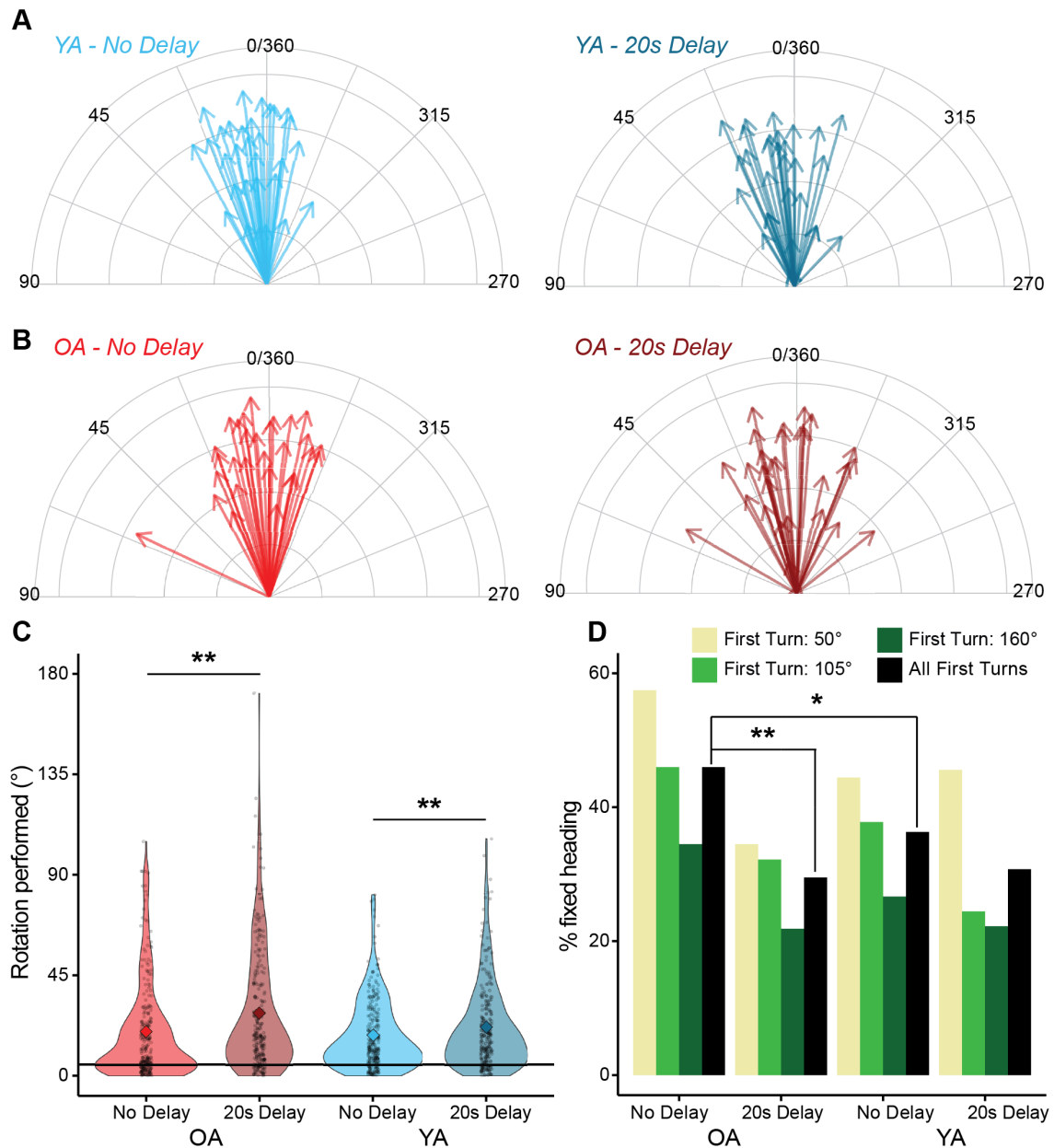


Figure 35: Testing results when already facing the landmark prior to answering.

Each arrow represents the average facing answer for (A) young and (B) older participants for (left) no delay and (right) 20s delay conditions. The length of the arrow represents the inverse circular standard deviation with a shorter length describing a larger standard deviation. C, average rotation performed between age groups and delay conditions. Violin plots show the distribution of data. The dots represent individual data, and the diamond is the average across individuals. The horizontal black line represents the threshold of "Fixed heading" (i.e. 5°). D, bars represent the percentage of trials where participants did not move across age groups and delay conditions. Data were separated by the first turn prior to the delay condition. * $p < 0.05$; ** $p < 0.01$.

Lastly, we checked whether participants would tend not to move for those trials (Figure 35D). We calculated the percentage of time participants moved less than 5° as a quantitative way to assess fixed answers (horizontal black line in Figure 35C). The reason for not only counting trials with 0° rotations is that participants might move their heads without noticing, as shown during the delay period (Figure 32B). Separating those results by the first turns, an ANOVA showed a main effect of age ($F(1,57)=4.18$; $p=0.045$), delay ($F(1,57)=10.54$; $p=0.002$) and first turn ($F(2,114)=11.08$; $p<0.001$). An interaction effect between age and delay ($F(1,57)=4.34$; $p=0.042$) and delay and first turn ($F(2,114)=5.54$; $p=0.005$) was also found. In addition, averaging the results across the first turns showed a significant decrease in the percentage of fixed heading after the delay period for older participants ($t(28)=2.93$; $p=0.007$). We did not find a difference for young participants ($t(29)=1.32$; $p=0.20$). Even more, there was a lower percentage of fixed heading for young participants compared to older when there was no delay period ($t(44.86)=-2.57$; $p=0.013$) but not for the twenty seconds delay ($t(48.20)=0.61$; $p=0.55$). Those results indicated that the delay condition impacted more older participants than young ones and that the signal drifted to more distant orientations.

The delay period increased the errors and no specific clustering of answers was found.

We tested the reduction of the representational space hypothesis. This hypothesis stated that the range of directions would be reduced to a selected few orientations with noise and delay. Therefore, the analysis aimed to assess whether the delay period led to increased clustering of answers corresponding to the only orientations available to the participants (Figure 36A). To test it, the circular standard deviation was computed across the answers given by participants, and an ANOVA showed a

main effect of age ($F(1,57)=16.93$; $p<0.001$), delay ($F(1,57)=11.52$; $p=0.001$) and expected rotation ($F(7,399)=2.56$; $p=0.014$). An interaction was found between delay and expected rotation ($F(7,399)=2.62$; $p=0.012$) but not for age and delay ($F(1,57)=0.12$; $p=0.73$) nor age and expected rotation ($F(7,399)=0.52$; $p=0.82$). However, when looking at the data pattern between the delay conditions, we did not find a systematic decrease in the circular standard deviation after a delay period, invalidating the hypothesis of a clustering of answers. On the contrary, the pattern indicated an increase in the circular standard deviation, suggesting a higher spread of answers. This was also the case when separating the trials over the first turns (Figure 36B-D).

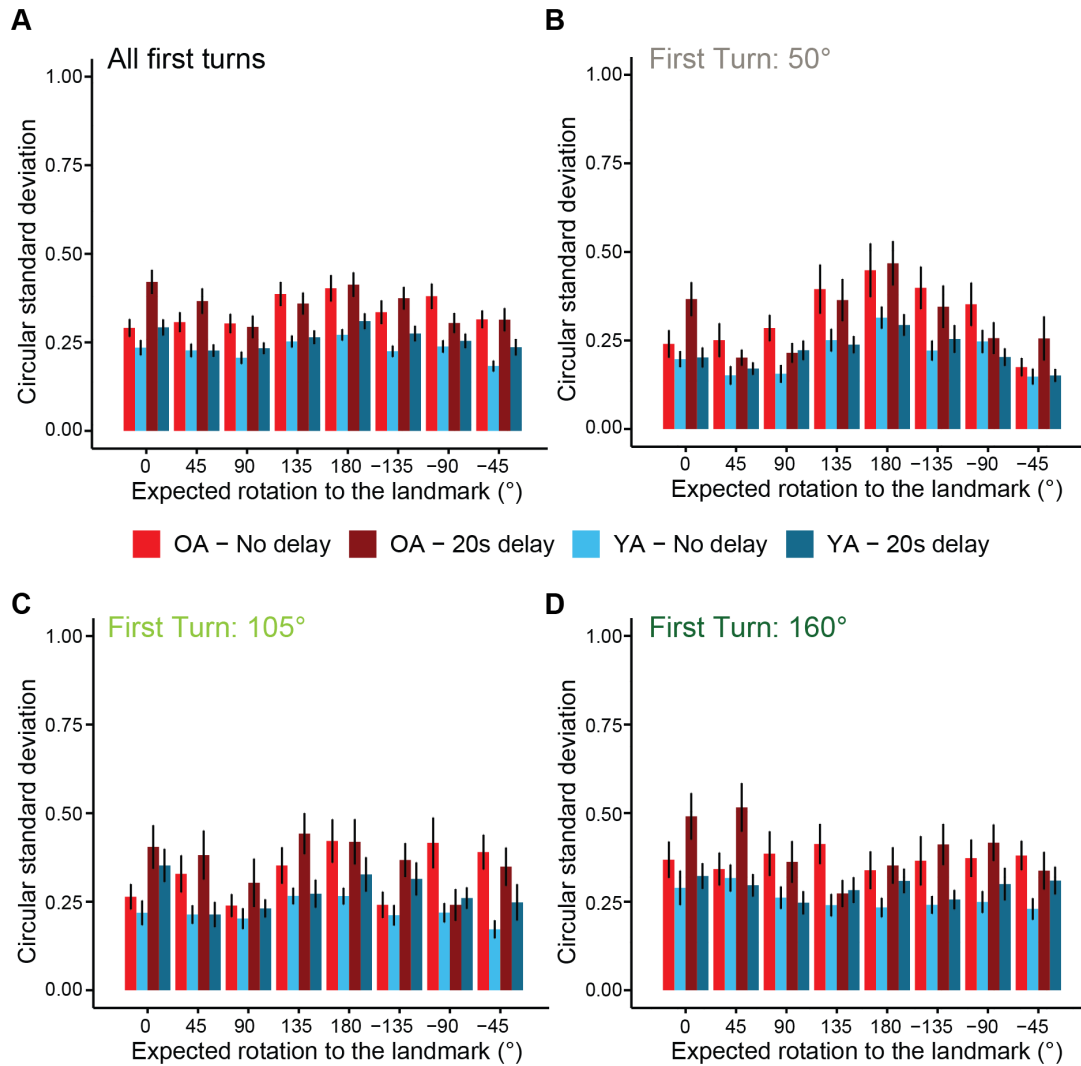


Figure 36: Checking the reduction of the representational space hypothesis.

To check for potential clustering of answers, the circular standard deviation was calculated for young (YA) and older (OA) adults for the two delay conditions. The data were either (A) combined or separated by the first turn (B, C, D) performed. The bars represent the average circular standard deviation. The black line represents the standard error of the distribution.

3.4 Discussion

The chapter aimed to investigate the ageing effect on the HD system. To check our hypotheses, we designed a new experiment where participants first learned a distant landmark and were tested by facing it after being rotated to different orientations. Our

results found that the pattern of angular errors was proportionally higher for smaller expected rotations to the landmark (45°) than for large ones (180°). The first turn influenced only the 45° and 90° turns, where participants performed worst for increased in first turns. In addition, older participants performed generally worse than young participants as they made larger angular errors overall. Both age groups were negatively impacted by the delay effect, especially for the particular case of 0° expected rotations. However, we did not find any specific clustering of answers after the delay, as suggested by the reduction of the representational space hypothesis from Zhang (1996). We found that both young and older participants had a higher spread of answers after the delay period. This observation suggested that their heading perception drifted randomly to another orientation and not to the same ones as first suggested. Those results are in accordance with the current literature that suggests a deficit in spatial navigation during ageing (Lester et al., 2017). Moreover, the effect seen is likely not due to a deficit in learning as both age groups performed extensive learning and had to pass a strict threshold of 8° . Debrief questionnaires indicated that participants remembered the position of the landmark at any time during the testing when the colour gradient was present. We also did not find any age difference when participants had to place back the landmark after performing a block of trials.

To obtain a precise answer from the participant, we calculated their absolute angular error in relation to the landmark they placed during each day. Separating the trials by the expected rotation to the landmark suggested that higher angular errors occur for larger rotations (e.g. 180°), especially for older adults. However, this measure did not consider that the amount to rotate was variable due to the different orientations faced prior to answering. Therefore, a separate measure was computed by dividing the angular errors via their associated expected rotation, giving a comparable metric.

We observed that greater errors would come from smaller expected rotation (i.e. 45°). Furthermore, those trials could be separated by the first turn executed, and its influence was observed only for the smaller expected rotation, where larger first turns led to increased errors. Taken together, those results suggest that the main source of errors for larger expected rotation (from 90° to 180°) is the accumulation of noise during the execution of the answers. For the smaller expected rotation trials (45°), the error might come from the increase of noise during the completion of the first turn. We argue that participants took longer to answer for those larger expected rotations as the distance was greater. Then, the noise from the velocity integration could accumulate longer than the 45° expected rotations during the answer phase. Previous studies on motion perception in humans found similar results where participants had a systematic bias in their velocity integration during passive translation (Crane, 2012; Zanchi et al., 2022). For active translation, path integration tasks also showed similar results where noise accumulation played a significant role in the error (Stangl et al., 2020).

The reduction of the representational space hypothesis was tested by introducing a delay period before participants answered. The goal was to check whether the delay would lead to a clustering of answers, as hypothesised by Zhang (1996) or to an increase of noise in the HD signal (Shinder and Taube, 2014). Our results showed that the angular errors increased after the delay period across the expected rotations. To further differentiate between the two possible hypotheses, we looked at the clustering of answers after the delay but did not find any systematic clustering for both age groups. This observation would suggest that during the delay period, the HD activity bump could drift slowly randomly. In addition, when investigating the difference between the two age groups, the largest effects are found for the small expected rotations such as 45° and 0° . In fact, for the trials when the expected rotation was equal to 0° , participants were already facing the landmark before

answering and should not move. Those trials removed a potential effect of the translation to perform as a source of noise, and only the first turn and the delay period played a role. We found that both age groups tended to move more after the delay period. This result suggests that there is an accumulation of noise during the delay and the HD system might become more noisy, leading to a faster drift of the HD bump. In addition, we separated those trials by the first turn executed prior. We observed for both age groups that lower turns (e.g. 50°) led to a higher chance for the participant to not move during the no-delay condition. This suggests that the HD system was sensitive to the noise produced by the first turn, similar to the results found for the 45° expected rotations.

During the debrief questionnaire, we asked participants to explain their strategy to solve the task. Then, it was possible to separate those answers into two strategies. On the one hand, some participants only used idiothetic cues (i.e. body-based). On the other hand, participants explained that they formed a mental image of the colour gradient and imagined the colour they were facing while rotating. This strategy can be seen as approximating allothetic cues, even though it required some vestibular input from the rotation. In addition, some participants described using a mixture of both strategies. Interestingly, most older participants reported that they only used the body-based strategy, whereas young participants were more flexible and used both strategies. Those results found for young participants align with previous works looking at cue combinations where young adults usually combine both idiothetic and allothetic optimally (Chen et al., 2017). For older adults, previous studies found a deficit in the multisensory integration of sensory cues (Bates and Wolbers, 2014; Colombo et al., 2017). For example, Bates and Wolbers (2014) tested young and older participants in a homing task. The authors used three conditions where participants could use the landmarks to answer, body-based cues or a combination of

both cue types. Their results showed that older participants could combine both cues to increase their performance, but the Bayesian integration was sub-optimal for landmarks. This observation can be related to the evidence that older participants have a deficit in their allocentric reference frame (Wiener et al., 2013; Bécu et al., 2023). In contrast, their egocentric reference frame seems less impacted (Bian and Andersen, 2013). Those evidences could be a reason why older participants in our study did not use the colour gradient during the rotations. They mostly used it after answering to reset their heading toward the position of the landmark. However, our task did not explicitly test those hypotheses within the task and only got it from the written feedback from participants.

Lastly, the design of the experiment was created to be accompanied by a modelling approach. The aim was to understand better the neural mechanisms that could explain the observed performance deficits in older adults. In the next chapter, we developed a computational model based on established neural network models of the HD system. We developed it to investigate ageing by including different sources of noise. In addition, the behavioural task was implemented within the model and by modifying the noise values, we tried to explain the behavioural results.

3.5 Contributions

Matthieu Bernard (MB) completed this project in a collaborative effort with Malika Schaumburg (MS) and Thomas Wolbers (TW). MB and TW conceptualised the work. MB managed the project administration. MB programmed the VR task. MB and MS acquired the data. MB analysed the data and visualised the results. TW supervised the work.

CHAPTER 3: A computational modelling approach to characterise age-related changes in the HD circuit.

4.1 Introduction

Several models investigating the properties of the HD system have been proposed throughout the years (McNaughton et al., 1991; Skaggs et al., 1995; Zhang, 1996; Byrne et al., 2007; Page et al., 2014; Bicanski and Burgess, 2016; Page and Jeffery, 2018; Yan et al., 2021). The majority replicated the properties found in the rodent (for review, see Taube (2007)) and the insect literature (Seelig and Jayaraman, 2015; Green et al., 2017; Kim et al., 2017). In contrast, others tried to link them to other spatial navigation features, such as cue combination (Harootonian et al., 2022) or path integration (Castegnaro et al., 2023). However, none of these models investigated how ageing would impact the HD system. A common way to model ageing is to increase the amount of noise within the model or delete neurons. Zhang's model (1996) investigated the impact of noise in the system, but deleting part of a ring attractor with recurrent connections was detrimental to its functioning. Therefore, it is essential to define those pitfalls and create a model that can successfully explore the effects of ageing. In his seminal work, Marr (1982) defined three levels of analysis to understand information-processing processes. First, the computation level defines what the system is doing. In our case, the HD system measures the animal's facing direction. Second, the algorithm

level asks what processes the HD system employs to create the heading representation in the brain. Previous papers suggest the ring attractor network to be a good candidate (Clark and Taube, 2012; Knierim and Zhang, 2012). Third, the implementation level illustrates how the HD system is implemented in the brain. For this study, we had to make hypotheses on this implementation level to determine how ageing affects the HD system.

Physiological changes such as synaptic changes (Morrison and Baxter, 2012), loss of cerebral volume (Burke and Barnes, 2006; Raz and Rodrigue, 2006; Moffat et al., 2006; Hughes et al., 2012), or deficiency in the vestibular system (Neuhauser et al., 2008; Agrawal et al., 2009; Anson and Jeka, 2015) happen during the ageing of the brain. All those factors could lead to defects within the HD network, and developing a new model could assess their relative contribution. For example, age-dependent synapse changes can be modelled as noisy connections or disconnections by changing the weights between neurons in the model. Removing neurons from the network could approximate losses of cerebral volume. Finally, the HD model could integrate vestibular deficit by increasing the noise level.

The tuning curve generated by the model can be described via several measures to assess the impact of the noise on the model. The tuning curve's peak firing rate, its variance, and the full-width-half-maximum (FWHM) of the tuning curve or the drift between the real HD and model HD can be recorded anytime during a simulation. All those measures can assert whether or not different levels of noise influence the stability and precision of the HD signal. If the tuning curve gets broader and drifts without rotational inputs, the heading signal will be less precise than a sharper tuning curve that is more stable with time. Those hypotheses can be compared with the results found in the experiment from Chapter 2. Indeed, we found differences in

performances between young and old adults, and a modelling approach could try to characterise this disparity.

To complete those objectives, this chapter will first create a model expanding on the previous ones published in the literature. Specifically, it will try to overcome the issues facing Zhang's model (1996) that could not efficiently study ageing. Next, an exploration of different noise sources will investigate their impact on the shape and behaviour of the tuning curve. Finally, this study will model the behavioural experiment carried out during Chapter 2 and examine if it can replicate the results between young and old adults by changing the noise levels. We end with an outlook on further analyses and modifications of the model.

4.2 Materials and Methods

4.2.1 The base HD attractor model

Researchers have modelled the HD system using a continuous ring attractor network in several studies exploring the properties of the system. These models date back to the seminal work by Zhang (1996), using a single attractor ring. More recently, different ring architectures were developed to characterise the addition of inputs to the system (Bicanski and Burgess, 2016; Page and Jeffery, 2018; Yan et al., 2021).

Our model used a 3-ring architecture (Figure 37A) and separated excitatory and inhibitory connections to follow Dale's principle that a neuron could not have both (Eccles, 1976). Lesion studies showed that the generation circuitry would be located in the LMN (Blair et al., 1998; Bassett et al., 2007; Sharp and Koester, 2008), so we implemented two rings mutually supporting each other. Those two rings would project inhibitory connections to a third ring situated in the ADN either on its left side

(clockwise (CW)) or its right side (counterclockwise (CCW)). The ADN ring would back-project excitatory connections to those rings. To calculate the neural dynamic, we used a firing-rate neuron model to model the activation of each neuron u within each ring as follows:

$$u_{new} = u_{old} + \frac{dt}{\tau} k \quad \text{with } k = I - w * u_{other} \quad (1)$$

where the new activation u_{new} was calculated for each time step t and its time constant τ . The equation input used the previous activity state u_{old} , any additional current I and the connections to other neurons u_{other} multiplied by a weight w positive for excitatory or negative for inhibitory. Activation is mapped to the firing rate with a sigmoid transfer function:

$$f_{u_{new}}(t) = \frac{1}{1 + e^{-\alpha(u_{new} - \beta)}} \quad (2)$$

where α and β determine the sigmoid shape. This sigmoid normalises the firing rate to range from 0 to 1 (Figure 37C).

Connections weights followed a Gaussian distribution (Figure 37D). It was centred for the excitatory ring and shifted to the right for the CW ring and the left for the CCW ring. Three individual factors controlled the level of the weights of each ring so their contributions could be increased or decreased. Since AHV cells (Stackman and Taube, 1998; Bassett and Taube, 2001) were not explicitly modelled, the activity packet was translated by changing the inhibitory factors. Indeed, those factors could be manipulated by increasing the factor in one ring (e.g. CW) and decreasing it in the other (e.g. CCW). This imbalance between those factors would allow the bump to translate in the direction where the inhibition is the least (in the example, the CCW

direction). Then, we fitted incremental changes in inhibitory factors to obtain different translation speeds. The resulting speed profile of the bump of activity was computed to obtain the differences in inhibitory factors (ΔF_{inh}) for changes in the angular head velocity of the agent (V_{ang}):

$$\Delta F_{inh}(t) = \sqrt{a + b * V_{ang}} + c \quad (3)$$

where parameters a , b and c scaled the function to match the physical head velocity changes and the rotational speed of the bump.

The activity bump was generated and maintained by sending background drives in all three rings. The background drive followed a probability mass function similar to a Poisson distribution. This input is thought to mimic the signal received from the vestibular system as lesions to the vestibular organs extinguish the HD signal (Stackman and Taube, 1997; Stackman et al., 2002). In addition, we modelled the visual input as described in Bicanski and Burgess (2016), where a separate ring had a one-to-one connection with the excitatory ring (Figure 37B). Those connections allowed the stabilisation of the signal by sending a small current to the neurons in the excitatory ring that are associated with the current heading of the agent. This approach aligned with previous works investigating the importance of vision and landmarks to keep the HD signal stable over time (Bicanski and Burgess, 2016; Page and Jeffery, 2018; Yan et al., 2021).

To calculate the HD over the neuron assembly firing rate, we used a similar equation to Song and Wang (2005):

$$\theta(t) = \arctan\left(\frac{\sum_i^N r_i \sin(\vartheta_i)}{\sum_i^N r_i \cos(\vartheta_i)}\right) \quad (4)$$

where $\theta(t)$ is the estimated population HD of the neuron assembly N at time t , r is the rate value of the neuron i and ϑ is its preferred heading direction. This equation allowed the model to calculate the HD of the agent during the simulations.

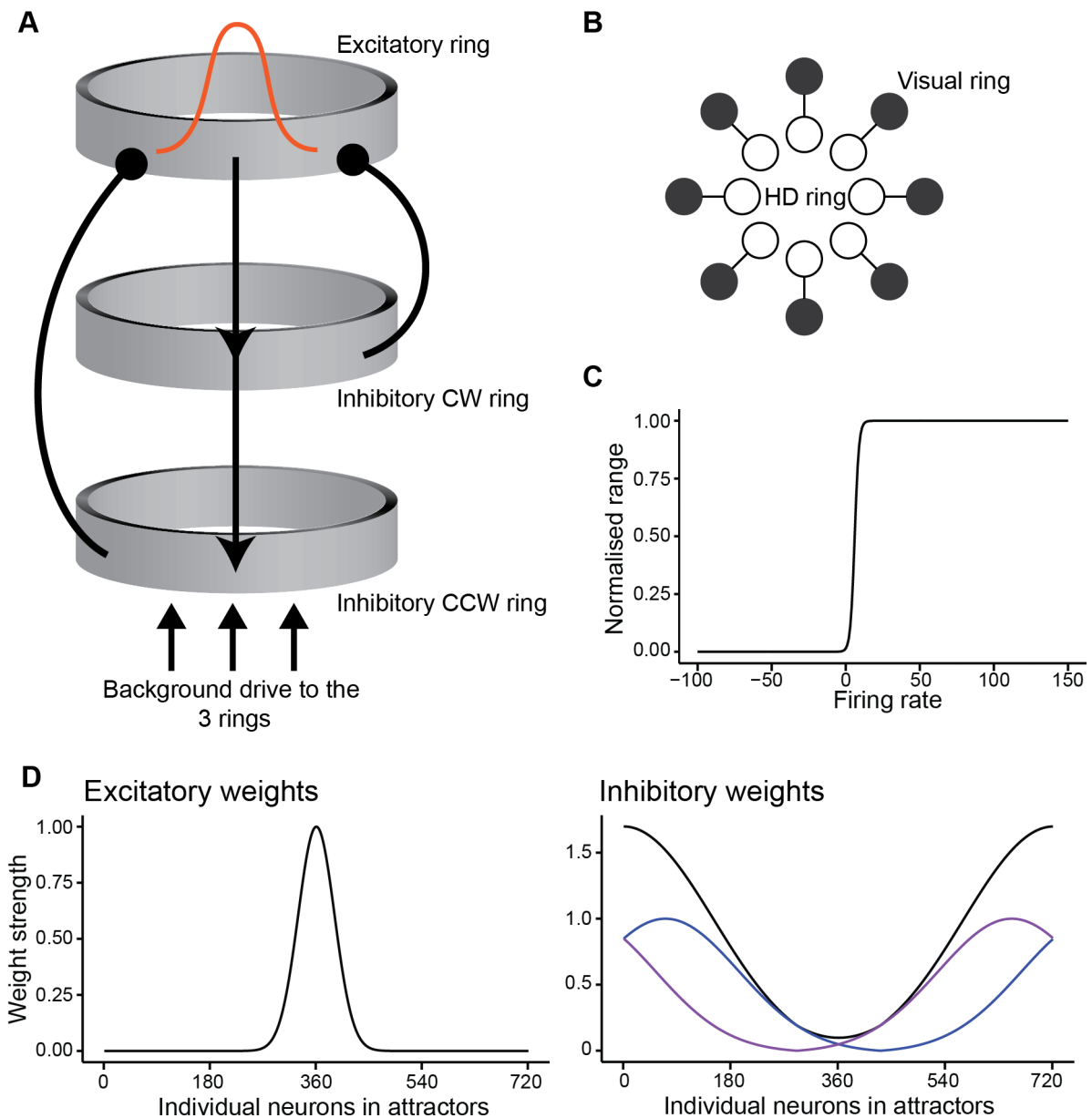


Figure 37: Architecture of the model.

A, the 3-ring structure with one ring sending excitatory connections to 2 separate rings that are sending back inhibitory connections either to the left (CCW) or right (CCW) side. Background drive is sent to each ring. *B*, the visual ring with one-on-one connections to the excitatory HD ring. Panel adapted from Bicanski and Burgess (2016). *C*, sigmoid function transforming the firing rate to a normalised range. *D*, excitatory (left) and inhibitory (right) weights distributions for one neuron to the other neurons. For inhibitory weights, blue corresponds to CW, purple to CCW and black to a combination of both sets of weights.

Finally, we implemented Zhang (1996) model by using the code from Yan et al. (2021) to compare it to the one developed in this study. In this continuous attractor network architecture, neurons had excitatory recurrent connections. The self-connection maintains the HD signal without external inputs such as the background drive. For more details about its implementation, see Yan et al. (2021).

Parameters	Values for 361nn	Values for 721nn
Number of neurons on each ring	361	721
τ	0.04	0.04
dt	0.002	0.002
α	0.7	0.7
β	6	6
a	146.20	1.36
b	47.70	2.49
c	-12.09	-1.17
Factor Excitatory	0.45	0.225
Factor Inhibitory CW	1.15	0.575
Factor Inhibitory CCW	1.15	0.575
Factor Feedback	5	5
Background drive Excitatory	28	28
Background drive Inhibitory	0.15	0.15

Table 4.1: Model parameters for the 361 and 721 neurons networks.

4.2.2 Source of noises

We implemented different noise sources to characterise the model and changed their values before running any simulation. The first source was related to the amount of noise added within the Gaussian distributions of the weights. The second source was associated with the background drive. Lastly, we implemented neuron death by

randomly deleting neurons on the three rings. A dead neuron would lose all its connections with other neurons and have a firing rate of 0 during the whole simulation.

4.2.3 Modelling of the HD behavioural task

In addition to the basic model, we decided to implement the task participants performed in the study from Chapter 2. For simplicity, the agent stayed static at the centre of the environment the whole time. The arena with the colour gradient was achieved by linking the colours to the visual ring. We hypothesised that the agent could (re)orient itself when looking at the colours like participants. In addition, the agent knew it was facing the landmark when the activity bump of the excitatory ring was within 356° to 4° since every participant learned the position with an accuracy of 8° . The model computed the agent's physical heading and the HD of the neuron assembly at every step during a simulation.

We separated each trial into six different phases (Figure 38). A, the agent fixed the same heading for one second to allow the realignment between the physical heading and the activity bump. B, the agent rotated to face the starting orientation. C, the agent faced the same orientation for one second to let the bump stabilise after the rotation. D, the arena disappeared, and the participants rotated by a given amount. E, the delay condition happened where the agent remained stationary for either 20 seconds (the delay condition) or 1 second (the no-delay condition). F, the agent rotated until the activity bump was aligned with the landmark. Then, the agent's physical heading was recorded to measure the absolute angular error of the trial.

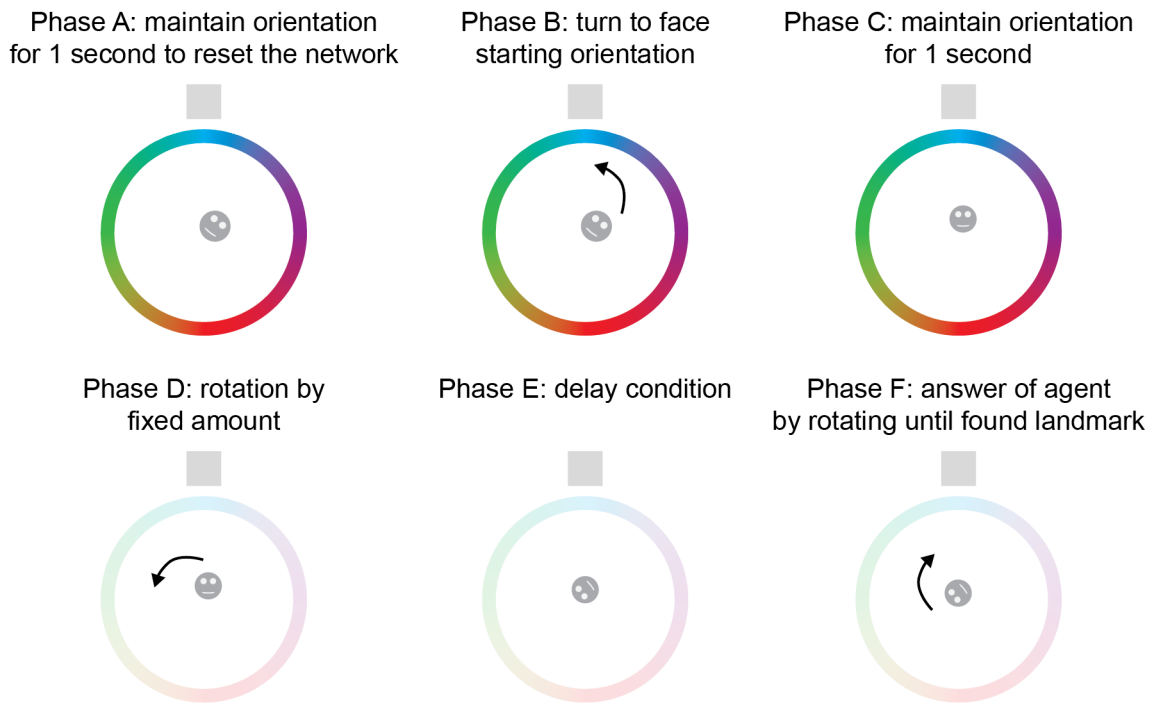


Figure 38: Task phases performed by the agent during a trial.

The virtual agent followed six phases to replicate the trials participants performed in Chapter 2. The agent always knew the position of the landmark (grey square) and could see the arena (coloured ring) during phases A, B and C. During those phases, the agent knew its rotation from visual ring inputs.

During phases A, B and C, the excitatory ring received visual inputs since the arena with the colour gradient was present in the task. The arena was absent for phases D, E and F, so the excitatory ring did not receive visual inputs. However, it maintained one-to-one connections with the visual ring to update its orientation to follow the HD bump of the excitatory ring. The goal was to have the agent estimate the colour it was facing, similar to the strategy reported by participants in Chapter 2.

Each agent had a trial sequence that used 30 unique trials with the following combination of expected amounts to answer: 0° , 40° , 90° , 135° and 180° , delay: 0s and 20s and first turn: 50° , 105° and 160° . Every trial was done two times for a total of 60 trials. The order of the trials was shuffled across agents. Importantly, the model did not reset the rate of each ring between two consecutive trials, and the starting heading

of the agent was the last one from the previous trial. This way, the visual feedback at the start of the trial had to reset the agent heading with the HD ring heading.

In addition, we wanted to match the agent velocities to the ones produced by the participant from the behavioural experiment. We created two distributions by calculating the velocity when participants performed the first turn (phase D) and while answering (phase F). Those distributions included both young and older participants. After calculating those distributions, we removed the 5% most extreme values on each side of the distributions to avoid outliers (Figure 39A-B). At the start of a trial, the model randomly picked a value from the two distributions. In addition, during the answer phase, participants could either rotate back toward the starting orientation (i.e. at phase C) or continue in the same direction and complete the circle. We computed the percentage of chance participants used one strategy over the other, and each agent followed one of those percentages (Figure 39C).

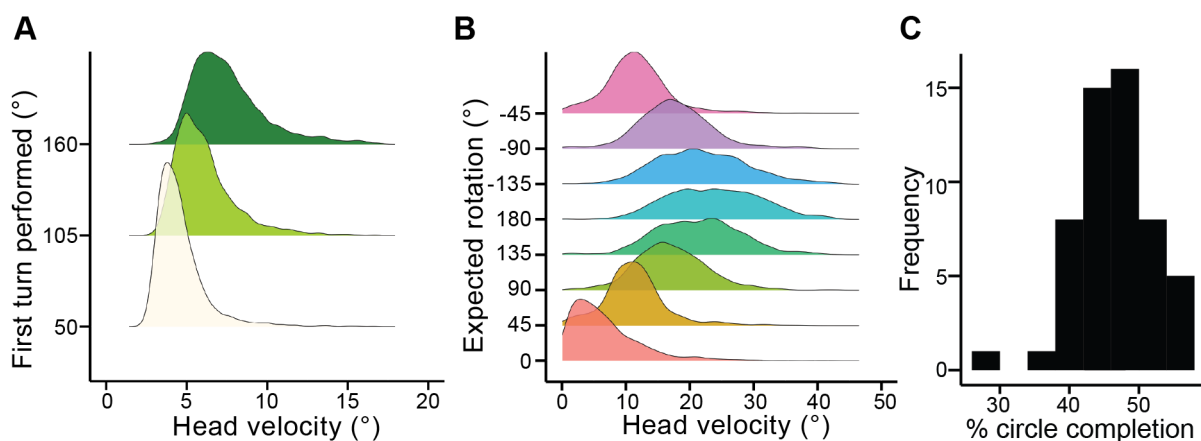


Figure 39: Participant distributions used in the model.

Head velocity distributions of participants separated by (A) the first turn performed and (B) the expected rotation to the landmark. C, percentage of time participants performed a full circle while answering.

4.2.4 Processing and Analysis of the Simulations

We investigated if the base model could follow heading trajectories. The goal was to test whether this speed profile allowed the model to follow a trajectory when changes in velocity occurred. To test this, we sampled trajectories of four minutes from four participants, two young and two old, during the learning task. Then, we calculated the cumulative drift occurring during the trajectory by computing the difference between the agent's physical HD and the activity bump's HD. We ran trajectories under two conditions, with and without visual input. We also compared when the model had no noise or a small amount of weight noise (2.5%).

Next, we tested the impact of neuron death in Zhang's model and ours. Indeed, Zhang (1996) discussed the impact of noise on weights but not neuron death in his study. We included a single dead neuron for Zhang's model and 1% for our model while creating a constant small velocity input. Each simulation ran until the HD bump completed an entire loop or until the bump flattened. Then, we plotted the trajectory of the bump over time while checking when it was passing near a dead neuron.

In addition, the sources of noise were systematically characterised across a suitable parameter range (Table 4.2). Each simulation lasted one minute, and the model received no velocity or visual input. Then, we extracted several measures from those simulations: the excitatory tuning curve's shape and the activity bump's HD, FWHM and peak rate over time. We also ran 50 simulations with a more comprehensive set of noise levels to explore their influence on the accumulation of drift, FWHM and peak rate in more detail (Yellow cells in Table 4.2). We assessed the presence of drift by looking at three measures: the accumulation of drift between every step, either signed or absolute values, and the maximum separation between the initial and final HD. For

the BG, due to the erratic bump shape, a Gaussian function was fitted on top of the bump to calculate the FWHM and peak rate on the fitted curve.

Weight noise	Background noise	Neuron death
0	0	0
5	10	5
10	20	10
15	30	15
20	40	20
25	50	25
30	60	30

Table 4.2: Percentage of noise for individual static simulation (rows) for each type of noise (columns). White cells, simulation ran only for analysis of the shape of the tuning curve.

Moreover, a separate analysis investigated neuron death during the behavioural task simulation. Indeed, we found that with enough neuron death, the network drifted to reach a stable position and would get stuck in local minima. The activity bump could move and continue its translation only with a substantial velocity input into the network. During the behavioural task, the velocity distribution differed for each orientation faced by the agent before answering (i.e. rotation to performed, Figure 39B). On average, 180° orientations had a faster velocity than orientations such as 45° or 0°. In this analysis, the behavioural task was run using the same first turn (105°). One hundred agents with damaged ring attractors repeated each condition three times. The conditions varied the number of neurons in each ring (361 or 721) and the neuron's death (1% to 15% for 361 neurons and 1% to 30% for 721 neurons). The velocity during the answer phase varied by calculating the average value and decreasing or increasing the value by adding one or two standard deviations. For each trial, the simulation ran until an answer was given by the agent or

until the activity bump got stuck in local minima at a position while answering. Then, we computed the probability of trials getting stuck in local minima across conditions.

Finally, we investigated the impact of the noise sources on the performance during the behavioural task. For each set of noise (Table 4.3), 30 agents performed the task and used the modified trial sequence while the individual noise levels were modified (Figure 38). Then, we extracted several measures for the different phases of the trials. We defined the angular error as the angular difference between the HD of the agent and the one of the bump. Those values were extracted at the end of each phase (Figure 38). In addition, we calculated the rate of change by computing the velocity of the HD of the agent and the bump. Then, the values were subtracted from each other and averaged for each phase. The final rate of change values would either be positive if the agent's velocity was faster or negative when the velocity of the bump was faster on average.

Weight noise	Background noise	Neuron death
0	0	0
5	5	1
10	10	3
15	15	5
20	20	7
25	25	10
30	50	13

Table 4.3: Percentage of noise for individual task simulation (rows) for each type of noise (columns).

4.3 Results

The model can follow trajectories from human participants.

After creating the model, we tested whether the HD of the excitatory bump followed changes in velocity and direction similar to participants. We extracted movement trajectories of two minutes from four participants (two young and two older). Our model followed trajectories without drift when the visual feedback was present (Figure 40). However, when removing the visual feedback, drift accumulated between the real HD and the HD of the attractor.

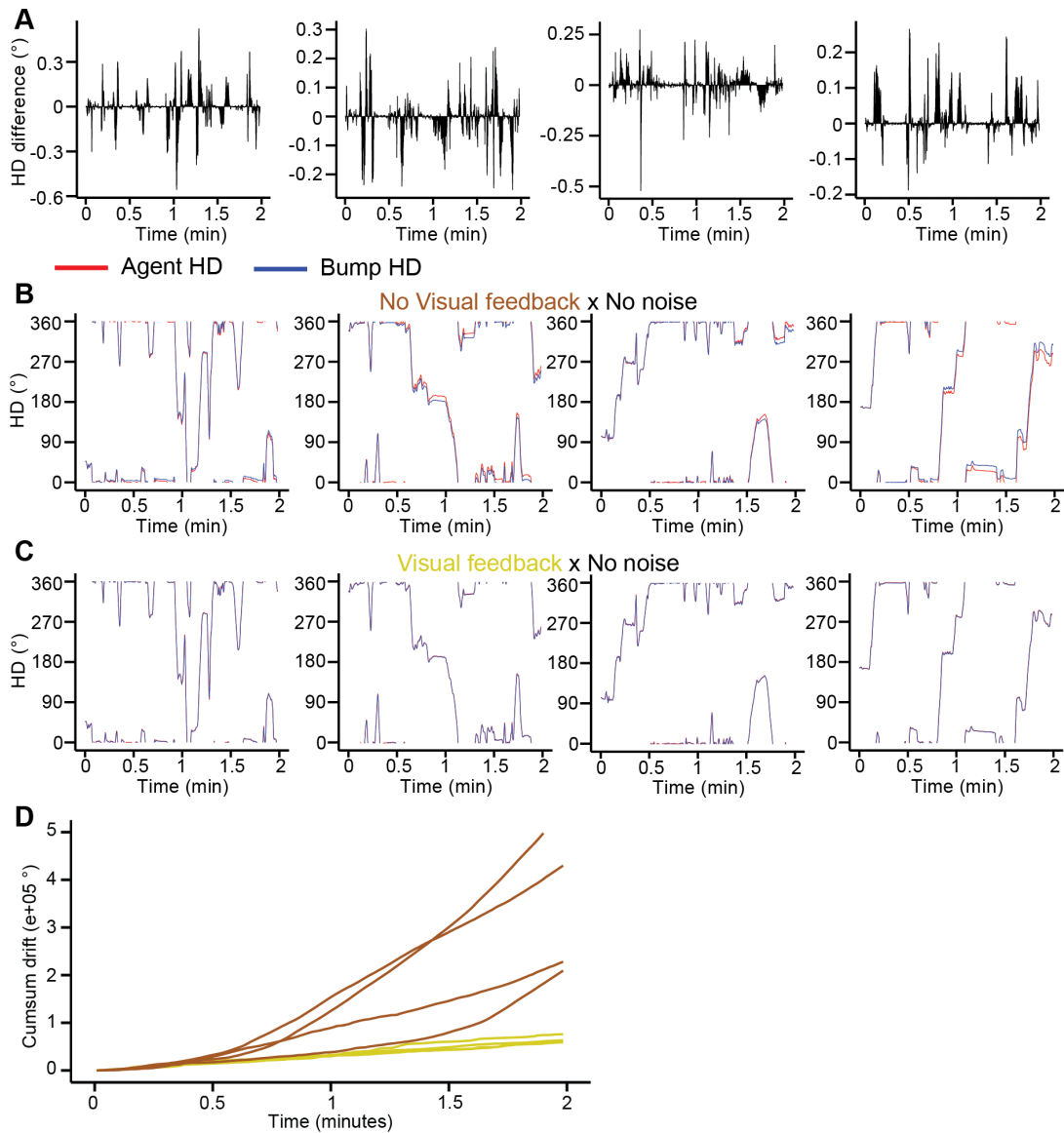


Figure 40: Human trajectory followed by the model and measure of drift.

A, velocity profile of four trajectories taken from participant data (2 young and 2 older adults). B-C, trajectories performed by the agent when visual feedback was present (B) or not (C). The red lines correspond to the real heading trajectory of the agent and the blue lines correspond to the HD bump. D, cumulative sum of drift between the agent heading and the bump heading.

Zhang's model cannot accommodate neuron death.

One way to model the effects of ageing is to increase the noise level in the model. We included three distinct sources of noise: weights, neurons and background drive. In his seminal study, Zhang's model only investigated the effect of noise on the weights but did not assess the impact of neuron death (Zhang, 1996). Therefore, we replicated his model, removed a single neuron from the attractor (red line in Figure 41A), and let the bump move in one direction. We found that when the bump reached the dead neuron, the bump would collapse, and the signal would flatten (Figure 41A). This result provided evidence that Zhang's attractor stopped functioning when a minor disruption occurred. We performed the same simulation with our model while having 1% of neuron death (red lines in Figure 41B). The simulation showed that the bump completed a full circle by passing through the dead neurons without getting flat (Figure 41B).

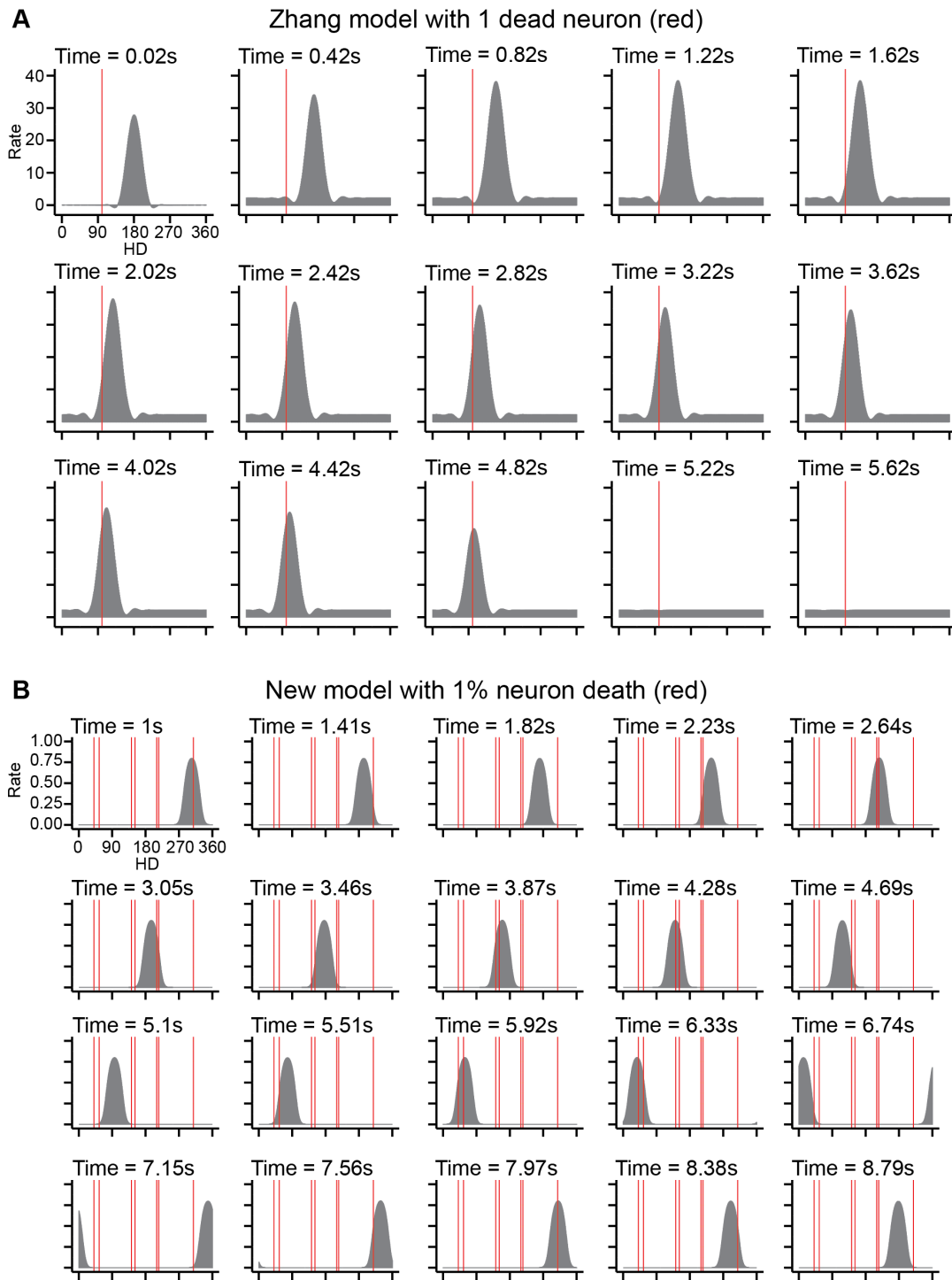


Figure 41: Simulation of Zhang and new model with the addition of neuron death.

A, simulation of Zhang attractor model after removing a single neuron (red line) and letting the bump move in one direction. Upon reaching the dead neuron, the bump collapsed. *B*, simulation of the model developed in this chapter after adding 1% neuron death (red lines). The bump passed all dead neurons and maintained its shape.

The noise types influence differently the shape and stability of the HD bump.

Next, we looked at the influence of individual noise on the shape of the bump when the state was at rest for simulations of two minutes. For the noise of the weights, we found a fuzzier bump and the heading would move to another position after a few seconds. (Figure 42A). There was no consistent drift for the background drive, but we observed a fuzzier bump leading to the HD, FWHM and peak to jitter (Figure 42B). For the neuron death, the shape of the bump got wider (from 47 for 5% to 68 for 20%), and we noticed that it moved to another position after a few seconds, similar to weight noise (Figure 42C).

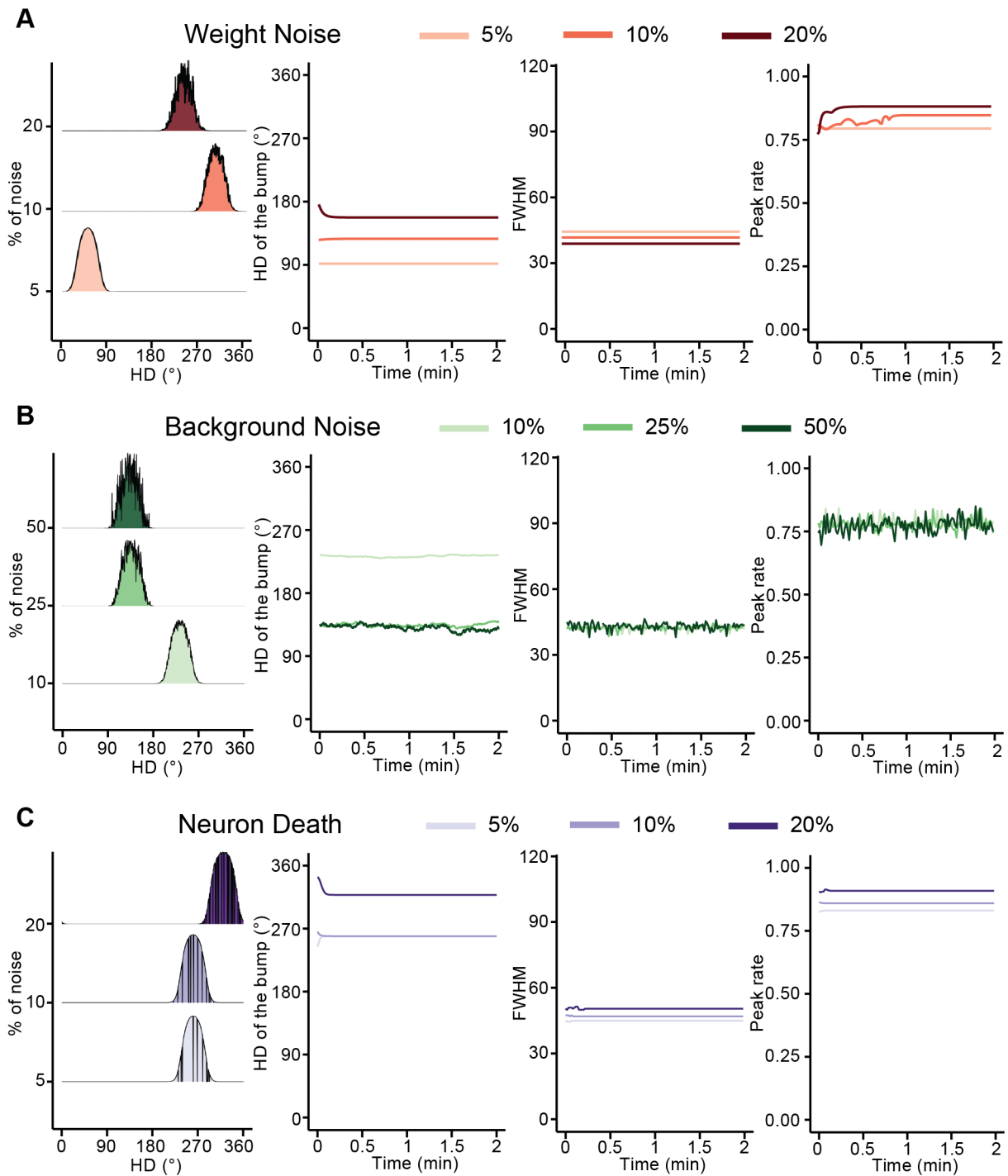


Figure 42: Influence of noise levels on the shape of the tuning curve.

Left to right, tuning curves from the excitatory ring for different noise levels after 1 minute of simulation; the HD over time; the FWHM over time; and the peak rate over time. These measures were calculated for (A) noise on the weights, (B) noise in the background drive and (C) neuron death. Simulations lasted 2 minutes, and no velocity input was given.

To characterise those changes further, we ran 50 simulations to obtain a broader range of noise levels. Each simulation lasted two minutes and did not include velocity input. For weight noise, the cumulative sum of changes indicated a random drift to a stable position (Figure 43A). The FWHM stayed the same but the peak rate reduced for higher weight noise values (Figure 43A). Next, we increased the levels of background drive noise and found that the absolute cumulative sum was greater than the step cumulative sum (Figure 43B). We also observed a larger amplitude in the maximum separation over higher noise levels (Figure 43B). This result is linked to the erratic shape and signal seen in Figure 43B. Finally, when increasing the percentage of neuron death, we did not find a specific pattern of change in HDs (Figure 43C). However, we found the same pattern of random drift to a stable position as weight noise, as seen in Figure 43C. In addition, we noticed a significant increase in FWHM for large neuron death percentage (Figure 43C).

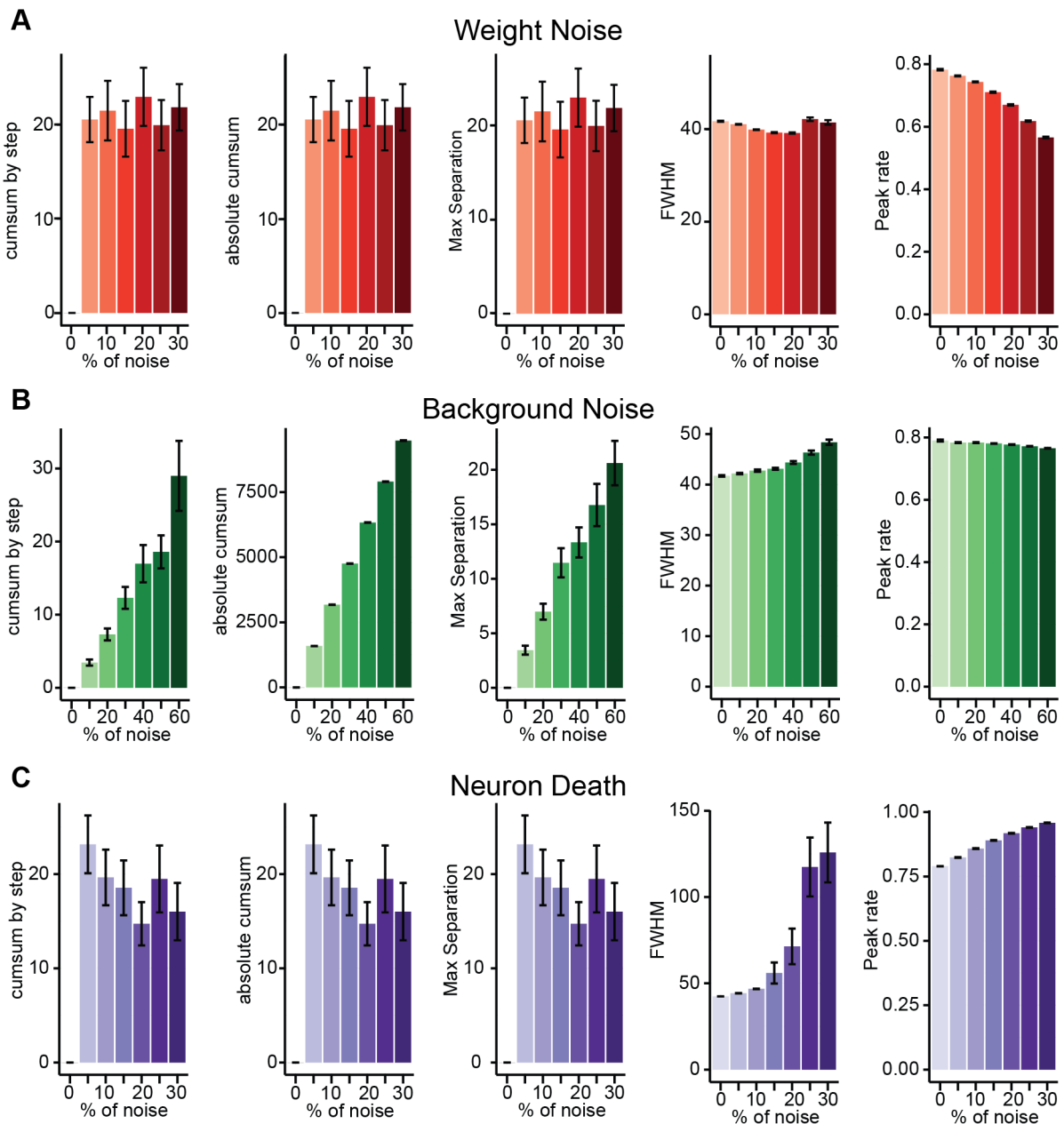


Figure 43: Influence of noise levels on the behaviour of the HD model.

Left to right, the cumulative sum of HD changes over simulation steps; the absolute cumulative sum of HD changes; the separation from the initial HD and the final HD; the average FWHM; the average peak rate. These measures were calculated for (A) noise on the weights, (B) noise in the background drive and (C) neuron death. Simulations lasted 2 minutes, and no velocity input was given. The black lines represent the standard error.

Neuron death reduces the responsiveness of the HD network at low velocities.

After looking at the model from a static perspective, we investigated its behaviour while it performed the behavioural task from Chapter 2. The agent completed trials similar to actual participants, with rotations with and without visual feedback and answering to face the learned direction (for more details, see the Methods section from Chapters 2 and 3). The static simulation results suggested that the bump started to move and reach a stable position with increased neuron death. Indeed, the attractor was not continuous anymore, and the initial HD settled into a local energy minimum of the network (Brody et al., 2003). Therefore, we explored if it happened during the task simulation where velocity inputs are present. We quantified this measure by calculating the probability of the bump getting stuck in local minima and not moving for at least one second while a velocity input was present (i.e. during the answer phase).

Our results indicated that the probability of getting stuck in local minima increased when incrementing neuron death (Figure 44A). This effect was attenuated when we added more neurons within each attractor and kept the percentage of dead neurons constant (Figure 44A). By doubling the number of neurons in the network (from 361 to 721), we obtained the same distribution and range of values when the percentage of neuron death doubled (maximum from 15% for 361 to 30% for 721, Figure 44A).

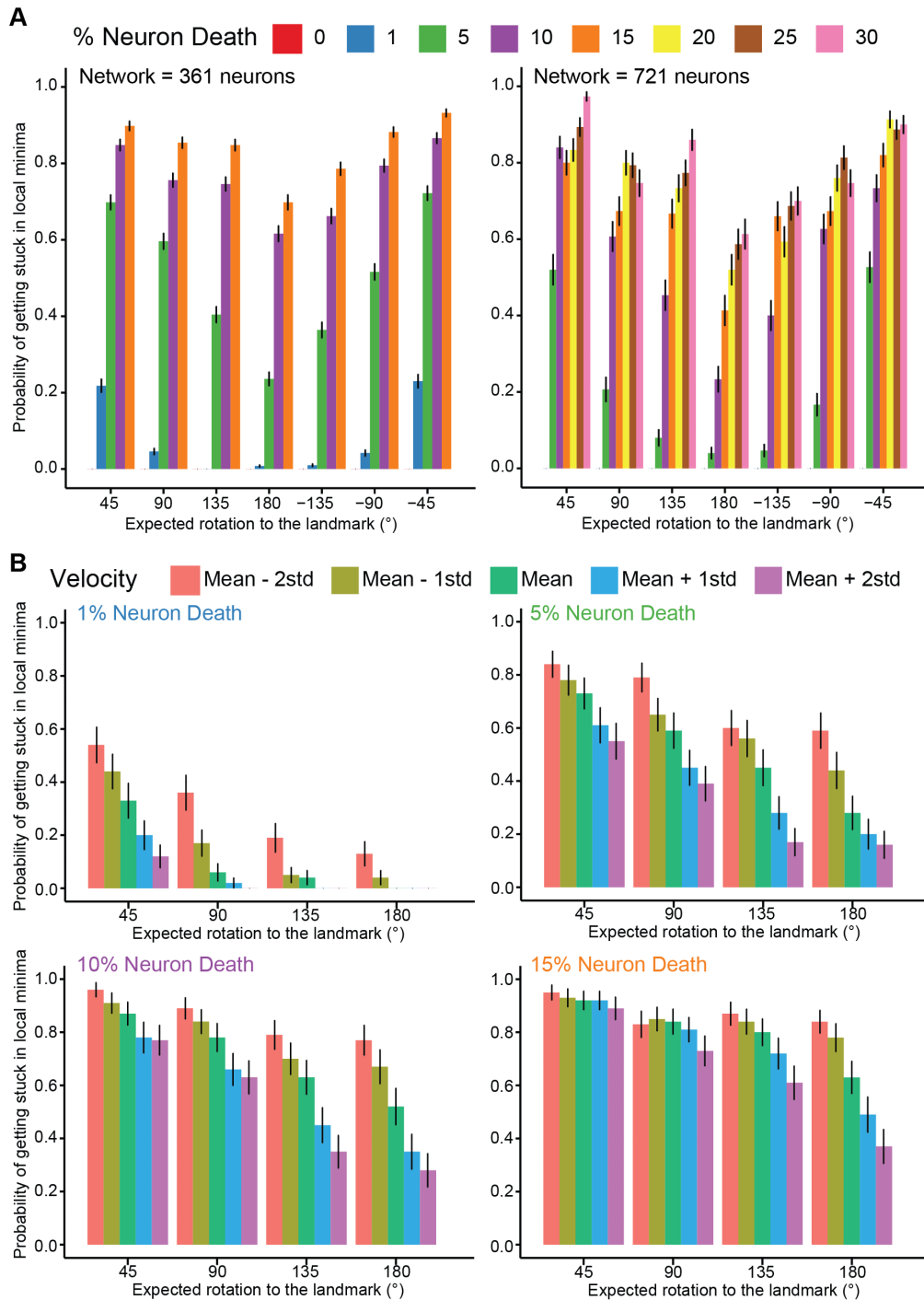


Figure 44: Probability for the attractor to get stuck in local minima when performing the task.

A, average probability for the attractor with (left) 361 and (right) 721 neurons separated by expected rotation to the landmark. The maximal percentage of neuron death was set to 15% for 361 and 30% for 721 neurons. *B*, average probability for the attractor with 361 neurons separated by expected rotation to the landmark. The different colours represent the velocity used during the answer phase. Neuron death was set to (top left) 1%, (top right) 5%, (bottom left) 10% and (bottom right) 15%. The black lines represent the standard error.

Finally, we found a link between the probability of getting stuck in local minima and the velocity input received. Indeed, the mean velocity value across the rotations during the answer phase differed. For example, this value was larger for rotation at 180° than for 45° (see Figure 39B). Hence, we observed an inverse bell-shape distribution where the probability was lower for 180° rotation and increased for 45° (Figure 44B). In addition, we also varied the velocity values for the rotation performed and found that for slower velocity, the probability of getting stuck in local minima was higher than for faster velocity (Figure 44B). This observation was the same for the different levels of neuron death percentage (Figure 44B).

The noise types influence differently the agent performance on the behavioural task.

Lastly, we tested the effect of individual noise type while the agent performed the behavioural task. Due to the complexity of a single trial, we took timestamps from the end of the different trial phases (Figure 38). Each trial started with active visual feedback to allow the bump to reset to the same heading as the agent's (Phase A, timestamps -1 to 0). Next, the agent rotated to face the starting orientation (Phase B, timestamps 0 to 1) and waited a second in this orientation (Phase C, timestamps 1 to 2). Then, the first turn started (Phase D, timestamps 2 to 3), followed by the delay condition (Phase E, timestamps 3 to 4). After the delay, the agent rotated to face the landmark (Phase F, timestamp 4 to 5). To assess the impact of the noise, we calculated two measures and assessed their change throughout the trial for the different noise levels. First, we looked at the angular error by taking the difference between the agent HD and the bump HD at every timestamp. Second, we computed the average rate of change during every phase by looking at the difference in velocity

between the heading of the agent and the bump. We also looked at the influence of the delay condition by separating the data using this condition.

We compared the evolution of angular error over the trial across delay conditions and for each weight noise level. The resetting of the HD worked over trials until the weight noise was larger than 15%. This would suggest that some accumulation of error could happen for high noise levels, even with visual feedback present. We found increased angular error after the first turn (Phase D, Figure 45) and the answer phase (Phase F, Figure 45) for both conditions. In addition, the 20-second delay condition produced a larger error (Phase E, Figure 45). This was the case up to 15% weight noise where the difference between the conditions got minimal.

Furthermore, we noticed an overall increase in the rate of change at every phase without visual feedback (B, D and F) for higher noise levels (Figure 46). Additionally, the rate of change was negative during the delay phase (E) showing that the HD bump was drifting to another location while the heading of the agent remained static. This is an indication that the HD bump was moving to local minima, as found in the static simulations.

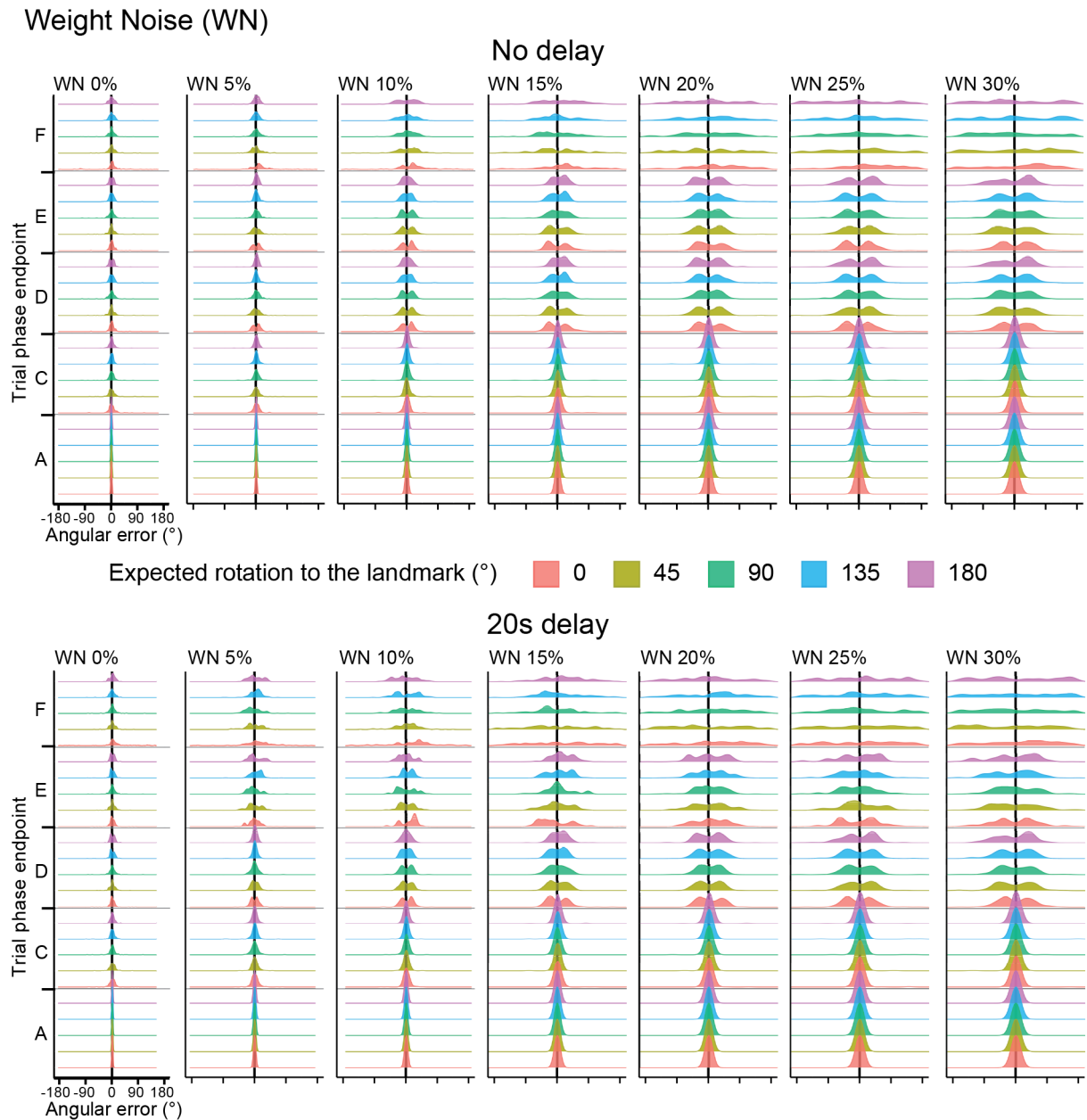


Figure 45: Evolution of the angular error over the trial phases for increased weight noise across delay conditions.

The density plots show the distributions of angular error measured at the end of the trial phases. The vertical black line represents 0° . The plots were separated by expected rotation to the landmark (colours), by phases (letters on the y-axis), by delay conditions (top - no delay, bottom - 20s delay) and by increased noise on the weights (columns). Phase A, reset of the network; Phase C, facing starting orientation; Phase D, performing the first turn; Phase E, delay condition; Phase F; answer from the agent.

Weight Noise (WN)

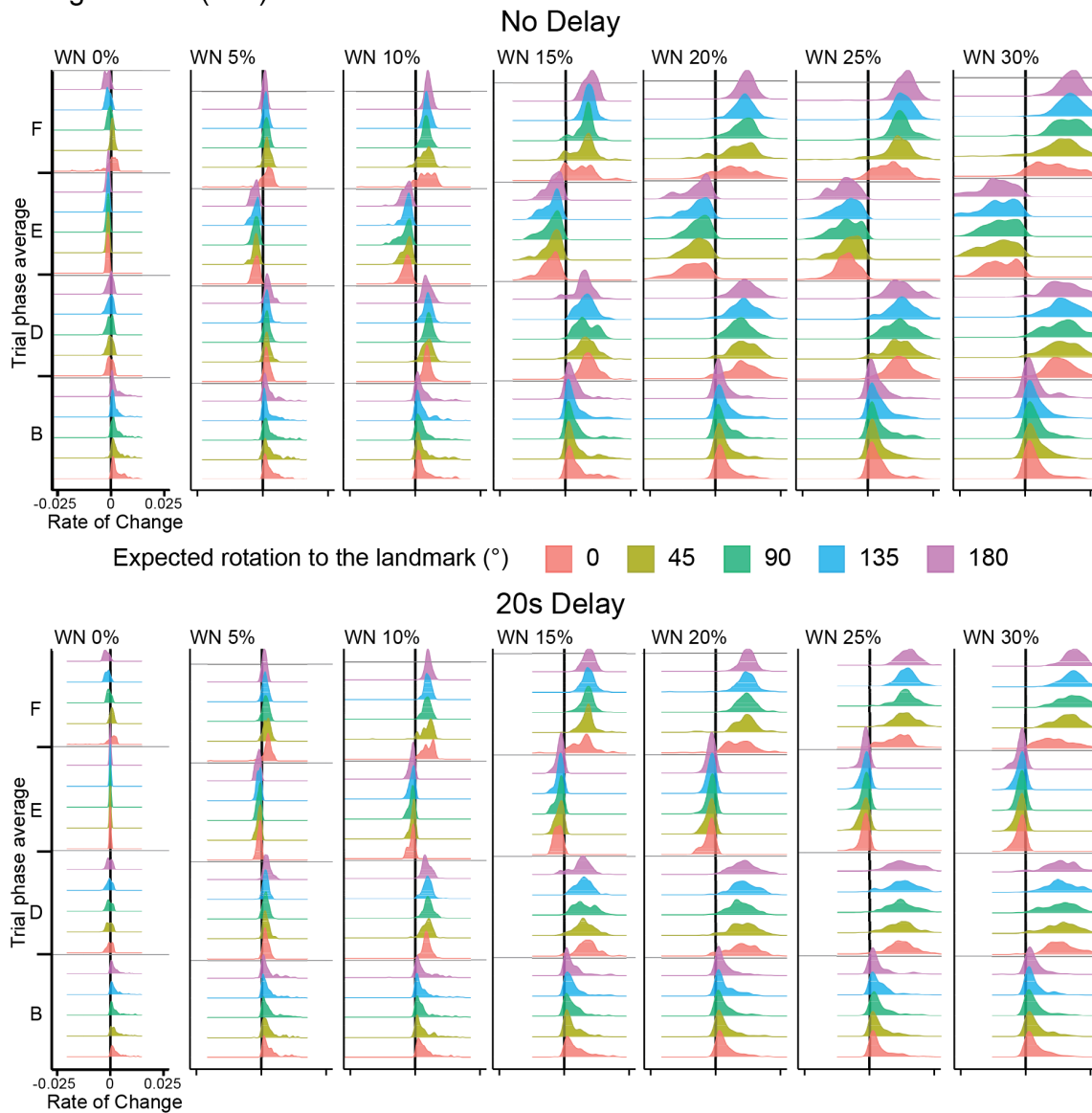


Figure 46: Evolution of the rate of change over the trial phases for increased weight noise across delay conditions.

The density plots show the distributions of the rate of change measured at the end of the trial phases. The vertical black line represents 0. The plots were separated by expected rotation to the landmark (colours), by phases (letters on the y-axis), by delay conditions (top - no delay, bottom - 20s delay) and by increased noise on the weights (columns). Phase A, reset of the network; Phase C, facing starting orientation; Phase D, performing the first turn; Phase E; delay condition; Phase F; answer from the agent.

We did not find a systematic increase in the angular error associated with higher background drive noise levels for both delay conditions (Figure 47). The spread of angular errors was due to the loss of visual feedback from Phase A to Phase C (Figure 47). However, we found a negative rate of change across the phases, with its fastest during the delay phase (E, Figure 48). This rate of change was due to the network's erratic bump, which had an unstable HD compared to the agent heading. Indeed, our static simulations showed that the HD of the bump varied across time while the average HD stayed at the same position. Those changes in HD would create faster velocity values than the agent's, producing the negative rate of change values in Figure 48.

Background noise (BG)

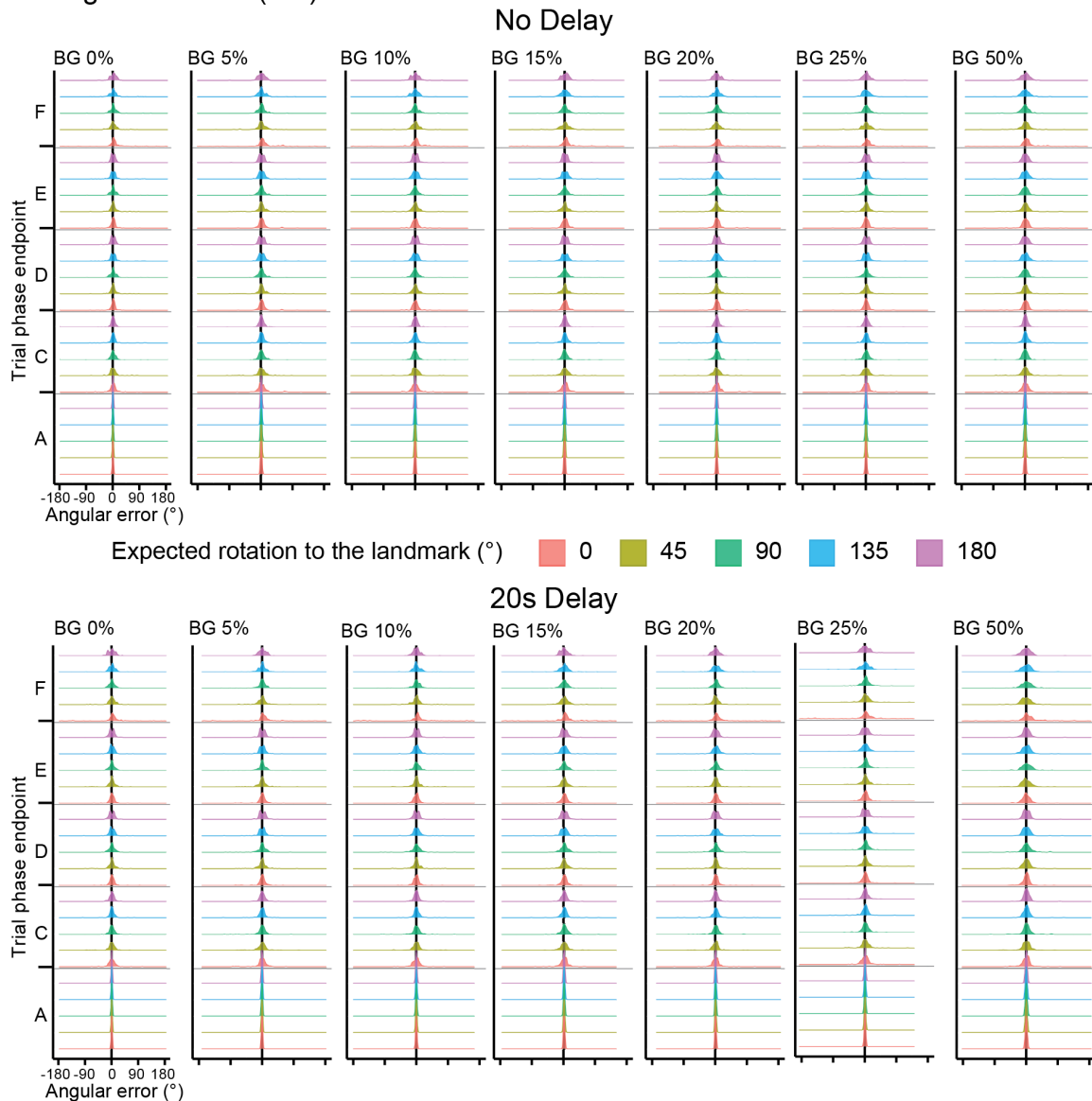


Figure 47: Evolution of the angular error over the trial phases for increased background noise across delay conditions.

The density plots show the distributions of angular error measured at the end of the trial phases. The vertical black line represents 0° . The plots were separated by expected rotation to the landmark (colours), by phases (letters on the y-axis), by delay conditions (top - no delay, bottom - 20s delay) and by increased noise on the background drive (columns). Phase A, reset of the network; Phase C, facing starting orientation; Phase D, performing the first turn; Phase E; delay condition; Phase F; answer from the agent.

Background noise (BG)

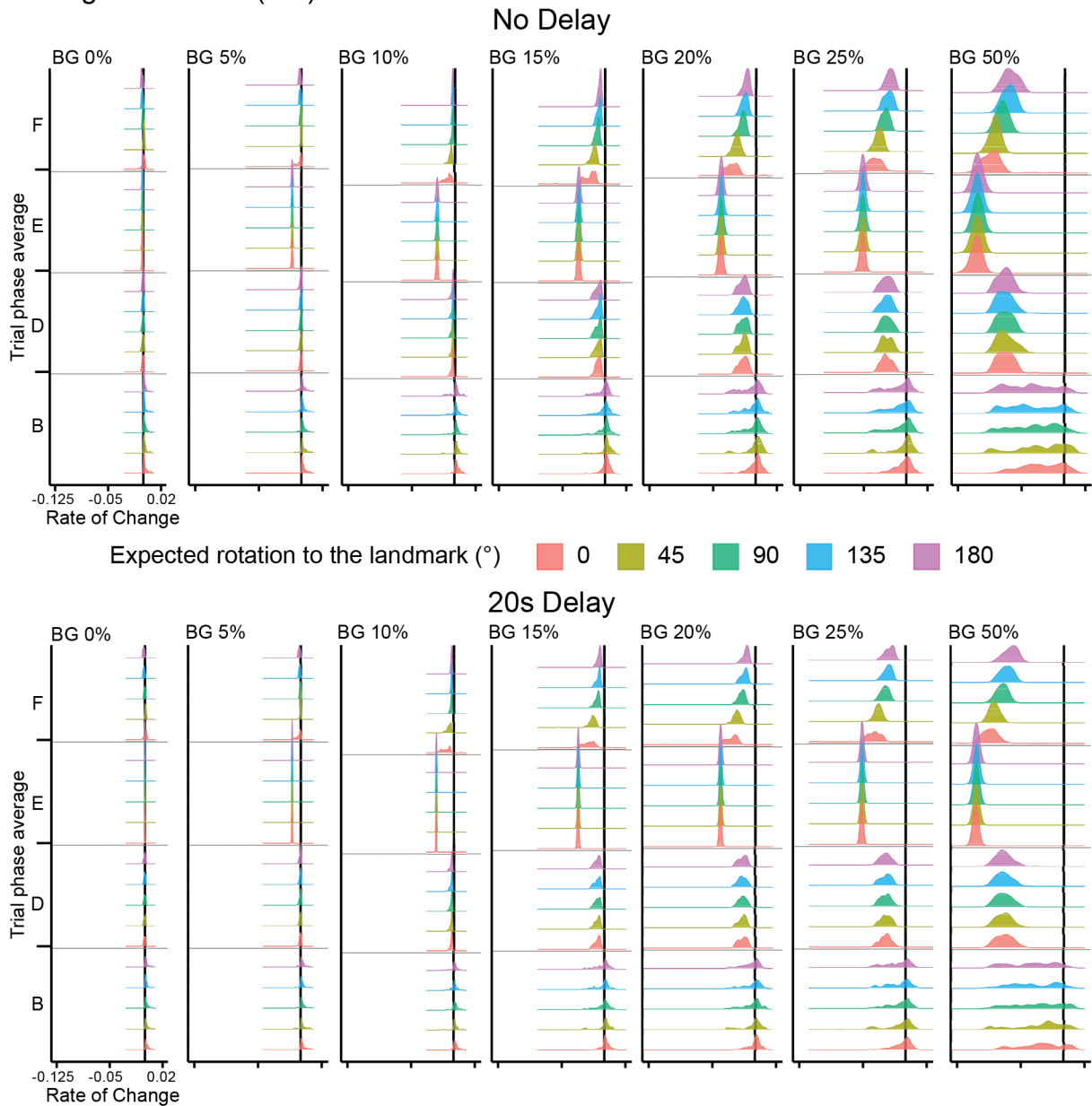


Figure 48: Evolution of the rate of change over the trial phases for increased background noise across delay conditions.

The density plots show the distributions of the rate of change measured at the end of the trial phases. The vertical black line represents 0° . The plots were separated by expected rotation to the landmark (colours), by phases (letters on the y-axis), by delay conditions (top - no delay, bottom - 20s delay) and by increased noise on the background drive (columns). Phase A, reset of the network; Phase C, facing starting orientation; Phase D, performing the first turn; Phase E; delay condition; Phase F; answer from the agent.

Finally, we assessed the impact of neuron death on the performance of the behavioural task. Our current model could not reset appropriately after each trial for large percentages of neuron death (e.g. 7% and higher). As seen in Phase A (Figure 49), some trials still had an error above 45° , with values reaching up to 180° , even when visual feedback was present. Those errors could lead to an accumulation of angular errors over the trials. In addition, we found a large spread of angular errors at every phase without visual feedback (D, E and F, Figure 49). From our previous simulation, we hypothesised that the spread came from the higher probability of getting stuck in local minima in the trials. Indeed, with a high neuron death and slow velocity, the HD bump can get stuck to some location within the attractor ring.

We found more evidence of the probability of getting stuck in local minima by analysing the rate of change in the different phases. During the delay phase (phase E, Figure 50), we noticed a constant negative rate of change where the HD bump would start to move to the stable position. Interestingly, the rate of change was faster and had a higher spread during the no-delay period compared to the 20-second delay. Since the measure was an average over the whole phase, it indicated that the bump did not reach the stable position during the no-delay and was still moving. During the 20-second condition, the bump had enough time to reach the position and stayed static, decreasing the average rate of change.

Further evidence from the answer phase (phase F) showed that most trials had a positive rate of change, especially for the 20-second delay (Figure 50). These results can be explained as only the agent HD moved while the HD bump was stuck in local minima. Lastly, the first turn phase (phase D) distribution was dispersed on both sides with positive and negative rate of change values (Figure 50). This range indicated that the bump was not stuck in local minima in every trial.

Neuron death (ND)

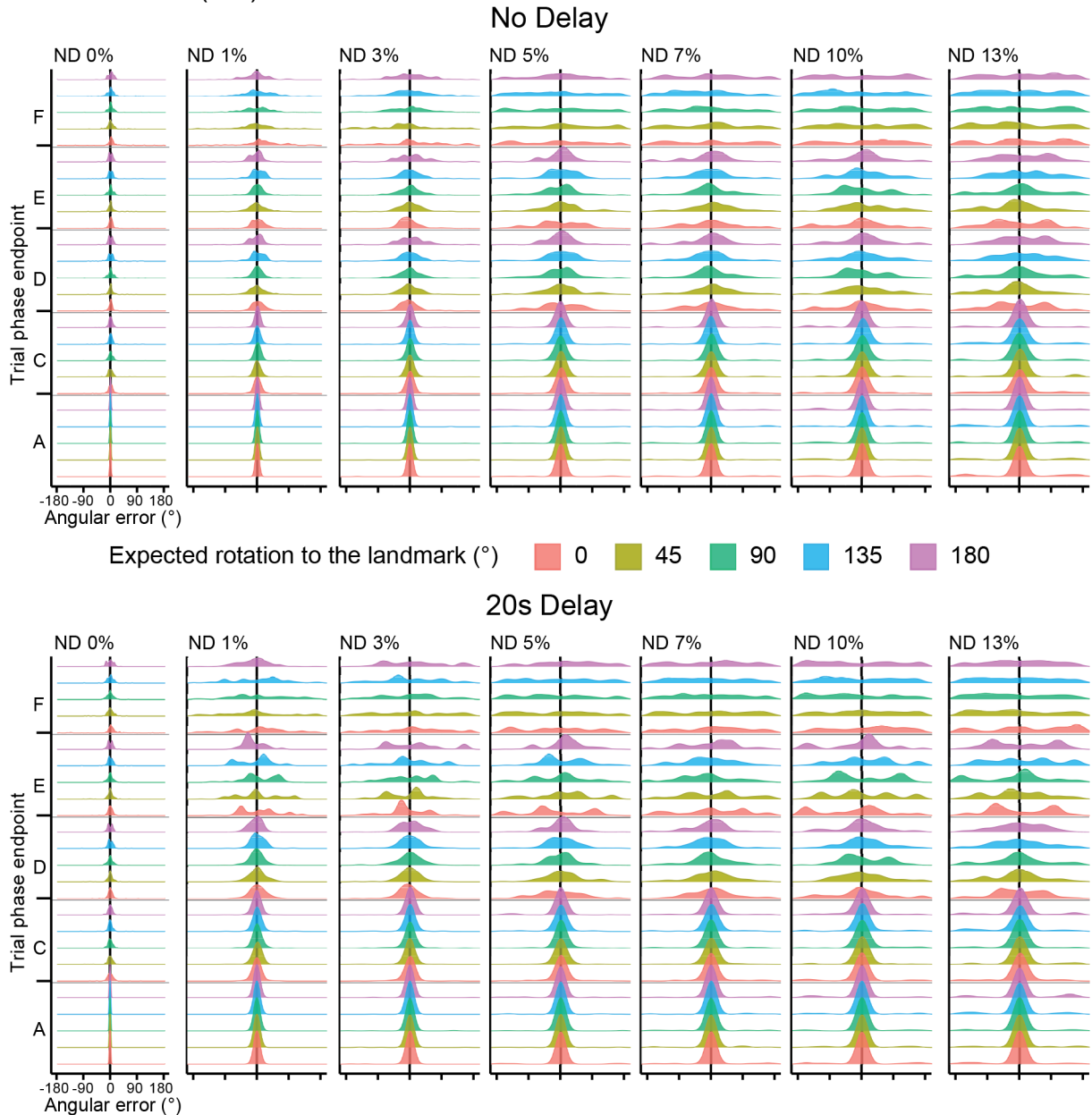


Figure 49: Evolution of the angular error over the trial phases for increased neuron death across delay conditions.

The density plots show the distributions of angular error measured at the end of the trial phases. The vertical black line represents 0° . The plots were separated by expected rotation to the landmark (colours), by phases (letters on the y-axis), by delay conditions (top - no delay, bottom - 20s delay) and by increased neuron death (columns). Phase A, reset of the network; Phase C, facing starting orientation; Phase D, performing the first turn; Phase E; delay condition; Phase F; answer from the agent.

Neuron death (ND)

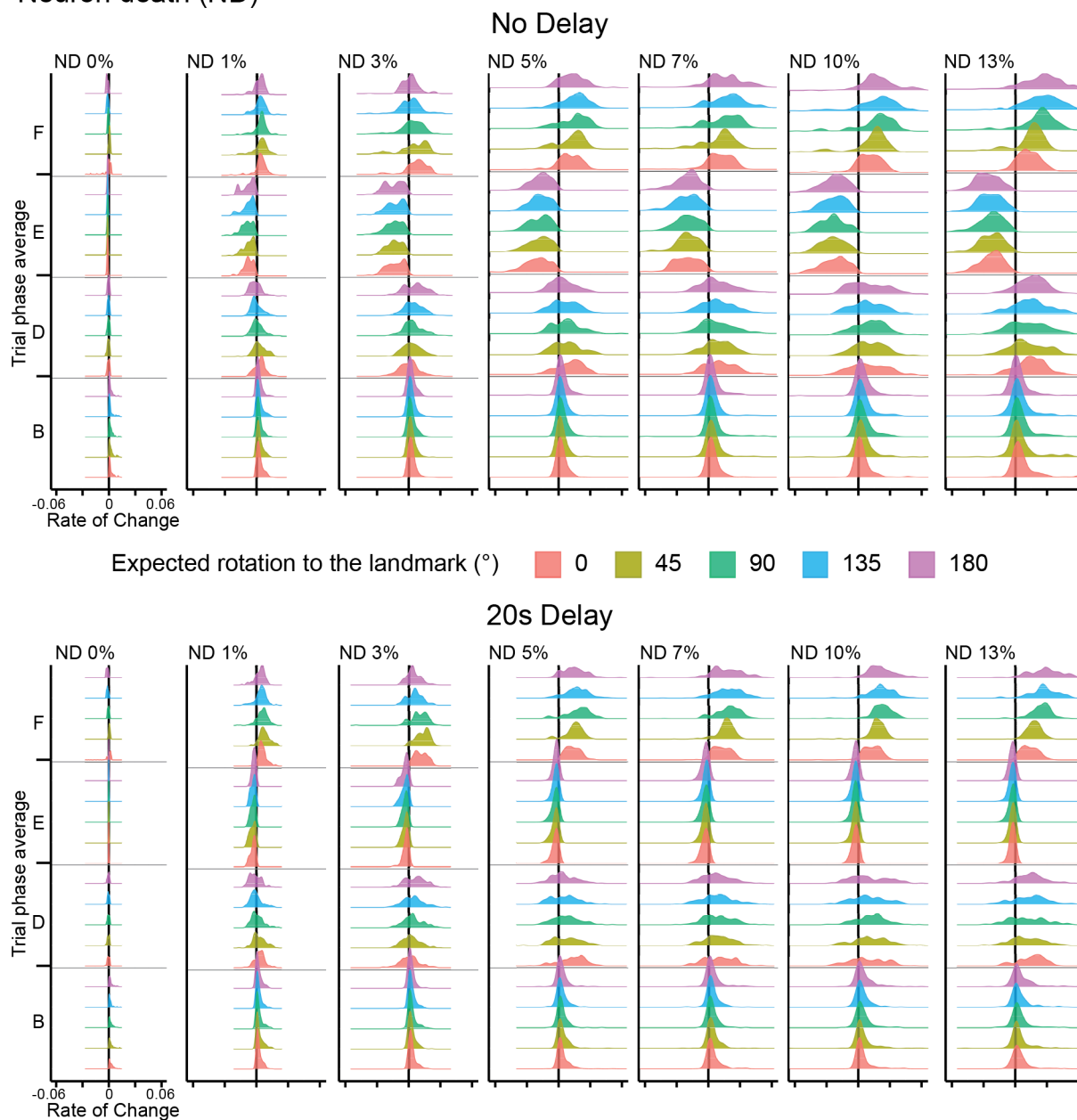


Figure 50: Evolution of the rate of change over the trial phases for increased neuron death across delay conditions.

The density plots show the distributions of the rate of change measured at the end of the trial phases. The vertical black line represents 0° . The plots were separated by expected rotation to the landmark (colours), by phases (letters on the y-axis), by delay conditions (top - no delay, bottom - 20s delay) and by increased neuron death (columns). Phase A, reset of the network; Phase C, facing starting orientation; Phase D, performing the first turn; Phase E; delay condition; Phase F; answer from the agent.

4.4 Discussion

In this chapter, we developed a new model based on previous architecture from the literature (Bicanski and Burgess, 2016). The goal was to implement three distinct noise sources to investigate the effect of ageing on the HD system. We showed that each noise source impacted and modified the behaviour of the HD attractor dynamics. First, noise on the weights increased the spikiness of the bump and pushed it to a stable position where it would get stuck in local minima. Second, noise on the background drive also increased the spikiness of the bump and created an erratic signal jittering around the current HD. Third, neuron death made the bump wider and also pushed the bump to local minima and became unresponsive without substantial velocity inputs.

To the best of our knowledge, no previous HD model tried to investigate how ageing could impact the system. Seminal models such as Zhang (1996) only described the influence of noise on the weights. One reason is that his model was not built to survive some types of noise, such as neuron death. We implemented his model to assess it, killing a single neuron within the ring attractor. The attractor model did not maintain the HD bump when it went over the dead neuron. This problem arose from the inner structure of the model as the author opted for recurrent connections on each neuron, allowing the creation and maintenance of the bump. Therefore, the firing rate at the bump's peak would drop to zero when it passed onto a dead neuron. This signal's drop would then propagate on neighbouring neurons, and their signal would decrease and have no excitation. To avoid this problem, our model moved to a 3-ring structure with the addition of a background drive, inspired by a previous model from Bicanski and Burgess (2016). This structure had the advantage of separating the generation of the signal from the connections between neurons in the rings. Our model could then study

neuron death while maintaining the attractor bump even when going through those neurons.

In this chapter, we investigated three sources of noise (weight, background drive and neuron death) and their impact on HD network dynamics by manipulating their level individually. We found that after increasing noise in the weights or killing neurons within the rings, the bump moved from its origin to a stable position. Then, it maintained its position until it received a driving force strong enough to push it, such as velocity inputs. This phenomenon has been described previously by Zhang (1996) and can be understood as a reduction of representational space. It is described as the reduction of the possible states (i.e. headings) that the attractor network can maintain over time. However, the author linked it to a high noise level on the weights, where we only found it for neuron death. As explained above, this can be due to the architectural difference between our models, as ours separated excitatory and inhibitory connections between rings. We hypothesised that with increased dead neurons, there is lower inhibition in the rings, as suggested by the increase of FWHM and peak rate. In addition, the stable position where the bump moved was random and changed across simulations. However, whether this observation arose from a specific arrangement of dead neurons is uncertain. Indeed, with the random location of dead neurons across the three rings, finding an efficient metric to measure the position impact is complex. Nevertheless, future work on this model should expand on this.

In addition, this signal drift happens during static and movement phases but when no visual feedback is present. This observation is in accordance with the literature, where several studies have shown that the PFD of HD cells drifts when the animal is placed in darkness (Taube et al., 1990b; Goodridge et al., 1998; Yoder et al., 2011). However,

those studies did not use aged animals and compare the speed of drift, which was faster in our simulation for increased noise levels.

Furthermore, we did not see any constant drift or probability of getting stuck in local minima for high levels of background drive noise. The main impact of this type of noise was to make the bump noisier with high spiking, leading to an unstable HD as it would jitter. There was no direct evidence of increased angular error while performing the task on the individual noise level. This result suggests that older adults' HD systems could handle increased instability from the background drive coming from the vestibular regions. However, combining this noise with the other types might produce a detrimental impact by extending the influence of the noise on weights or neuron death.

The decision to add different noise sources was motivated by the current state of the literature on the impact of ageing. Each noise type approximated a physiological change happening in the brain during healthy ageing. Weight noise modelled synaptic change where connections between neurons would be impaired (Morrison and Baxter, 2012). Neuron death was linked to cerebral volume loss in different brain regions containing HD cells (Burke and Barnes, 2006; Raz and Rodrigue, 2006; Hughes et al., 2012). Background drive was associated with vestibular deficiency as both are the generating power of the HD system (Neuhauser et al., 2008; Agrawal et al., 2009; Anson and Jeka, 2015). To the best of our knowledge, our model is the first to address this question directly. The main goal was to implement an attractor model that could characterise different types of noise. However, the exact connectivity and architecture of the human HD system are still unknown. Thus, our model had to include simplifications, and revisions will be required in the future. One piece of evidence specific to the behavioural task we modelled was that we could not

replicate the range of errors we saw within our older group. Additional brain mechanisms could reduce the impact of cerebral loss but were not modelled (Davies, 2016; Wyss-Coray, 2016). As mentioned above, weight changes could compensate for the loss of dead neurons through some form of homeostasis regulation. This will be explored in future work.

Additionally, it would be interesting to look at damage to the drosophila HD circuit. Studies found a ring-like structure within their brain, but no studies investigated whether it is sensible to neuron death (Seelig and Jayaraman, 2015; Green et al., 2017; Kim et al., 2017). However, due to the short life span of the drosophila, neuron death might not happen naturally, and such mechanisms might not exist. On the contrary, mammals like humans and rodents have a longer life span, and neuron death happens (Morrison and Baxter, 2012). Then, we can hypothesise that the architecture of the attractor is different from the drosophila and can compensate for the loss of cerebral volumes.

Finally, the results from our model when it performed the behavioural task shed some light on the participants' data from Chapter 2 and the age difference found. We replicated the delay effect where the angular error increased after the 20-second delay by adding noise to the weights and with neuron death. This increase was found in participants from both age groups and could be explained by the HD bump drifting to local minima during the delay period. For neuron death, the increase in the range of angular errors could be linked to the accumulation of errors due to the inability to reset headings between trials properly. However, participants did not display this behaviour. Every participant knew the landmark's location, and they could remember it during the task at every trial. Therefore, this accumulation problem in our model could be due to nonoptimal parameters within the reset phase. The visual feedback might not be strong enough to return the HD from the bump to the agent HD.

Otherwise, the time for the reset phase could be too short if the distance between the two headings was too large. Lastly, it was challenging to assess the individual effect of the background drive in the model or the task. As mentioned, assessing it when combined with another type of noise would be more interesting. For future studies, we would get more insight into having participants perform vestibular checking prior to the task (Cohen, 2019). This would give important insight into their deficit, especially in older participants, and how it could affect their performance.

To conclude, this model was a first step in describing how the HD system is impacted by ageing and will help future studies to investigate this important aspect. Future work on this model and behavioural data should check the impact of combined noises on the ring attractor model. In addition, some parameters from the model can be tweaked from the results of our first characterisation. Indeed, the reduced representational space in the neuron death condition could be further characterised by checking its origin and properties in more detail.

4.5 Contributions

Matthieu Bernard (MB) completed this project in a collaborative effort with Andrej Bicanski (AB) and Thomas Wolbers (TW). MB, AB and TW conceptualised the work. MB managed the project administration. MB and AB developed the computational head direction model. MB analysed the data and visualised the results. AB and TW supervised the work.

General discussion

5.1 Summary

The work accomplished in this thesis brought new results on the HD system in humans, extending our understanding of the system. In the first chapter of the thesis, we replicated and expanded our knowledge of the HD system using neuroimaging methods and analysis. Previous work (Taube et al., 2013) hypothesised that recording HD signals in humans might be impossible with such studies. They justified that the HD system would require vestibular inputs, which are not present when the participant is lying in the scanner, head-fixed. However, similarly to previous neuroimaging studies (Baumann et al., 2010; Marchette et al., 2014; Chadwick et al., 2015; Shine et al., 2016), we found brain signals sensible to change in HD within the human brain. This study further proves that the HD system can update itself even without the direct presence of idiothetic cues. Sit and Goard (2023) also found the same results by recording HD cells when rodents were head-fixed.

Secondly, our study investigated an essential characteristic of the HD system: the stability of landmarks. Previous studies described the importance of landmarks for stabilising the HD signal (Knierim et al., 1995; Zugaro et al., 2001, 2003), but none actively assessed the impact of instability in humans. Therefore, we created a new task investigating how the HD system would react when landmarks had different spatial stability. Our results found that the RSC, coding for the permanence of landmarks (Auger et al., 2012; Auger and Maguire, 2013; Auger et al., 2015, 2017; Auger and Maguire, 2018a,b), and V1 could differentiate if landmarks were stable or unstable. Moreover, those two brain regions could discriminate between the HDs associated with the stable landmarks, while the thalamus could set apart only the

unstable landmarks. One explanation is that only idiothetic cues could separate the position of unstable landmarks as they moved across the environment, and those vestibular cues were reiterated during the scanner (as proposed by Shine et al. (2016)). Finally, the presubiculum and, more generally, the hippocampus decoded both types of landmarks. We suggested that it could be due to its role as an integrator between the allothetic and idiothetic cues.

In the second chapter, we investigated the impact of ageing on the HD system by testing young and older participants in a novel behavioural task. In contrast to past experiments, this task specifically isolated HD computation. We tested their memory by making them physically turn and then adding a delay condition before their answer. This new task had the advantage of providing full body-based cues using a HMD and immersive VR. We found that older adults produced larger angular errors on average than young participants. This age difference was not due to a memory deficit, as every participant precisely remembered the landmark's location. We also found a detrimental effect on angular error during the delay condition for both age groups. Those results provide the first evidence of a deficit of the HD system during ageing, possibly due to increased noise within this system.

In parallel to the behavioural task, we created a computational model to understand better the neural mechanisms that could explain the performance deficits in older adults. Recent theoretical models successfully looked at the effect of ageing on other spatial functions, such as cue combination (Harootonian et al., 2022) or path integration (Castegnarò et al., 2023). However, previous HD models did not systematically investigate the effect of ageing by looking at different increases in noise in the system (McNaughton et al., 1991; Skaggs et al., 1995; Zhang, 1996; Byrne et al., 2007; Page et al., 2014; Bicanski and Burgess, 2016; Page and Jeffery,

2018; Yan et al., 2021). Therefore, in the third chapter, we created a HD model inspired by previous ring attractor architectures (Bicanski and Burgess, 2016) and integrated three distinct noise sources to investigate ageing. Those types of noise were linked to known physiological changes happening in the ageing brain: synaptic change (Morrison and Baxter, 2012), loss of cerebral volume (Burke and Barnes, 2006; Raz and Rodrigue, 2006; Moffat et al., 2006; Hughes et al., 2012) and vestibular deficit (Neuhauser et al., 2008; Agrawal et al., 2009; Anson and Jeka, 2015). The model translated them to noise on the weights, neuron death and noise on the background drive (which is thought to generate the signal in the attractor ring). The first characterisation investigated how increased noise impacted the system when the HD bump was static. Noise on the weights and eliminating neurons from the rings drove the bump to drift to a stable position and stay stuck in these local minima. The background drive produced an erratic bump with a jittering position. Moreover, we implemented the second chapter's behavioural task to assess the impact of noise sources on participant performances. Our results showed that increased noise on weights and neuron death led to an overall increase in the angular error that could be due to an accumulation of noise over trials and drift to local minima. Cumulatively, those results showed that with increased noise within the HD system, the impact is similar to those found in our participants and could be responsible for impairments in the overall spatial navigation skills found in older adults (Lester et al., 2017).

5.2 Limitations

There are limitations to the work carried out during the experiments associated with the three chapters of this thesis. The first limitation is that we did not collect any measure of the vestibular system in the neuroimaging or behavioural studies.

However, vestibular degeneration is common in old age and is thought to impact spatial navigation skills (Neuhauser et al., 2008; Agrawal et al., 2009; Anson and Jeka, 2015). Clinical tasks exist to test the participant's balance but require additional material to ensure a complete and precise measure (Cohen, 2019). Multiple rodent studies have described the importance of vestibular signals for the generation and updating of the HD system (Stackman and Taube, 1997; Stackman et al., 2002). Therefore, participants with a damaged vestibular system could explain some individual variability seen in the results of the behavioural task. For the neuroimaging study from the first chapter, a recent study developed an approach to look at the inner ear's vestibular organs using neuroimaging data (Ahmadi et al., 2021). This new method would allow future analysis to use brain images from the dataset of Chapter 1 to check if there are structural differences between participants and if they are related to variations in performance.

MVPA analysis has been developed and used for over a decade with many applications in the spatial navigation field (Haxby et al., 2001; Hassabis et al., 2009; Bonnici et al., 2012). However, there is no consensus on the exact methods to apply as it depends on the data and the hypothesis. The same debate exists on how to perform the group-level statistical analysis of decoding accuracy. Most studies consider permutation-based statistics the best choice when the number of permutations is high enough. Nevertheless, this statistic can sometimes not be used as in Chapter 1, when we compared stable vs unstable landmarks. We were limited to 128 unique permutations and had to do simple t-tests to compare the average decoding against the chance level. Recent statistical methods tried to find a better approach, such as the *ith*-test from Allefeld et al. (2016) and expanded by Hirose (2021). They developed a statistical analysis called the information prevalence hypothesis, testing whether the significant results from the subjects' sample can be

applied to a larger population. This method still needs to be used more widely within the neuroimaging field to assess its correct functioning.

We also noticed individual differences in the performance and strategy used in both tasks from Chapters 1 and 2. It could play a role in the findings by leaving the participants free to use their own strategy to solve the task. In the first study, we found differences in how participants responded when they needed to point towards unstable landmarks. Unfortunately, our analysis could not assess the impact of those individualities on the HD signals. For the behavioural study, the difference in strategy found between age groups has also been described in previous studies (Colombo et al., 2017; Lester et al., 2017). However, similar to Chapter 1, we found individual differences within each age group. Investigating the impact of those differences in future studies could be beneficial, and this topic has already been discussed in previous papers (Hegarty et al., 2006; Wolbers and Hegarty, 2010).

Finally, we created a new model to characterise potential degradations of the HD system during healthy ageing. However, this model only approximates a complex biological system like the brain. Indeed, our model's structure only integrates parts of the complete HD system. Further mechanisms and brain regions not included in the model exist and may modify some of the results (Davies, 2016; Wyss-Coray, 2016). In addition, the chapter only investigated individual types of noises, and future work should combine them. This future characterisation might help to understand the effect of ageing in more depth since those deficits most likely coexist and interact between themselves within the brain.

5.3 Implications and Future Perspective

In sum, the work outlined in this thesis has laid the foundation for future studies to investigate the impact of ageing on the HD system. Previous studies did not explore this question in the rodent and human literature, but investigating those changes in more depth could help to understand the mechanisms underlying age-related navigational decline. Our behavioural study and the associated model directly compared young and older participants and first characterised how the HD system is impacted by ageing. In addition, while the first chapter did not test older participants, the perception of landmark stability could be altered with ageing. Previous reports suggest that the RSC is degraded with ageing (Moffat et al., 2006; Antonova et al., 2009), which could lead older adults to perceive stable landmarks as unstable. Then, we can hypothesise that the tuning curve associated with those landmarks would either get wider or shift to different orientations. Even more, the landmark stability in ageing could be assessed with the work from Yan et al. (2021) that modelled the relation between landmarks and the HD system. However, their model used Zhang (1996) architecture, and we showed that it cannot correctly investigate ageing. Nonetheless, we could combine their approach with the model from Chapter 3 to test those hypotheses and increase the ecological validity of our model. Altogether, those studies could help open future research to investigate those open questions of ageing and disease in human and animal models.

In addition, the new behavioural task from Chapter 2 could be developed for usage in a clinical setting. Indeed, the task was simple to perform, and older participants learned it successfully. We can assume that patients with mild cognitive impairment (MCI) or suffering from Alzheimer's disease (AD) could perform the task. Previous studies indicate that several critical regions related to HD are sensitive to early AD

pathology, such as the thalamus, RSC and hippocampus (Braak and Braak, 1995; Nestor et al., 2003; Pengas et al., 2010; Serino et al., 2014). Behaviourally, both rodent AD models (Crouzier et al., 2018) and human patients (Aguirre and D'Esposito, 1999; Coughlan et al., 2018) display symptoms of disorientation, which could be linked to damage from the HD system. In addition, other spatial navigation cells using HD inputs, such as grid cells, are impaired with AD (Kunz et al., 2015; Jun et al., 2020). However, it is unknown how the HD computation is altered in early AD, but finding a way to measure it could be a way to identify at-risk patients. We could assess if the task developed in Chapter 2 could be used. A few adjustments to the task would be necessary to fit the clinical settings where time and space are limited. The number of trials should be reduced to avoid some repetitions of symmetrical orientations. The task should also be able to be performed without active movement while keeping physical rotation by letting the patient stand in the middle of the environment.

Recently, we have observed an increasing number of studies using electrophysiological recordings in human patients (Ekstrom et al., 2003; Manning et al., 2009; Mukamel et al., 2010; Jacobs et al., 2010; Stangl et al., 2020). Those patients allowed researchers to study the neurophysiological basis of spatial navigation with similar resolution as in the rodent literature. Recent technological advances have also enabled ambulatory setups, which are ideal for testing spatial tasks (Topalovic et al., 2020, 2023). Giving full idiothetic cues to the patients while they perform a task is critical for replicating naturalistic behaviour. This goal was already at the origin of developing immersive VR tasks for human experiments to create closer real-world navigation. Nevertheless, no published studies looked at the HD system, and this work should be carried out in the future. Indeed, we could use the task from Chapter 2 without immersive VR, as HMDs are usually incompatible

with those patients due to the electrodes. We could replace the circular arena with a coloured curtain and the virtual landmark with a physical one. This physical setup would be possible as previous studies used it in the context of the Morris water maze (Laczó et al., 2010). Then, it would be feasible to investigate how the brain signal related to HD cells is modulated during the task, specifically during the delay period. This way, we could assess whether the constant drift suggested by the model is happening or if there is a drift to a stable position, as hypothesised by neuron death. Nonetheless, the study of those implanted patients is challenging. They are usually rare, present in special clinics and have limited time to complete tasks. In addition, doctors decide the electrodes' placement, and the number of ROIs available is usually limited to the hippocampus and, in some cases, the RSC (Lehongre et al., 2022). Lastly, those patients are usually young, which could make ageing studies challenging to carry out.

To conclude, this thesis hopes to encourage future studies to investigate the HD system and spatial navigation in the context of ageing. Understanding and treating spatial navigation deficits arising with age is critical as they lead to everyday impairments. Older adults with those deficits suffer from reduced mobility, leading to other problems such as diminished social interaction, fall risk, lower physical activity, etc (Burns, 1999; Ferrucci et al., 2016; Freiburger et al., 2020). Altogether, those deficits have been identified as major psychological risk factors for developing dementia (Hendriks et al., 2023). Using spatial navigation tests to identify those at-risk populations early is essential to treat them accordingly and reduce the risk of more severe pathology.

Bibliography

- Agrawal, Y., Carey, J. P., Della Santina, C. C., Schubert, M. C., and Minor, L. B. (2009). Disorders of balance and vestibular function in US adults: data from the National Health and Nutrition Examination Survey, 2001-2004. *Archives of Internal Medicine*, 169(10):938–944. 10.1001/archinternmed.2009.66.
- Aguirre, G. K. and D'Esposito, M. (1999). Topographical disorientation: a synthesis and taxonomy. *Brain*, 122(9):1613–1628. 10.1093/brain/122.9.1613.
- Aguirre, G. K., Mattar, M. G., and Magis-Weinberg, L. (2011). de Bruijn cycles for neural decoding. *NeuroImage*, 56(3):1293–1300. 10.1016/j.neuroimage.2011.02.005.
- Ahmadi, S.-A., Raiser, T. M., Rühl, R. M., Flanagin, V. L., and zu Eulenburg, P. (2021). IE-Map: a novel in-vivo atlas and template of the human inner ear. *Scientific Reports*, 11(1):3293. 10.1038/s41598-021-82716-0.
- Alexander, A. S., Place, R., Starrett, M. J., Chrastil, E. R., and Nitz, D. A. (2023). Rethinking retrosplenial cortex: Perspectives and predictions. *Neuron*, 111(2):150–175. 10.1016/j.neuron.2022.11.006.
- Allefeld, C., Görgen, K., and Haynes, J.-D. (2016). Valid population inference for information-based imaging: From the second-level t-test to prevalence inference. *NeuroImage*, 141:378–392. 10.1016/j.neuroimage.2016.07.040.
- Allefeld, C. and Haynes, J.-D. (2014). Searchlight-based multi-voxel pattern analysis of fMRI by cross-validated MANOVA. *NeuroImage*, 89:345–357. 10.1016/j.neuroimage.2013.11.043.
- Amit, D. J. (1989). *Modeling Brain Function: The World of Attractor Neural Networks*. Cambridge University Press.
- Amorim, M.-A. (2003). "What is my avatar seeing?": The coordination of "out-of-body" and "embodied" perspectives for scene recognition across views. *Visual Cognition*, 10(2):157–199. 10.1080/713756678.
- Anson, E. and Jeka, J. (2015). Perspectives on Aging Vestibular Function. *Frontiers in Neurology*, 6:269. 10.3389/fneur.2015.00269.
- Antonova, E., Parslow, D., Brammer, M., Dawson, G. R., Jackson, S. H. D., and Morris, R. G. (2009). Age-related neural activity during allocentric spatial memory. *Memory (Hove, England)*, 17(2):125–143. 10.1080/09658210802077348.
- Astur, R. S., Taylor, L. B., Mamelak, A. N., Philpott, L., and Sutherland, R. J. (2002). Humans with hippocampus damage display severe spatial memory impairments in a virtual Morris water task. *Behavioural Brain Research*, 132(1):77–84. 10.1016/s0166-4328(01)00399-0.
- Auger, S. D. and Maguire, E. A. (2013). Assessing the mechanism of response in the retrosplenial cortex of good and poor navigators. *Cortex*, 49(10):2904–2913. 10.1016/j.cortex.2013.08.002.
- Auger, S. D. and Maguire, E. A. (2018a). Dissociating Landmark Stability from Orienting Value Using Functional Magnetic Resonance Imaging. *Journal of Cognitive Neuroscience*, 30(5):698–713. 10.1162/jocn_a_01231.

- Auger, S. D. and Maguire, E. A. (2018b). Retrosplenial Cortex Indexes Stability beyond the Spatial Domain. *The Journal of Neuroscience*, 38(6):1472–1481. 10.1523/JNEUROSCI.2602-17.2017.
- Auger, S. D., Mullally, S. L., and Maguire, E. A. (2012). Retrosplenial Cortex Codes for Permanent Landmarks. *PLoS ONE*, 7(8):e43620. 10.1371/journal.pone.0043620.
- Auger, S. D., Zeidman, P., and Maguire, E. A. (2015). A central role for the retrosplenial cortex in de novo environmental learning. *eLife*, 4:e09031. 10.7554/eLife.09031.
- Auger, S. D., Zeidman, P., and Maguire, E. A. (2017). Efficacy of navigation may be influenced by retrosplenial cortex-mediated learning of landmark stability. *Neuropsychologia*, 104:102–112. 10.1016/j.neuropsychologia.2017.08.012.
- Bartsch, T., Schönfeld, R., Müller, F. J., Alfke, K., Leplow, B., Aldenhoff, J., Deuschl, G., and Koch, J. M. (2010). Focal lesions of human hippocampal CA1 neurons in transient global amnesia impair place memory. *Science (New York, N.Y.)*, 328(5984):1412–1415. 10.1126/science.1188160.
- Bassett, J. P. and Taube, J. S. (2001). Neural correlates for angular head velocity in the rat dorsal tegmental nucleus. *The Journal of Neuroscience: The Official Journal of the Society for Neuroscience*, 21(15):5740–5751. 10.1523/JNEUROSCI.21-15-05740.2001.
- Bassett, J. P., Tullman, M. L., and Taube, J. S. (2007). Lesions of the Tegmentomammillary Circuit in the Head Direction System Disrupt the Head Direction Signal in the Anterior Thalamus. *Journal of Neuroscience*, 27(28):7564–7577. 10.1523/JNEUROSCI.0268-07.2007.
- Bates, S. L. and Wolbers, T. (2014). How cognitive aging affects multisensory integration of navigational cues. *Neurobiology of Aging*, 35(12):2761–2769. 10.1016/j.neurobiolaging.2014.04.003.
- Baumann, O., Chan, E., and Mattingley, J. B. (2010). Dissociable neural circuits for encoding and retrieval of object locations during active navigation in humans. *Neuroimage*, 49(3):2816–25. 10.1016/j.neuroimage.2009.10.021.
- Behzadi, Y., Restom, K., Liou, J., and Liu, T. T. (2007). A Component Based Noise Correction Method (CompCor) for BOLD and Perfusion Based fMRI. *NeuroImage*, 37(1):90–101. 10.1016/j.neuroimage.2007.04.042.
- Bian, Z. and Andersen, G. J. (2013). Aging and the Perception of Egocentric Distance. *Psychology and aging*, 28(3):813–825. 10.1037/a0030991.
- Bicanski, A. and Burgess, N. (2016). Environmental Anchoring of Head Direction in a Computational Model of Retrosplenial Cortex. *Journal of Neuroscience*, 36(46):11601–11618. 10.1523/JNEUROSCI.0516-16.2016.
- Blair, H. T., Cho, J., and Sharp, P. E. (1998). Role of the Lateral Mammillary Nucleus in the Rat Head Direction Circuit: A Combined Single Unit Recording and Lesion Study. *Neuron*, 21(6):1387–1397. 10.1016/S0896-6273(00)80657-1.
- Blair, H. T. and Sharp, P. E. (1996). Visual and vestibular influences on head-direction cells in the anterior thalamus of the rat. *Behavioral Neuroscience*, 110(4):643–660. 10.1037//0735-7044.110.4.643.

- Bonnici, H. M., Kumaran, D., Chadwick, M. J., Weiskopf, N., Hassabis, D., and Maguire, E. A. (2012). Decoding representations of scenes in the medial temporal lobes. *Hippocampus*, 22(5):1143–1153. 10.1002/hipo.20960.
- Braak, H. and Braak, E. (1995). Staging of Alzheimer's disease-related neurofibrillary changes. *Neurobiology of Aging*, 16(3):271–278; discussion 278–284. 10.1016/0197-4580(95)00021-6.
- Brody, C. D., Romo, R., and Kepecs, A. (2003). Basic mechanisms for graded persistent activity: discrete attractors, continuous attractors, and dynamic representations. *Current Opinion in Neurobiology*, 13(2):204–211. 10.1016/s0959-4388(03)00050-3.
- Burgess, N. (2006). Spatial memory: how egocentric and allocentric combine. *Trends in Cognitive Sciences*, 10(12):551–557. 10.1016/j.tics.2006.10.005.
- Burke, S. N. and Barnes, C. A. (2006). Neural plasticity in the ageing brain. *Nature Reviews Neuroscience*, 7(1):30–40. 10.1038/nrn1809.
- Burns, P. C. (1999). Navigation and the mobility of older drivers. *The Journals of Gerontology. Series B, Psychological Sciences and Social Sciences*, 54(1):S49–55. 10.1093/geronb/54b.1.s49.
- Byrne, P., Becker, S., and Burgess, N. (2007). Remembering the past and imagining the future. *Psychological review*, 114(2):340–375. 10.1037/0033-295X.114.2.340.
- Bécu, M., Sheynikhovich, D., Ramanoël, S., Tatur, G., Ozier-Lafontaine, A., Authié, C. N., Sahel, J.-A., and Arleo, A. (2023). Landmark-based spatial navigation across the human lifespan. *eLife*, 12:e81318. 10.7554/eLife.81318.
- Castegnarò, A., Ji, Z., Rudzka, K., Chan, D., and Burgess, N. (2023). Overestimation in angular path integration precedes Alzheimer's dementia. *Current Biology*, 33(21):4650–4661.e7. 10.1016/j.cub.2023.09.047.
- Chadwick, M., Jolly, A., Amos, D., Hassabis, D., and Spiers, H. (2015). A Goal Direction Signal in the Human Entorhinal/Subicular Region. *Current Biology*, 25(1):87–92. 10.1016/j.cub.2014.11.001.
- Chen, L. L., Lin, L.-H., Green, E. J., Barnes, C. A., and McNaughton, B. L. (1994). Head-direction cells in the rat posterior cortex. *Experimental Brain Research*, 101(1):8–23. 10.1007/BF00243212.
- Chen, X., McNamara, T. P., Kelly, J. W., and Wolbers, T. (2017). Cue combination in human spatial navigation. *Cognitive Psychology*, 95:105–144. 10.1016/j.cogpsych.2017.04.003.
- Cho, J. and Sharp, P. E. (2001). Head direction, place, and movement correlates for cells in the rat retrosplenial cortex. *Behavioral Neuroscience*, 115(1):3–25.
- Chrastil, E. R. and Warren, W. H. (2021). Executing the homebound path is a major source of error in homing by path integration. *Journal of Experimental Psychology: Human Perception and Performance*, 47(1):13–35. 10.1037/xhp0000875.
- Claessen, M. H. G. and van der Ham, I. J. M. (2017). Classification of navigation impairment: A systematic review of neuropsychological case studies. *Neuroscience and Biobehavioral Reviews*, 73:81–97. 10.1016/j.neubiorev.2016.12.015.

- Clark, B. J., Bassett, J. P., Wang, S. S., and Taube, J. S. (2010). Impaired head direction cell representation in the anterodorsal thalamus after lesions of the retrosplenial cortex. *J Neurosci*, 30(15):5289–302. 10.1523/JNEUROSCI.3380-09.2010.
- Clark, B. J. and Taube, J. S. (2011). Intact landmark control and angular path integration by head direction cells in the anterodorsal thalamus after lesions of the medial entorhinal cortex. *Hippocampus*, 21(7):767–782. 10.1002/hipo.20874.
- Clark, B. J. and Taube, J. S. (2012). Vestibular and attractor network basis of the head direction cell signal in subcortical circuits. *Frontiers in Neural Circuits*, 6:7. 10.3389/fncir.2012.00007.
- Cohen, H. S. (2019). A review on screening tests for vestibular disorders. *Journal of Neurophysiology*, 122(1):81–92. 10.1152/jn.00819.2018.
- Colombo, D., Serino, S., Tuena, C., Pedrolì, E., Dakanalis, A., Cipresso, P., and Riva, G. (2017). Egocentric and allocentric spatial reference frames in aging: A systematic review. *Neuroscience and Biobehavioral Reviews*, 80:605–621. 10.1016/j.neubiorev.2017.07.012.
- Committeri, G., Galati, G., Paradis, A.-L., Pizzamiglio, L., Berthoz, A., and LeBihan, D. (2004). Reference frames for spatial cognition: different brain areas are involved in viewer-, object-, and landmark-centered judgments about object location. *Journal of Cognitive Neuroscience*, 16(9):1517–1535. 10.1162/0898929042568550.
- Coughlan, G., Laczó, J., Hort, J., Minihane, A.-M., and Hornberger, M. (2018). Spatial navigation deficits — overlooked cognitive marker for preclinical Alzheimer disease? *Nature Reviews Neurology*, 14(8):496–506. 10.1038/s41582-018-0031-x.
- Coutrot, A., Manley, E., Goodroe, S., Gahnstrom, C., Filomena, G., Yesiltepe, D., Dalton, R. C., Wiener, J. M., Hölscher, C., Hornberger, M., and Spiers, H. J. (2022). Entropy of city street networks linked to future spatial navigation ability. *Nature*, 604(7904):104–110. 10.1038/s41586-022-04486-7.
- Coutrot, A., Silva, R., Manley, E., de Cothi, W., Sami, S., Bohbot, V. D., Wiener, J. M., Hölscher, C., Dalton, R. C., Hornberger, M., and Spiers, H. J. (2018). Global Determinants of Navigation Ability. *Current biology: CB*, 28(17):2861–2866.e4. 10.1016/j.cub.2018.06.009.
- Crane, B. T. (2012). Direction Specific Biases in Human Visual and Vestibular Heading Perception. *PLOS ONE*, 7(12):e51383. 10.1371/journal.pone.0051383.
- Crouzier, L., Gilabert, D., Rossel, M., Trousse, F., and Maurice, T. (2018). Topographical memory analyzed in mice using the Hamlet test, a novel complex maze. *Neurobiology of Learning and Memory*, 149:118–134. 10.1016/j.nlm.2018.02.014.
- Darwin, C. (1859). *On the origin of species by means of natural selection , or, The preservation of favoured races in the struggle for life*. 1859, London.
- Davies, K. J. A. (2016). Adaptive Homeostasis. *Molecular aspects of medicine*, 49:1–7. 10.1016/j.mam.2016.04.007.

- Desikan, R. S., Ségonne, F., Fischl, B., Quinn, B. T., Dickerson, B. C., Blacker, D., Buckner, R. L., Dale, A. M., Maguire, R. P., Hyman, B. T., Albert, M. S., and Killiany, R. J. (2006). An automated labeling system for subdividing the human cerebral cortex on MRI scans into gyral based regions of interest. *NeuroImage*, 31(3):968–980. 10.1016/j.neuroimage.2006.01.021.
- Destrieux, C., Fischl, B., Dale, A., and Halgren, E. (2010). Automatic parcellation of human cortical gyri and sulci using standard anatomical nomenclature. *NeuroImage*, 53(1):1–15. 10.1016/j.neuroimage.2010.06.010.
- Diersch, N. and Wolbers, T. (2019). The potential of virtual reality for spatial navigation research across the adult lifespan. *The Journal of Experimental Biology*, 222(Pt Suppl 1):jeb187252. 10.1242/jeb.187252.
- Eccles, J. (1976). From electrical to chemical transmission in the central nervous system. *Notes and Records of the Royal Society of London*, 30(2):219–230. 10.1098/rsnr.1976.0015.
- Ekstrom, A. D. (2015). Why vision is important to how we navigate. *Hippocampus*, 25(6):731–735. 10.1002/hipo.22449.
- Ekstrom, A. D., Arnold, A. E. G. F., and Iaria, G. (2014). A critical review of the allocentric spatial representation and its neural underpinnings: toward a network-based perspective. *Frontiers in Human Neuroscience*, 8:803. 10.3389/fnhum.2014.00803.
- Ekstrom, A. D., Huffman, D. J., and Starrett, M. (2017). Interacting networks of brain regions underlie human spatial navigation: a review and novel synthesis of the literature. *Journal of Neurophysiology*, 118(6):3328–3344. 10.1152/jn.00531.2017.
- Ekstrom, A. D. and Isham, E. A. (2017). Human spatial navigation: Representations across dimensions and scales. *Current opinion in behavioral sciences*, 17:84–89. 10.1016/j.cobeha.2017.06.005.
- Ekstrom, A. D., Kahana, M. J., Caplan, J. B., Fields, T. A., Isham, E. A., Newman, E. L., and Fried, I. (2003). Cellular networks underlying human spatial navigation. *Nature*, 425(6954):184–188. 10.1038/nature01964.
- Etienne, A. S. and Jeffery, K. J. (2004). Path integration in mammals. *Hippocampus*, 14(2):180–192. 10.1002/hipo.10173.
- Fallahnezhad, M., Le Mero, J., Zenelaj, X., Vincent, J., Rochefort, C., and Rondi-Reig, L. (2023). Cerebellar control of a unitary head direction sense. *Proceedings of the National Academy of Sciences of the United States of America*, 120(9):e2214539120. 10.1073/pnas.2214539120.
- Ferrucci, L., Cooper, R., Shardell, M., Simonsick, E. M., Schrack, J. A., and Kuh, D. (2016). Age-Related Change in Mobility: Perspectives From Life Course Epidemiology and Geroscience. *The Journals of Gerontology Series A: Biological Sciences and Medical Sciences*, 71(9):1184–1194. 10.1093/gerona/glw043.
- Finkelstein, A., Derdikman, D., Rubin, A., Foerster, J. N., Las, L., and Ulanovsky, N. (2015). Three-dimensional head-direction coding in the bat brain. *Nature*, 517(7533):159–164. 10.1038/nature14031.

- Finkelstein, A., Rouault, H., Romani, S., and Ulanovsky, N. (2019). Dynamic control of cortical head-direction signal by angular velocity. preprint, Neuroscience. 10.1101/730374.
- Flavell, J. H., Everett, B. A., Croft, K., and Flavell, E. R. (1981). Young children's knowledge about visual perception: Further evidence for the Level 1–Level 2 distinction. *Developmental Psychology*, 17(1):99–103. 10.1037/0012-1649.17.1.99.
- Freeman, S. H., Kandel, R., Cruz, L., Rozkalne, A., Newell, K., Frosch, M. P., Hedley-Whyte, E. T., Locascio, J. J., Lipsitz, L., and Hyman, B. T. (2008). Preservation of Neuronal Number Despite Age-Related Cortical Brain Atrophy In Elderly Subjects Without Alzheimer Disease. *Journal of neuropathology and experimental neurology*, 67(12):1205–1212. 10.1097/NEN.0b013e31818fc72f.
- Freiberger, E., Sieber, C. C., and Kob, R. (2020). Mobility in Older Community-Dwelling Persons: A Narrative Review. *Frontiers in Physiology*, 11:881. 10.3389/fphys.2020.00881.
- Gallistel, C. R. (1990). *The organization of learning*. The organization of learning. The MIT Press, Cambridge, MA, US.
- Geuter, S., Qi, G., Welsh, R. C., Wager, T. D., and Lindquist, M. A. (2018). Effect Size and Power in fMRI Group Analysis. 10.1101/295048.
- Goodridge, J. P., Dudchenko, P. A., Worboys, K. A., Golob, E. J., and Taube, J. S. (1998). Cue control and head direction cells. *Behavioral Neuroscience*, 112(4):749–761. 10.1037//0735-7044.112.4.749.
- Goodridge, J. P. and Taube, J. S. (1997). Interaction between the postsubiculum and anterior thalamus in the generation of head direction cell activity. *J Neurosci*, 17(23):9315–30.
- Goodridge, J. P. and Touretzky, D. S. (2000). Modeling Attractor Deformation in the Rodent Head-Direction System. *Journal of Neurophysiology*, 83(6):3402–3410. 10.1152/jn.2000.83.6.3402.
- Graham, J. A., Dumont, J. R., Winter, S. S., Brown, J. E., LaChance, P. A., Amon, C. C., Farnes, K. B., Morris, A. J., Streltsov, N. A., and Taube, J. S. (2023). Angular head velocity cells within brainstem nuclei projecting to the head direction circuit. *The Journal of Neuroscience: The Official Journal of the Society for Neuroscience*, pages JN–RM–0581–23. 10.1523/JNEUROSCI.0581-23.2023.
- Green, J., Adachi, A., Shah, K. K., Hirokawa, J. D., Magani, P. S., and Maimon, G. (2017). A neuronal circuit architecture for angular integration in *Drosophila*. *Nature*, 546(7656):101–106. 10.1038/nature22343.
- Grieves, R. M. and Jeffery, K. J. (2017). The representation of space in the brain. *Behavioural Processes*, 135:113–131. 10.1016/j.beproc.2016.12.012.
- Grieves, R. M., Shinder, M. E., Rosow, L. K., Kenna, M. S., and Taube, J. S. (2022). The Neural Correlates of Spatial Disorientation in Head Direction Cells. *eNeuro*, 9(6). 10.1523/ENEURO.0174-22.2022.
- Hafting, T., Fyhn, M., Molden, S., Moser, M.-B., and Moser, E. I. (2005). Microstructure of a spatial map in the entorhinal cortex. *Nature*, 436(7052):801–806. 10.1038/nature03721.

- Harootyan, S. K., Ekstrom, A. D., and Wilson, R. C. (2022). Combination and competition between path integration and landmark navigation in the estimation of heading direction. *PLOS Computational Biology*, 18(2):e1009222. 10.1371/journal.pcbi.1009222.
- Harris, M. A. and Wolbers, T. (2012). Ageing effects on path integration and landmark navigation. *Hippocampus*, 22(8):1770–1780. 10.1002/hipo.22011.
- Hashimoto, R., Tanaka, Y., and Nakano, I. (2010). Heading disorientation: a new test and a possible underlying mechanism. *European Neurology*, 63(2):87–93. 10.1159/000276398.
- Hassabis, D., Chu, C., Rees, G., Weiskopf, N., Molyneux, P. D., and Maguire, E. A. (2009). Decoding Neuronal Ensembles in the Human Hippocampus. *Current Biology*, 19(7-3):546–554. 10.1016/j.cub.2009.02.033.
- Haxby, J. V., Gobbini, M. I., Furey, M. L., Ishai, A., Schouten, J. L., and Pietrini, P. (2001). Distributed and overlapping representations of faces and objects in ventral temporal cortex. *Science*, 293(5539):2425–30. 10.1126/science.1063736.
- Hegarty, M., Montello, D. R., Richardson, A. E., Ishikawa, T., and Lovelace, K. (2006). Spatial abilities at different scales: Individual differences in aptitude-test performance and spatial-layout learning. *Intelligence*, 34(2):151–176. 10.1016/j.intell.2005.09.005.
- Hendriks, S., Ranson, J. M., Peetoom, K., Lourida, I., Tai, X. Y., de Vugt, M., Llewellyn, D. J., and Köhler, S. (2023). Risk Factors for Young-Onset Dementia in the UK Biobank. *JAMA Neurology*. 10.1001/jamaneurol.2023.4929.
- Heward, M., Hicks, B., Hedges, B., Gaden, R., and Wiener, J. M. (2023). Experiences of age-related declining navigation abilities and impact on use of outdoor environments: a qualitative study of young-old adults with self-reported memory difficulties. *Ageing & Society*, pages 1–21. 10.1017/S0144686X23000612.
- Hirose, S. (2021). Valid and powerful second-level group statistics for decoding accuracy: Information prevalence inference using the i-th order statistic (i-test). *NeuroImage*, 242:118456. 10.1016/j.neuroimage.2021.118456.
- Hopfield, J. J. (1982). Neural networks and physical systems with emergent collective computational abilities. *Proceedings of the National Academy of Sciences of the United States of America*, 79(8):2554–2558.
- Hughes, E. J., Bond, J., Svrckova, P., Makropoulos, A., Ball, G., Sharp, D. J., Edwards, A. D., Hajnal, J. V., and Counsell, S. J. (2012). Regional changes in thalamic shape and volume with increasing age. *NeuroImage*, 63(3):1134–1142. 10.1016/j.neuroimage.2012.07.043.
- Ishikawa, T. and Montello, D. R. (2006). Spatial knowledge acquisition from direct experience in the environment: Individual differences in the development of metric knowledge and the integration of separately learned places. *Cognitive Psychology*, 52(2):93–129. 10.1016/j.cogpsych.2005.08.003.
- Israël, I., Grasso, R., Georges-Francois, P., Tsuzuku, T., and Berthoz, A. (1997). Spatial memory and path integration studied by self-driven passive linear displacement. I. Basic properties. *Journal of Neurophysiology*, 77(6):3180–3192. 10.1152/jn.1997.77.6.3180.

- Jackson, D. A. (1993). Stopping Rules in Principal Components Analysis: A Comparison of Heuristical and Statistical Approaches. *Ecology*, 74(8):2204–2214. 10.2307/1939574.
- Jacob, P.-Y., Casali, G., Spieser, L., Page, H., Overington, D., and Jeffery, K. (2017). An independent, landmark-dominated head direction signal in dysgranular retrosplenial cortex. *Nature neuroscience*, 20(2):173–175. 10.1038/nn.4465.
- Jacobs, J., Kahana, M. J., Ekstrom, A. D., Mollison, M. V., and Fried, I. (2010). A sense of direction in human entorhinal cortex. *Proceedings of the National Academy of Sciences*, 107(14):6487–6492. 10.1073/pnas.0911213107.
- Jain, D., Jakhalekar, I. R., and Deshmukh, S. S. (2017). Navigational Strategies and Their Neural Correlates. *Journal of the Indian Institute of Science*, 97(4):511–525. 10.1007/s41745-017-0053-1.
- Jun, H., Bramian, A., Soma, S., Saito, T., Saido, T. C., and Igarashi, K. M. (2020). Disrupted Place Cell Remapping and Impaired Grid Cells in a Knockin Model of Alzheimer’s Disease. *Neuron*, 107(6):1095–1112.e6. 10.1016/j.neuron.2020.06.023.
- Kiltner, K., Groten, R., and Slater, M. (2012). The Sense of Embodiment in Virtual Reality. *Presence: Teleoperators and Virtual Environments*, 21(4):373–387. 10.1162/PRES_a_00124.
- Kim, S., Sapiurka, M., Clark, R. E., and Squire, L. R. (2013). Contrasting effects on path integration after hippocampal damage in humans and rats. *Proceedings of the National Academy of Sciences*, 110(12):4732–4737. 10.1073/pnas.1300869110.
- Kim, S. S., Rouault, H., Druckmann, S., and Jayaraman, V. (2017). Ring attractor dynamics in the *Drosophila* central brain. *Science*, 356(6340):849–853. 10.1126/science.aal4835.
- Klatzky, R. L. (1998). Allocentric and Egocentric Spatial Representations: Definitions, Distinctions, and Interconnections. In Freksa, C., Habel, C., and Wender, K. F., editors, *Spatial Cognition: An Interdisciplinary Approach to Representing and Processing Spatial Knowledge*, pages 1–17. Springer Berlin Heidelberg, Berlin, Heidelberg.
- Knierim, J., Kudrimoti, H., and McNaughton, B. (1995). Place cells, head direction cells, and the learning of landmark stability. *The Journal of Neuroscience*, 15(3):1648–1659. 10.1523/JNEUROSCI.15-03-01648.1995.
- Knierim, J. J. and Zhang, K. (2012). Attractor Dynamics of Spatially Correlated Neural Activity in the Limbic System. *Annual Review of Neuroscience*, 35(1):267–285. 10.1146/annurev-neuro-062111-150351.
- Koch, C., Li, S.-C., Polk, T. A., and Schuck, N. W. (2020). Effects of aging on encoding of walking direction in the human brain. *Neuropsychologia*, page 107379. 10.1016/j.neuropsychologia.2020.107379.
- Kornienko, O., Latuske, P., Bassler, M., Kohler, L., and Allen, K. (2018). Non-rhythmic head-direction cells in the parahippocampal region are not constrained by attractor network dynamics. *eLife*, 7:e35949. 10.7554/eLife.35949.

- Kunz, L., Schröder, T. N., Lee, H., Montag, C., Lachmann, B., Sariyska, R., Reuter, M., Stirnberg, R., Stöcker, T., Messing-Floeter, P. C., Fell, J., Doeller, C. F., and Axmacher, N. (2015). Reduced grid-cell-like representations in adults at genetic risk for Alzheimer's disease. *Science*, 350(6259):430–433. 10.1126/science.aac8128.
- Laczó, J., Andel, R., Vyhnaek, M., Vlcek, K., Magerova, H., Varjassyova, A., Tolar, M., and Hort, J. (2010). Human analogue of the morris water maze for testing subjects at risk of Alzheimer's disease. *Neuro-Degenerative Diseases*, 7(1-3):148–152. 10.1159/000289226.
- Lehongre, K., Lambrecq, V., Whitmarsh, S., Frazzini, V., Cousyn, L., Soleil, D., Fernandez-Vidal, S., Mathon, B., Houot, M., Lemaréchal, J.-D., Clemenceau, S., Hasboun, D., Adam, C., and Navarro, V. (2022). Long-term deep intracerebral microelectrode recordings in patients with drug-resistant epilepsy: Proposed guidelines based on 10-year experience. *NeuroImage*, 254:119116. 10.1016/j.neuroimage.2022.119116.
- Lester, A. W., Moffat, S. D., Wiener, J. M., Barnes, C. A., and Wolbers, T. (2017). The Aging Navigational System. *Neuron*, 95(5):1019–1035. 10.1016/j.neuron.2017.06.037.
- Liu, R., Chang, L., and Wickern, G. (1984). The dorsal tegmental nucleus: an axoplasmic transport study. *Brain Research*, 310(1):123–132. 10.1016/0006-8993(84)90015-5.
- Loh, K. Y. and Ogle, J. (2004). Age related visual impairment in the elderly. *The Medical Journal of Malaysia*, 59(4):562–568.
- Maguire, E. A. (2001). The retrosplenial contribution to human navigation: a review of lesion and neuroimaging findings. *Scandinavian Journal of Psychology*, 42(3):225–238. 10.1111/1467-9450.00233.
- Maguire, E. A., Burgess, N., and O'Keefe, J. (1999). Human spatial navigation: cognitive maps, sexual dimorphism, and neural substrates. *Current Opinion in Neurobiology*, 9(2):171–177. 10.1016/S0959-4388(99)80023-3.
- Maguire, E. A., Woollett, K., and Spiers, H. J. (2006). London taxi drivers and bus drivers: A structural MRI and neuropsychological analysis. *Hippocampus*, 16(12):1091–1101. 10.1002/hipo.20233.
- Manning, J. R., Jacobs, J., Fried, I., and Kahana, M. J. (2009). Broadband shifts in local field potential power spectra are correlated with single-neuron spiking in humans. *Journal of Neuroscience*, 29(43):13613–13620.
- Marchette, S. A., Vass, L. K., Ryan, J., and Epstein, R. A. (2014). Anchoring the neural compass: coding of local spatial reference frames in human medial parietal lobe. *Nat Neurosci*, 17(11):1598–606. 10.1038/nn.3834.
- Marquardt, J., Mohan, P., Spiliopoulou, M., Glanz, W., Butryn, M., Kuehn, E., Schreiber, S., Maass, A., and Diersch, N. (2022). Individual movement patterns in real-world navigation as a digital marker of cognitive health in the elderly. *Alzheimer's & Dementia*, 18(S7):e063058. 10.1002/alz.063058.
- Marr, D. (1982). *Vision: A Computational Investigation into the Human Representation and Processing of Visual Information*. W. H. Freeman and Company, USA.

- May, M. (2004). Imaginal perspective switches in remembered environments: Transformation versus interference accounts. *Cognitive Psychology*, 48(2):163–206. 10.1016/S0010-0285(03)00127-0.
- May, M., Péruch, P., and Savoyant, A. (1995). Navigating in a virtual environment with map-acquired knowledge: Encoding and alignment effects. *Ecological Psychology*, 7(1):21–36. 10.1207/s15326969eco0701_2.
- McNaughton, B. L., Chen, L. L., and Markus, E. J. (1991). "Dead reckoning," landmark learning, and the sense of direction: a neurophysiological and computational hypothesis. *Journal of Cognitive Neuroscience*, 3(2):190–202. 10.1162/jocn.1991.3.2.190.
- Merrill, D. A., Chiba, A. A., and Tuszyński, M. H. (2001). Conservation of neuronal number and size in the entorhinal cortex of behaviorally characterized aged rats. *The Journal of Comparative Neurology*, 438(4):445–456. 10.1002/cne.1327.
- Mittelstaedt, M. L. and Mittelstaedt, H. (1980). Homing by path integration in a mammal. *Naturwissenschaften*, 67(11):566–567. 10.1007/BF00450672.
- Moffat, S. D. (2009). Aging and Spatial Navigation: What Do We Know and Where Do We Go? *Neuropsychology Review*, 19(4):478–489. 10.1007/s11065-009-9120-3.
- Moffat, S. D., Elkins, W., and Resnick, S. M. (2006). Age differences in the neural systems supporting human allocentric spatial navigation. *Neurobiology of Aging*, 27(7):965–972. 10.1016/j.neurobiolaging.2005.05.011.
- Morrison, J. H. and Baxter, M. G. (2012). The Aging Cortical Synapse: Hallmarks and Implications for Cognitive Decline. *Nature reviews. Neuroscience*, 13(4):240–250. 10.1038/nrn3200.
- Mou, W., McNamara, T. P., Valiquette, C. M., and Rump, B. (2004). Allocentric and egocentric updating of spatial memories. *Journal of Experimental Psychology. Learning, Memory, and Cognition*, 30(1):142–157. 10.1037/0278-7393.30.1.142.
- Mueller, E. A., Moore, M. M., Kerr, D. C., Sexton, G., Camicioli, R. M., Howieson, D. B., Quinn, J. F., and Kaye, J. A. (1998). Brain volume preserved in healthy elderly through the eleventh decade. *Neurology*, 51(6):1555–1562. 10.1212/wnl.51.6.1555.
- Mukamel, R., Ekstrom, A. D., Kaplan, J., Iacoboni, M., and Fried, I. (2010). Single-neuron responses in humans during execution and observation of actions. *Current biology*, 20(8):750–756. 10.1016/j.cub.2010.02.045.
- Nau, M., Navarro Schröder, T., Frey, M., and Doeller, C. F. (2020). Behavior-dependent directional tuning in the human visual-navigation network. *Nature Communications*, 11(1):3247. 10.1038/s41467-020-17000-2.
- Nestor, P. J., Fryer, T. D., Smielewski, P., and Hodges, J. R. (2003). Limbic hypometabolism in Alzheimer's disease and mild cognitive impairment. *Annals of Neurology*, 54(3):343–351. 10.1002/ana.10669.

- Neuhauser, H. K., Radtke, A., von Brevern, M., Lezius, F., Feldmann, M., and Lempert, T. (2008). Burden of Dizziness and Vertigo in the Community. *Archives of Internal Medicine*, 168(19):2118–2124. 10.1001/archinte.168.19.2118.
- O'Keefe, J. and Dostrovsky, J. (1971). The hippocampus as a spatial map. Preliminary evidence from unit activity in the freely-moving rat. *Brain Research*, 34(1):171–175. 10.1016/0006-8993(71)90358-1.
- Page, H. J. I. and Jeffery, K. J. (2018). Landmark-Based Updating of the Head Direction System by Retrosplenial Cortex: A Computational Model. *Frontiers in Cellular Neuroscience*, 12. 10.3389/fncel.2018.00191.
- Page, H. J. I., Walters, D. M., Knight, R., Piette, C. E., Jeffery, K. J., and Stringer, S. M. (2014). A theoretical account of cue averaging in the rodent head direction system. *Philosophical Transactions of the Royal Society B: Biological Sciences*, 369(1635):20130283. 10.1098/rstb.2013.0283.
- Parsons, L. M. (1987). Imagined spatial transformation of one's body. *Journal of Experimental Psychology: General*, 116(2):172–191. 10.1037/0096-3445.116.2.172.
- Patenaude, B., Smith, S. M., Kennedy, D. N., and Jenkinson, M. (2011). A Bayesian model of shape and appearance for subcortical brain segmentation. *NeuroImage*, 56(3):907–922. 10.1016/j.neuroimage.2011.02.046.
- Pengas, G., Hodges, J. R., Watson, P., and Nestor, P. J. (2010). Focal posterior cingulate atrophy in incipient Alzheimer's disease. *Neurobiology of Aging*, 31(1):25–33. 10.1016/j.neurobiolaging.2008.03.014.
- Petrucchio, L., Lavian, H., Wu, Y. K., Svava, F., Štíh, V., and Portugues, R. (2023). Neural dynamics and architecture of the heading direction circuit in zebrafish. *Nature Neuroscience*, 26(5):765–773. 10.1038/s41593-023-01308-5.
- Peyrache, A., Lacroix, M. M., Petersen, P. C., and Buzsáki, G. (2015). Internally organized mechanisms of the head direction sense. *Nat Neurosci*, 18(4):569–75. 10.1038/nn.3968.
- Poulter, S., Hartley, T., and Lever, C. (2018). The Neurobiology of Mammalian Navigation. *Current biology: CB*, 28(17):R1023–R1042. 10.1016/j.cub.2018.05.050.
- Qi, Y. and Mou, W. (2023). Sources of systematic errors in human path integration. *Journal of Experimental Psychology: Human Perception and Performance*, 49(2):197–225. 10.1037/xhp0001076.
- Quillen, D. A. (1999). Common Causes of Vision Loss in Elderly Patients. *American Family Physician*, 60(1):99–108.
- Ranck, J. B. (1984). Head-direction cells in the deep cell layers of dorsal presubiculum in freely moving rats. *Society for Neuroscience Abstracts*, 10. citeulike-article-id:496729.
- Rapp, P. R., Deroche, P. S., Mao, Y., and Burwell, R. D. (2002). Neuron number in the parahippocampal region is preserved in aged rats with spatial learning deficits. *Cerebral Cortex (New York, N.Y.: 1991)*, 12(11):1171–1179. 10.1093/cercor/12.11.1171.

- Rapp, P. R. and Gallagher, M. (1996). Preserved neuron number in the hippocampus of aged rats with spatial learning deficits. *Proceedings of the National Academy of Sciences of the United States of America*, 93(18):9926–9930. 10.1073/pnas.93.18.9926.
- Raz, N. and Rodrigue, K. M. (2006). Differential aging of the brain: Patterns, cognitive correlates and modifiers. *Neuroscience and biobehavioral reviews*, 30(6):730–748. 10.1016/j.neubiorev.2006.07.001.
- Renart, A., Song, P., and Wang, X.-J. (2003). Robust Spatial Working Memory through Homeostatic Synaptic Scaling in Heterogeneous Cortical Networks. *Neuron*, 38(3):473–485. 10.1016/S0896-6273(03)00255-1.
- Robertson, R. G., Rolls, E. T., Georges-Francois, P., and Panzeri, S. (1999). Head direction cells in the primate pre-subiculum. *Hippocampus*, 9(3):206–19. 10.1002/(SICI)1098-1063(1999)9:3<206::AID-HIPO2>3.0.CO;2-H.
- Sadalla, E. K. and Montello, D. R. (1989). Remembering Changes in Direction. *Environment and Behavior*, 21(3):346–363. 10.1177/0013916589213006.
- Sargolini, F., Fyhn, M., Hafting, T., McNaughton, B. L., Witter, M. P., Moser, M.-B., and Moser, E. I. (2006). Conjunctive representation of position, direction, and velocity in entorhinal cortex. *Science (New York, N.Y.)*, 312(5774):758–762. 10.1126/science.1125572.
- Seelig, J. D. and Jayaraman, V. (2015). Neural dynamics for landmark orientation and angular path integration. *Nature*, 521(7551):186–191. 10.1038/nature14446.
- Segen, V., Ying, J., Morgan, E., Brandon, M., and Wolbers, T. (2022). Path integration in normal aging and Alzheimer’s disease. *Trends in Cognitive Sciences*, 26(2):142–158. 10.1016/j.tics.2021.11.001.
- Serino, S., Cipresso, P., Morganti, F., and Riva, G. (2014). The role of egocentric and allocentric abilities in Alzheimer’s disease: a systematic review. *Ageing Research Reviews*, 16:32–44. 10.1016/j.arr.2014.04.004.
- Sharp, P. E., Blair, H. T., and Cho, J. (2001a). The anatomical and computational basis of the rat head-direction cell signal. *Trends in Neurosciences*, 24(5):289–294. 10.1016/S0166-2236(00)01797-5.
- Sharp, P. E. and Koester, K. (2008). Lesions of the mammillary body region severely disrupt the cortical head direction, but not place cell signal. *Hippocampus*, 18(8):766–784. 10.1002/hipo.20436.
- Sharp, P. E., Tinkelman, A., and Cho, J. (2001b). Angular velocity and head direction signals recorded from the dorsal tegmental nucleus of gudden in the rat: implications for path integration in the head direction cell circuit. *Behavioral Neuroscience*, 115(3):571–588. 10.1037/0735-7044.115.3.571.
- Shelton, A. L. and McNamara, T. P. (1997). Multiple views of spatial memory. *Psychonomic Bulletin & Review*, 4(1):102–106. 10.3758/BF03210780.
- Shinder, M. E. and Taube, J. S. (2014). Self-motion improves head direction cell tuning. *Journal of Neurophysiology*, 111(12):2479–2492. 10.1152/jn.00512.2013.

- Shine, J. P., Valdes-Herrera, J. P., Hegarty, M., and Wolbers, T. (2016). The Human Retrosplenial Cortex and Thalamus Code Head Direction in a Global Reference Frame. *J Neurosci*, 36(24):6371–81. 10.1523/JNEUROSCI.1268-15.2016.
- Siegler, I., Viaud-Delmon, I., Israël, I., and Berthoz, A. (2000). Self-motion perception during a sequence of whole-body rotations in darkness. *Experimental Brain Research*, 134(1):66–73. 10.1007/s002210000415.
- Sit, K. K. and Goard, M. J. (2023). Coregistration of heading to visual cues in retrosplenial cortex. *Nature Communications*, 14(1):1992. 10.1038/s41467-023-37704-5.
- Skaggs, W. E., Knierim, J. J., Kudrimoti, H. S., and McNaughton, B. L. (1995). A Model of the Neural Basis of the Rat's Sense of Direction. page 10.
- Song, L., E Constanthin, P., Lin, N., Tian, Y., and An, L. (2020). Injury to the human retrosplenial cortex: Two cases and a review of the literature. *Trends in Medicine*, 20(3). 10.15761/TiM.1000230.
- Song, P. and Wang, X.-J. (2005). Angular path integration by moving "hill of activity": a spiking neuron model without recurrent excitation of the head-direction system. *The Journal of Neuroscience: The Official Journal of the Society for Neuroscience*, 25(4):1002–1014. 10.1523/JNEUROSCI.4172-04.2005.
- Stackman, R. W., Clark, A. S., and Taube, J. S. (2002). Hippocampal spatial representations require vestibular input. *Hippocampus*, 12(3):291–303. 10.1002/hipo.1112.
- Stackman, R. W. and Taube, J. S. (1997). Firing Properties of Head Direction Cells in the Rat Anterior Thalamic Nucleus: Dependence on Vestibular Input. *The Journal of Neuroscience*, 17(11):4349–4358. 10.1523/JNEUROSCI.17-11-04349.1997.
- Stackman, R. W. and Taube, J. S. (1998). Firing properties of rat lateral mammillary single units: head direction, head pitch, and angular head velocity. *The Journal of Neuroscience: The Official Journal of the Society for Neuroscience*, 18(21):9020–9037. 10.1523/JNEUROSCI.18-21-09020.1998.
- Stangl, M., Achtzehn, J., Huber, K., Dietrich, C., Tempelmann, C., and Wolbers, T. (2018). Compromised Grid-Cell-like Representations in Old Age as a Key Mechanism to Explain Age-Related Navigational Deficits. *Current Biology*, 28(7):1108–1115.e6. 10.1016/j.cub.2018.02.038.
- Stangl, M., Kanitscheider, I., Riemer, M., Fiete, I., and Wolbers, T. (2020). Sources of path integration error in young and aging humans. *Nature Communications*, 11(1):2626. 10.1038/s41467-020-15805-9.
- Swenor, B. K., Lee, M. J., Varadaraj, V., Whitson, H. E., and Ramulu, P. Y. (2020). Aging With Vision Loss: A Framework for Assessing the Impact of Visual Impairment on Older Adults. *The Gerontologist*, 60(6):989–995. 10.1093/geront/gnz117.
- Takahashi, N., Kawamura, M., Shiota, J., Kasahata, N., and Hirayama, K. (1997). Pure topographic disorientation due to right retrosplenial lesion. *Neurology*, 49(2):464–469. 10.1212/wnl.49.2.464.
- Taube, J. S. (1995). Head direction cells recorded in the anterior thalamic nuclei of freely moving rats. *J Neurosci*, 15(1 Pt 1):70–86. 10.1523/JNEUROSCI.15-01-00070.1995.

- Taube, J. S. (2007). The head direction signal: origins and sensory-motor integration. *Annu Rev Neurosci*, 30:181–207. 10.1146/annurev.neuro.29.051605.112854.
- Taube, J. S. and Muller, R. U. (1998). Comparisons of head direction cell activity in the postsubiculum and anterior thalamus of freely moving rats. *Hippocampus*, 8(2):87–108. 10.1002/(SICI)1098-1063(1998)8:2<87::AID-HIPO1<3.0.CO;2-4.
- Taube, J. S., Muller, R. U., and Ranck, J. B. (1990a). Head-direction cells recorded from the postsubiculum in freely moving rats. I. Description and quantitative analysis. *J Neurosci*, 10(2):420–35.
- Taube, J. S., Muller, R. U., and Ranck, J. B. (1990b). Head-direction cells recorded from the postsubiculum in freely moving rats. II. Effects of environmental manipulations. *J Neurosci*, 10(2):436–47.
- Taube, J. S., Valerio, S., and Yoder, R. M. (2013). Is navigation in virtual reality with fMRI really navigation? *Journal of Cognitive Neuroscience*, 25(7):1008–1019. 10.1162/jocn_a_00386.
- Thompson, P. M., Hayashi, K. M., de Zubicaray, G., Janke, A. L., Rose, S. E., Semple, J., Herman, D., Hong, M. S., Dittmer, S. S., Doddrell, D. M., and Toga, A. W. (2003). Dynamics of Gray Matter Loss in Alzheimer’s Disease. *The Journal of Neuroscience*, 23(3):994–1005. 10.1523/JNEUROSCI.23-03-00994.2003.
- Tolman, E. C. (1948). Cognitive maps in rats and men. *Psychological Review*, 55(4):189–208. 10.1037/h0061626.
- Tong, F. (2003). Primary visual cortex and visual awareness. *Nature Reviews Neuroscience*, 4(3):219–229. 10.1038/nrn1055.
- Topalovic, U., Aghajan, Z. M., Villaroman, D., Hiller, S., Christov-Moore, L., Wishard, T. J., Stangl, M., Hasulak, N. R., Inman, C. S., Fields, T. A., Rao, V. R., Eliashiv, D., Fried, I., and Suthana, N. (2020). Wireless Programmable Recording and Stimulation of Deep Brain Activity in Freely Moving Humans. *Neuron*, 108(2):322–334.e9. 10.1016/j.neuron.2020.08.021.
- Topalovic, U., Barclay, S., Ling, C., Alzuhair, A., Yu, W., Hoxhikyan, V., Chandrakumar, H., Rozgic, D., Jiang, W., Basir-Kazeruni, S., Maoz, S. L., Inman, C. S., Stangl, M., Gill, J., Bari, A., Fallah, A., Eliashiv, D., Pouratian, N., Fried, I., Suthana, N., and Markovic, D. (2023). A wearable platform for closed-loop stimulation and recording of single-neuron and local field potential activity in freely moving humans. *Nature Neuroscience*, 26(3):517–527. 10.1038/s41593-023-01260-4.
- Ueda, S., Nagamachi, K., Nakamura, J., Sugimoto, M., Inami, M., and Kitazaki, M. (2021). The effects of body direction and posture on taking the perspective of a humanoid avatar in a virtual environment. *PLoS ONE*, 16(12):e0261063. 10.1371/journal.pone.0261063.
- Vann, S. D. and Aggleton, J. P. (2004). Testing the importance of the retrosplenial guidance system: effects of different sized retrosplenial cortex lesions on heading direction and spatial working memory. *Behavioural Brain Research*, 155(1):97–108. 10.1016/j.bbr.2004.04.005.
- Viejo, G. and Peyrache, A. (2020). Precise coupling of the thalamic head-direction system to hippocampal ripples. *Nature Communications*, 11(1):2524. 10.1038/s41467-020-15842-4.

- Waller, D., Montello, D. R., Richardson, A. E., and Hegarty, M. (2002). Orientation specificity and spatial updating of memories for layouts. *Journal of Experimental Psychology. Learning, Memory, and Cognition*, 28(6):1051–1063. 10.1037//0278-7393.28.6.1051.
- Wang, R. F. and Spelke, E. S. (2000). Updating egocentric representations in human navigation. *Cognition*, 77(3):215–250. 10.1016/s0010-0277(00)00105-0.
- Warren, W. H., Blackwell, A. W., and Morris, M. W. (1989). Age differences in perceiving the direction of self-motion from optical flow. *Journal of Gerontology*, 44(5):P147–153. 10.1093/geronj/44.5.p147.
- Wiener, J. M., Büchner, S. J., and Hölscher, C. (2009). Taxonomy of Human Wayfinding Tasks: A Knowledge-Based Approach. *Spatial Cognition & Computation*, 9(2):152–165. 10.1080/13875860902906496.
- Wiener, J. M., Condappa, O. d., Harris, M. A., and Wolbers, T. (2013). Maladaptive Bias for Extrahippocampal Navigation Strategies in Aging Humans. *Journal of Neuroscience*, 33(14):6012–6017. 10.1523/JNEUROSCI.0717-12.2013.
- Wilmoth, J. R., Bas, D., Mukherjee, S., and Hanif, N. (2023). World Social Report 2023: Leaving No One Behind in an Ageing World.
- Wolbers, T. and Hegarty, M. (2010). What determines our navigational abilities? *Trends in Cognitive Sciences*, 14(3):138–146. 10.1016/j.tics.2010.01.001.
- Wolbers, T. and Wiener, J. M. (2014). Challenges for identifying the neural mechanisms that support spatial navigation: The impact of spatial scale. *Frontiers in Human Neuroscience*, 8. 10.3389/fnhum.2014.00571.
- Wolbers, T., Wiener, J. M., Mallot, H. A., and Büchel, C. (2007). Differential Recruitment of the Hippocampus, Medial Prefrontal Cortex, and the Human Motion Complex during Path Integration in Humans. *The Journal of Neuroscience*, 27(35):9408–9416. 10.1523/JNEUROSCI.2146-07.2007.
- Wyss-Coray, T. (2016). Ageing, neurodegeneration and brain rejuvenation. *Nature*, 539(7628):180–186. 10.1038/nature20411.
- Yan, Y., Burgess, N., and Bicanski, A. (2021). A model of head direction and landmark coding in complex environments. *PLOS Computational Biology*, 17(9):e1009434. 10.1371/journal.pcbi.1009434.
- Yoder, R. M., Clark, B. J., Brown, J. E., Lamia, M. V., Valerio, S., Shinder, M. E., and Taube, J. S. (2011). Both visual and idiothetic cues contribute to head direction cell stability during navigation along complex routes. *Journal of Neurophysiology*, 105(6):2989–3001. 10.1152/jn.01041.2010.
- Yoder, R. M., Peck, J. R., and Taube, J. S. (2015). Visual Landmark Information Gains Control of the Head Direction Signal at the Lateral Mammillary Nuclei. *The Journal of Neuroscience*, 35(4):1354–1367. 10.1523/JNEUROSCI.1418-14.2015.
- Zacks, J. M., Vettel, J. M., and Michelon, P. (2003). Imagined viewer and object rotations dissociated with event-related fMRI. *Journal of Cognitive Neuroscience*, 15(7):1002–1018. 10.1162/089892903770007399.

- Zanchi, S., Cuturi, L. F., Sandini, G., and Gori, M. (2022). How much I moved: Robust biases in self-rotation perception. *Attention, Perception, & Psychophysics*, 84(8):2670–2683. 10.3758/s13414-022-02589-x.
- Zhang, K. (1996). Representation of spatial orientation by the intrinsic dynamics of the head-direction cell ensemble: a theory. *Journal of Neuroscience*, 16(6):2112–2126. 10.1523/JNEUROSCI.16-06-02112.1996.
- Zugaro, M. B., Arleo, A., Berthoz, A., and Wiener, S. I. (2003). Rapid spatial reorientation and head direction cells. *J Neurosci*, 23(8):3478–82. 10.1523/JNEUROSCI.23-08-03478.2003.
- Zugaro, M. B., Berthoz, A., and Wiener, S. I. (2001). Background, but not foreground, spatial cues are taken as references for head direction responses by rat anterodorsal thalamus neurons. *J Neurosci*, 21(14):RC154.

List of Figures

1	The two reference frames of spatial navigation.	12
2	The spatial navigation system in the human brain.	13
3	The head direction cell firing.	15
4	Head direction cells properties in a changing environment.	16
5	Simplified circuit of the regions involved in the HD system.	19
6	Summary of human brain regions sensitive to HD signal.	22
7	Schematic of ring attractor network dynamics in a HD model.	27
8	Percentage of people aged 65 years or over across world regions from 1950 and estimated until 2050.	30
9	Design of the task.	38
10	Environment of the task.	39
11	Design of the learning phase.	40
12	Design of a testing trial.	43
13	EPI slab of the brain.	45
14	Example of a design matrix created for univariate analysis and run- wise decoding.	50
15	MVPA analysis for run-wise and trial-wise decoding.	51
16	Example of a design matrix created for trial-wise decoding.	52
17	Learning results from participants.	54
18	Percentage of time a landmark was seen by a participant during a pointing trial.	56
19	Percentage of time a landmark was seen during a pointing trial across the learning phase for each individual participant.	57

20	Average pointing answer to the moons for participants during the criterion and testing tasks for each landmark.	59
21	Pointing answer to the moons during the criterion task and testing phase for each individual participant.	61
22	Decoding results for stable vs unstable landmarks and control conditions.	63
23	Decoding results for North vs South (Stable) and West vs East (Unstable) for the ROIs.	65
24	Decoding results for North vs South (Stable) and West vs East (Unstable) for the segmented ROIs	67
25	The reduction of the representational space.	75
26	Testing the hypothesis of the reduction of the representational space with the task.	76
27	Virtual environment used in immersive VR.	78
28	Design of the learning task with a trial example.	80
29	Design of the testing task with a trial example.	81
30	Learning performance across days.	85
31	Landmark placement between days	86
32	Control measures for equal performance between testing days and head movement during the delay phase.	87
33	Average angular error across delay conditions and age groups. . .	88
34	Ratio of angular error by expected rotation across delay conditions and age groups.	89
35	Testing results when already facing the landmark prior to answering.	91
36	Checking the reduction of the representational space hypothesis. .	94

37	Architecture of the model.	104
38	Task phases performed by the agent during a trial.	107
39	Participant distributions used in the model.	108
40	Human trajectory followed by the model and measure of drift.	113
41	Simulation of Zhang and new model with the addition of neuron death.	115
42	Influence of noise levels on the shape of the tuning curve.	117
43	Influence of noise levels on the behaviour of the HD model.	119
44	Probability for the attractor to get stuck in local minima when performing the task.	121
45	Evolution of the angular error over the trial phases for increased weight noise across delay conditions.	124
46	Evolution of the rate of change over the trial phases for increased weight noise across delay conditions.	125
47	Evolution of the angular error over the trial phases for increased background noise across delay conditions.	127
48	Evolution of the rate of change over the trial phases for increased background noise across delay conditions.	128
49	Evolution of the angular error over the trial phases for increased neuron death across delay conditions.	130
50	Evolution of the rate of change over the trial phases for increased neuron death across delay conditions.	131

List of Tables

2.1	Brain masks defining the ROIs used in the analysis	48
4.1	Model parameters for the 361 and 721 neurons networks.	105
4.2	Percentage of noise for individual static simulation (rows) for each type of noise (columns). White cells, simulation ran only for analysis of the shape of the tuning curve.	110
4.3	Percentage of noise for individual task simulation (rows) for each type of noise (columns).	111

Declaration of Honour

“I hereby declare that I prepared this thesis without the impermissible help of third parties and that none other than the aids indicated have been used; all sources of information are clearly marked, including my own publications.

In particular I have not consciously:

- fabricated data or rejected undesirable results,
- misused statistical methods with the aim of drawing other conclusions than those warranted by the available data,
- plagiarized external data or publications,
- presented the results of other researchers in a distorted way.

I am aware that violations of copyright may lead to injunction and damage claims by the author and also to prosecution by the law enforcement authorities.

I hereby agree that the thesis may be electronically reviewed with the aim of identifying plagiarism.

This work has not yet been submitted as a doctoral thesis in the same or a similar form in Germany, nor in any other country. It has not yet been published as a whole.”

Magdeburg, _____

Matthieu BERNARD